



THE HONG KONG
POLYTECHNIC UNIVERSITY

香港理工大學

Pao Yue-kong Library

包玉剛圖書館

Copyright Undertaking

This thesis is protected by copyright, with all rights reserved.

By reading and using the thesis, the reader understands and agrees to the following terms:

1. The reader will abide by the rules and legal ordinances governing copyright regarding the use of the thesis.
2. The reader will use the thesis for the purpose of research or private study only and not for distribution or further reproduction or any other purpose.
3. The reader agrees to indemnify and hold the University harmless from and against any loss, damage, cost, liability or expenses arising from copyright infringement or unauthorized usage.

IMPORTANT

If you have reasons to believe that any materials in this thesis are deemed not suitable to be distributed in this form, or a copyright owner having difficulty with the material being included in our database, please contact lbsys@polyu.edu.hk providing details. The Library will look into your claim and consider taking remedial action upon receipt of the written requests.

**DEVELOPMENT OF A NOVEL DIRECT EXPANSION
BASED STANDALONE ENHANCED
DEHUMIDIFICATION AIR CONDITIONING
SYSTEM FOR IMPROVED YEAR-ROUND INDOOR
HUMIDITY CONTROL**

CHEN WENJING

PhD

The Hong Kong Polytechnic University

2018

The Hong Kong Polytechnic University
Department of Building Services Engineering

**Development of a Novel Direct Expansion Based
Standalone Enhanced Dehumidification Air Conditioning
System for Improved Year-round Indoor Humidity
Control**

Chen Wenjing

**A thesis submitted in partial fulfillment of the requirements for the Degree of
Doctor of Philosophy**

June 2018

Certificate of Originality

I hereby declare that this thesis is my own work and that, to the best of my knowledge and belief, it reproduces no material previously published or written, nor material that has been accepted for the award of any other degree or diploma, except where due acknowledgement has been made in the text.

Chen Wenjing

Abstract

In buildings, controlling indoor air humidity at an appropriate level is critically important since this directly affects building occupants' thermal comfort, indoor air quality (IAQ) and the operating efficiency of building A/C systems. In hot and humid climates, such as Hong Kong, air conditioning (A/C) is usually required for up to 7 months from April to October in a year. At different seasons within the 7 months, however, space latent load that directly affects indoor air humidity level can vary significantly. On the other hand, direct expansion (DX) based A/C systems are widely used for indoor environmental control in various buildings in different climates, since they are simpler and more energy efficient, and generally cost less to own and maintain. However, the current trend in designing a conventional DX A/C system is to have a smaller moisture removal capacity in an attempt to boost its energy efficiency ratings. Furthermore, most DX A/C systems are equipped with single-speed compressors and fans, relying on on-off cycling compressor to maintain indoor air temperature only. Therefore, in hot and humid climates, such a DX A/C system, once installed, will have to be operated at different seasonal cooling load situations, and would hence have a hard time in trying to maintain the desired indoor air temperature and humidity at all times, unless supplementary measures to supply variable dehumidification ability are provided. However, these measures are usually complicated and costly, and may only be good during a specific season and become redundant in other seasons.

Therefore, a standalone DX based enhanced dehumidification air conditioning (EDAC) system is proposed to provide suitable indoor air humidity control at different seasons in hot and humid climates, without requiring any supplementary measures. The proposed EDAC system has two evaporators and could act as a dehumidifier on the days when

less or no additional cooling is required by employing one evaporator as a reheating coil (ADO mode), or as an enhanced dehumidification A/C system by operating the two evaporators together for achieving an improved indoor humidity control (EDAC mode).

A research project on the development of such an EDAC system for improved year-round indoor air humidity control in hot and humid climates through experiments and mathematical model has been carried out and the project results are presented in this Thesis.

This Thesis begins with reporting the establishment of a prototype experimental EDAC system consisting of a DX refrigeration plant (refrigerant side) and an air-distribution sub-system (air side). All its major operating parameters can be real-time measured and recorded using high precision measuring devices. The availability of the experimental EDAC system would help facilitate experimentally studying the operational characteristics of the EDAC system, experimentally validating a steady-stated EDAC mathematical model to be developed and developing a year-round control strategy for the EDAC system for improved indoor air humidity control in hot and humid climates.

Secondly, the Thesis presents an extensive experimental study on the operational characteristics of the experimental EDAC system at the EDAC mode in terms of the relationship between its output total cooling capacity (TCC) and equipment sensible heat ratio (E SHR), when both the evaporators were operated. The experimental results demonstrated that at a fixed inlet air state, varying refrigerant and air mass flow rates to both evaporators would significantly affect the operational characteristics. The resulted TCC and E SHR relationships were mutually constrained within an irregular

area in a TCC - E SHR diagram, thus providing variable dehumidification ability. The experimental results also demonstrated that inlet air temperature and relative humidity would significantly influence the operational characteristics of the EDAC system, resulting in shifted position of, and varied shape of an irregular area of TCC - E SHR relationship in a TCC - E SHR diagram.

Thirdly, the development and experimental validation of a physical-based steady-state mathematical model for the experimental EDAC system at the EDAC mode are presented. The model was developed by referring to the previous models for a two-evaporator A/C system. Using the validated EDAC model, a follow-up detailed modeling study was carried out to both demonstrate that the EDAC system was able to provide variable dehumidification ability and to optimize the sizing of the two evaporators used in the EDAC system. Furthermore, the modeling study results indicated that the EDAC system could produce variable dehumidification capacity. The modeling study results also suggested that a lower ratio of surface areas for the two evaporators in an EDAC system was beneficial to enlarging its variation ranges for both total cooling capacity (TCC) and equipment sensible heat ratio (E SHR).

Finally, the Thesis presents an experimental study on the development of a year-round control strategy for operating the EDAC system at both the ADO and EDAC mode for achieving improved year-round indoor humidity level in buildings located in hot and humid climates. The experimental results show that in hot and humid climates, the use of the EDAC system and the control strategy was able to achieve an improved year-round indoor humidity control, while still maintaining the required indoor air temperature control at a higher energy efficiency, as compared to the use of a conventional On-Off controlled single evaporator DX A/C system.

Publications arising from the Thesis

I. Journal Papers

- **Wenjing Chen**, Ming-yin Chan, Wenbing Weng, Huaxia Yan, Shiming Deng, An experimental study on the operational characteristics of a direct expansion based enhanced dehumidification air conditioning system. *Applied Energy*, 225 (2018): 922-933. (Based on Chapter 5).
- **Wenjing Chen**, Ming-yin Chan, Wenbing Weng, Huaxia Yan, Shiming Deng, Development of a steady-state physical-based mathematical model for a direct expansion based enhanced dehumidification air conditioning system. *International Journal of Refrigeration*, 91 (2018): 55-68. (Based on Chapter 6).
- **Wenjing Chen**, Ming-yin Chan, Shiming Deng, Huaxia Yan, Wenbing Weng, A direct expansion based enhanced dehumidification air conditioning system for improved year-round indoor humidity control in hot and humid climates. *Building and Environment*, 139 (2018): 95-109 (Based on Chapter 7).

II. Conference papers

- **Wenjing Chen**, Ming-yin Chan, Wenbing Weng, Shiming Deng. Modeling and experimental study on a direct expansion based enhanced dehumidification air conditioning system. 17th International Refrigeration and Air Conditioning Conference at Purdue, Accepted.

Acknowledgements

I must express my sincere grateful thanks to my Chief Supervisor, Dr. Chan Ming-yin, Assistant Professor and my Co-Supervisor, Dr. Deng Shiming, Professor, both from the Department of Building Services Engineering (BSE), The Hong Kong Polytechnic University, and my Co-Supervisor, Dr. Weng Wenbing, Professor, from School of Environment and Architecture, University of Shanghai for Science and Technology, for their readily available supervision, invaluable suggestions, patient guidance and continuous helps throughout the course of my study.

My special thanks go to the Hong Kong Polytechnic University for financially supporting this research work. I would like to thank Dr. Xia Yudong, Dr. Yan Huaxia and Mr. Fang Guanyu for their helps during my study. I would like also to thank the technicians in the heating, ventilation and air conditioning (HVAC) Laboratory of the BSE Department for their assistances in the experimental work.

Finally, my deepest gratitude goes to my parents, my girlfriend Miss. Zheng Xueying and all other family members. I could not have completed my work without their loves and continuous support throughout my life.

Table of Contents

	Page
Certificate of Originality	I
Abstract	II
Publications arising from the Thesis	V
Acknowledgements.....	VI
Table of Contents	VII
List of Figures.....	XI
List of Tables	XVI
Nomenclature	XVII
List of Abbreviations	XIX
Chapter 1 Introduction.....	1
Chapter 2 Literature review.....	5
2.1 Introduction	5
2.2 The fundamental issues about indoor humidity level.....	7
2.2.1 Source of indoor moisture	7
2.2.2 The importance of indoor air humidity control	7
2.3 The reasons for inadequate dehumidification encountered when using DX A/C systems	9
2.3.1 The design and selection of a DX A/C system.....	9
2.3.2 Space cooling load characteristics	10
2.3.3 Existing control strategies for DX A/C systems.....	13
2.4 Measures to deal with inadequate dehumidification at different load conditions	14

2.4.1 Measures in Period I	15
2.4.2 Measures in Period II.....	18
2.4.3 Measures in Period III	31
2.5 Modeling of DX A/C systems	32
2.5.1 Sub-models for the refrigerant-side of a DX A/C system	35
2.5.2 Sub-models for the air-side of a DX A/C system.....	38
2.5.3 Solving DX A/C system models.....	41
2.6 Conclusions	42
Chapter 3 Proposition	45
3.1 Background	45
3.2 Project title	45
3.3 Aims and objectives	46
3.4 Research methodologies.....	47
Chapter 4 The prototype experimental EDAC system	49
4.1 Introduction	49
4.2 Detailed configurations of the proposed EDAC system.....	50
4.3 Descriptions of the experimental EDAC system and its major components.....	52
4.4 Computerized instrumentation and data acquisition system	57
4.4.1 Sensors/ measuring devices for temperatures, pressures and flow rates.....	57
4.4.2 The data acquisition system.....	59
4.5 LabVIEW logging & control supervisory program.....	60
4.6 Summary	60
Chapter 5 Operational characteristics of the experimental EDAC system	62
5.1 Introduction	62

5.2	Experimental procedures and data interpretation	62
5.3	The measured operational characteristics of the EDAC system	66
5.3.1	The measured operational characteristics of the experimental EDAC system at Case T-26 or RH-50.....	67
5.3.2	The influence of different inlet air states on the operational characteristics of the experimental EDAC system (all the cases) .	79
5.3.3	Discussion.....	82
5.4	Conclusions	83
Chapter 6 Development of a steady-state mathematical model for the experimental EDAC system at the EDAC mode		85
6.1	Introduction	85
6.2	Development of a steady-state mathematical model for the EDAC system at the EDAC mode	86
6.2.1	Steady-state modeling of the experimental EDAC system at EDAC mode	87
6.2.2	Numerical procedure for solving the EDAC model	92
6.3	Experimental validation of the EDAC model	95
6.4	The follow-up modeling study	98
6.4.1	EDAC system's ability to provide variable dehumidification ability	98
6.4.2	Sizing optimization for the two evaporators in the EDAC system	102
6.4.3	Discussion.....	105
6.5	Conclusions	106
Chapter 7 Development of a control strategy for the EDAC system for its year- round operation.....		108

7.1 Introduction	108
7.2 Development of the year-round control strategy for the EDAC system.....	109
7.3 Experimental conditions.....	115
7.4 Experimental results and discussions	117
7.4.1 The measured operating performances of the EDAC system under the year-round control strategy at the ADO mode (Set A).....	118
7.4.2 The measured operating performances of the EDAC system under the year-round control strategy at the EDAC mode (Set B).....	121
7.4.3 Discussions	128
7.5 Conclusions	130
Chapter 8 Conclusion and future work.....	131
8.1 Conclusions	131
8.2 Proposed further work	133
Appendix Photos of the experimental EDAC system	135
References	143

List of Figures

	Page
Chapter 2	
Fig. 2.1	Schematic diagram of a typical DX A/C system 6
Fig. 2.2	Averaged monthly application SHRs between April and October in a master bedroom in Hong Kong [Li et al., 2006] 13
Fig. 2.3	Using the heat rejected from condenser for reheating air [Alsenz, 2002] 16
Fig. 2.4	Using the heat rejected from compressor for reheating air [Knight et al., 2008] 16
Fig. 2.5	Schematics of the novel isothermal dehumidifier [Han et al., 2013] 17
Fig. 2.6	The schematic diagram of a radiant panel assisted SSLC system [Han and Zhang, 2011] 19
Fig. 2.7	Schematic diagram of the SSLC system using two parallel compression cycles [Ling et al., 2010] 21
Fig. 2.8	Schematics of an experimental setup for a desiccant assisted SSLC A/C system [Subramanyam et al., 2004] 23
Fig. 2.9	Schematics of the structure and operational modes of a novel concept for a desiccant-enhanced DX A/C system [Tu et al., 2017] 24
Fig. 2.10	The variations in TCC and E SHR at different combinations of compressor and supply fan speeds [Li and Deng, 2007b] 25
Fig. 2.11	The inherent correlation between TCC and E SHR at different speed combinations of compressor and supply fan for a VS DX A/C system [Xu et al., 2010] 27

Fig. 2.12	Inherent correlations between output TCC and equipment SHR of the experimental VS DX A/C system at constant temperature group [Li et al., 2014]	28
Fig. 2.13	Inherent correlations between output TCC and Equipment SHR of the experimental VS DX A/C system at constant RH group [Li et al., 2014]	28
Fig. 2.14	The inherent correlation of the experimental VS DX A/C system at three different DS settings [Xia et al., 2017]	29

Chapter 4

Fig. 4.1	Schematics of the detailed configuration for the proposed EDAC system	51
Fig. 4.2	The schematic diagram of the DX refrigeration plant in the prototype experimental EDAC system	53
Fig. 4.3	The schematic diagram of the air side for the prototype experimental EDAC system	54

Chapter 5

Fig. 5.1	The measured operational characteristics of the prototype experimental EDAC system under various R_r and R_a (Case T-26)	67
Fig. 5.2	The influences of R_r on the evaporating pressures in HX1 and HX2, and the compressor suction pressure	69
Fig. 5.3	The factors affecting the evaporating pressures in HX1 and HX2, and compressor suction pressure	70

Fig. 5.4	The influences of varying R_r on the DSs at exits of HX1, HX2 and the compressor suction	72
Fig. 5.5	The influences of R_r on the mass flow rates through HX1, HX2 and compressor of the EDAC system (Points D, E, F correspond to the same shown in Fig. 5.1)	73
Fig. 5.6	The influences of varying R_a on the evaporating pressures in HX1 and HX2, and compressor suction pressure, at a fixed R_r	78
Fig. 5.7	The influences of varying R_a on the DSs at exits of HX1 and HX2, and the compressor suction	78
Fig. 5.8	The measured operational characteristics of the experimental EDAC system at the Constant T Group (Cases RH-40, RH-50 and RH-60)	80
Fig. 5.9	The operational characteristics of the EDAC system at the Constant RH Group (Cases T-22, T-24 and T-26)	81
 Chapter 6		
Fig. 6.1	A conceptual model for the experimental EDAC system at the EDAC mode	88
Fig. 6.2	An existing conceptual model for the DEAC system [Pan et al., 2012]	89
Fig. 6.3	Schematic diagram of the hydraulic network for the air-side in the proposed EDAC system	91
Fig. 6.4	Flow chart of the calculation procedure of the complete EDAC system model	94

Fig. 6.5	Comparison of the predicted and experimental TCC and ESHR at the inlet air state of 26 °C and 50% RH (Case RH-50 or T-26)	95
Fig. 6.6	Comparison of the predicted and experimental TCC values at all the five experimental cases	97
Fig. 6.7	Comparison of the predicted and experimental E SHR values at all the five experimental cases	98
Fig. 6.8	The operational characteristics of different DX A/C systems at the same inlet air state of 25 °C and 50% RH	100
Fig. 6.9	The operational characteristics of the EDAC system with different R_s values at an inlet air state of 26 °C and 50% RH	103
 Chapter 7		
Fig. 7.1	Flow chart of the year-round control strategy for the EDAC system for improved indoor humidity level	110
Fig. 7.2	Cascade PI controllers at Status 3	114
Fig. 7.3	Measured variations in indoor air temperature and RH in Test A1	120
Fig. 7.4	Measured variations in indoor air temperature and RH in Test A2	121
Fig. 7.5	Measured variations in indoor air temperature and RH in Test B1	123
Fig. 7.6	Measured variations in indoor air temperature and RH in Test B3	124
Fig. 7.7	Measured variations in indoor air temperature and RH in Test B2	126

Fig. 7.8	Measured variations in indoor air temperature and RH in Test B4	127
Fig. 7.9	Measured variations in indoor air temperature and RH in Test B5	128
Appendix		
Photo 1	Overview of the experimental EDAC system (1)	139
Photo 2	Overview of the experimental EDAC system (2)	140
Photo 3	Overview of the air duct of the experimental EDAC system (1)	141
Photo 4	Overview of the air duct of the experimental EDAC system (2)	142
Photo 5	Indoor Chamber of the Laboratory	143
Photo 6	Outdoor Chamber of the Laboratory	143
Photo 7	Refrigerant mass flow meters	144
Photo 8	Load generation unit	144
Photo 9	Air sampling device	145
Photo 10	Airflow rate measuring apparatus	145
Photo 11	Logging supervisory program	146
Photo 12	Control supervisory program	146

List of Tables

	Page
Chapter 4	
Table 4.1 Specifications of the main components used in the prototype experimental EDAC system	56
Table 4.2 Details of instrumentation and sensors used in the experimental EDAC system	59
Chapter 5	
Table 5.1 Five experimental cases with different inlet air settings	64
Table 5.2 The combinations of R_a and R_r used in the five experimental cases	64
Table 5.3 Measurement/calculation uncertainty of system operating parameters	66
Chapter 7	
Table 7.1 Statuses of the control valves and VCDs at different operating modes	111
Table 7.2 Experimental conditions and cases	116

Nomenclature

Variable	Description	Unit
A	area	m^2
C_{pa}	air specific heat at constant pressure	$\text{kJ}/(\text{kg}\cdot\text{K})$
DP	differential pressure	Pa
d	moisture content	g/kg
h	specific enthalpy	kJ/kg
m	mass flow rate	kg/s
P	pressure	kPa
Q_s	sensible output cooling capacity	kW
R	ratio	DL
RH	relative humidity	%
RH_i	indoor air relative humidity	%
$RH_{i,s}(\text{ADO})$	indoor air relative humidity set point at ADO mode	%
$RH_{i,s}(\text{EDAC})$	indoor air relative humidity set point at EDAC mode	%
T	temperature	$^{\circ}\text{C}$
T_i	indoor air temperature	$^{\circ}\text{C}$
$T_{i,s}(\text{ADO})$	indoor air temperature set point at ADO mode	$^{\circ}\text{C}$
$T_{i,s}(\text{EDAC})$	indoor air temperature set point at EDAC mode	$^{\circ}\text{C}$
T_o	outdoor air temperature	$^{\circ}\text{C}$
$T_{o,ac}$	outdoor air temperature above which air conditioning is required	$^{\circ}\text{C}$
T_s	supply air temperature	$^{\circ}\text{C}$
ΔRH	relative humidity control dead-band	%
ΔT	temperature control dead-band	$^{\circ}\text{C}$
η_{isen}	isentropic coefficient	-

η_{vol} volumetric coefficient

-

Subscripts

1 the first heat exchanger
2 the second heat exchanger
a air
calc calc
com compressor
cond condenser
duct air duct
fan supply fan
i indoor
o outdoor
r refrigerant
S supply air
s size / set
sc sub-cooling
suc compressor suction
w wet-bulb

List of Abbreviations

A/C	air conditioning
ANN	artificial neural network
CC	cooling coil
COP	coefficient of performance
DEAC	dual-evaporator air conditioning
DS	the degree of refrigerant superheat
DX	direct expansion
EEV	electronic expansion valve
EER	energy efficiency rating
EDAC	enhanced dehumidification air conditioning
E SHR	equipment sensible heat ratio
FM	refrigerant mass flow meter
FRMA	airflow rate measuring apparatus
HX1	the first heat exchanger
HX2	the second heat exchanger
IAQ	indoor air quality
LGU	load generating unit
MEAC	multi-evaporator air conditioning
MPC	model predictive control
PID	proportional-integral-derivative
RTD	resistance temperature device
SEAC	single evaporator air conditioning
SSLC	separate sensible and latent cooling
SV	solenoid valve

TCC	total cooling capacity
VCD	air volume control damper
VS	variable speed
VSD	variable speed drive

Chapter 1

Introduction

Achieving a comfortable indoor air temperature in air conditioned buildings may not be the sole goal for building air conditioning (A/C) installations. Appropriately controlling indoor air humidity at a suitable level is also essential for an A/C system, which is particularly true in hot and humid climates, since indoor air humidity directly affects building occupants' thermal comfort [Toftum and Fanger, 1999; Zhang and Yoshino, 2010], indoor air quality (IAQ) [Arens and Baughman, 1996] and the operating efficiency of building A/C installations [Berglund, 1998].

In hot and humid climates, such as Hong Kong, direct expansion (DX) air conditioning A/C systems are widely used for controlling indoor air temperature and humidity in various buildings, in particular in small- to medium-scale buildings, since DX A/C systems are simpler and more energy efficient, and generally cost less to own and maintain. However, it is often difficult and challenging for a conventional DX A/C system to provide desired humidity control due to the current design trends for A/C systems, variable space load conditions and commonly used control strategies for DX A/C systems. Therefore, supplementary measures, such as separate sensible and latent cooling (SSLCL) technology and variable speed (VS) technology, have been applied to assisting conventional DX A/C systems to provide variable dehumidification ability, so as to match the variable space load conditions. However, these measures are often complicated and costly, thus only commonly used in large-scaled installations but rarely for small systems such as residential A/C units.

To address the inadequacy in dealing with variable indoor space loads by using conventional DX A/C systems, and to avoid complicated and costly additional measures for providing adequate dehumidification ability, a novel DX based enhanced dehumidification air conditioning (EDAC) system with two evaporators has been proposed. Therefore, a research project to develop the proposed EDAC system through experiments and mathematical modeling has been carried out and the project results are presented in this thesis.

To begin with, a comprehensive literature review on various issues related to the development of the EDAC system is presented in Chapter 2. Firstly, the fundamental issues on indoor air humidity control including source of indoor moisture and the effects of indoor air humidity on indoor thermal comfort and indoor air quality (IAQ). Secondly, the reasons for inadequate dehumidification ability provided by conventional DX A/C systems are discussed. This is followed by reviewing the existing measures to dealing with inadequate dehumidification at different seasonal cooling load situations. Lastly, a review on the previous studies on the modeling of DX A/C systems and their major system components is presented.

Chapter 3 presents the research proposal, which covers the background, project title, objectives and research methodologies for the research project reported in this Thesis.

In Chapter 4, a description for a purposely established prototype experimental EDAC system to facilitate carrying out the research project reported in this Thesis is presented. Firstly, the configuration of the EDAC system is detailed. Then the prototype experimental EDAC system and its major components are described. This is followed by describing computerized measuring devices and a data acquisition system. Finally, a supervisory program used to operate and control the prototype experimental EDAC

system is detailed. The availability of the prototype experimental EDAC system is expected to be essential in successfully carrying out the research project.

Chapter 5 presents an experimental study on the operational characteristics of the experimental EDAC system in terms of the relationship between its output total cooling capacity (TCC) and equipment sensible heat ratio (E SHR), when both evaporators in the EDAC system were operated, i.e., at EDAC mode. During the experiments, constant compressor and supply fan speeds were used, but the refrigerant and air mass flow rates to both evaporators were varied, at different inlet air states to the experimental EDAC system. The experimental results demonstrated that at a fixed inlet air state, varying refrigerant and air mass flow rates to both evaporators would significantly affect the operational characteristics of the experimental EDAC system. The experimental results also demonstrated that both the inlet air temperature and relative humidity could influence the operational characteristics of the EDAC system.

Chapter 6 reports on the development of a steady-state mathematical model for the EDAC system at the EDAC mode, and the developed EDAC model was experimentally validated using the prototype experimental EDAC system, with an acceptable modeling accuracy. The model was developed with reference to the previous models for a two-evaporator DX A/C system. Using the validated model, a detailed modeling study was carried out to both demonstrate that the EDAC system was able to provide variable dehumidification ability and to optimize the sizing of the two evaporators used in the EDAC system.

In Chapter 7, based on the experimental and modeling studies reported on Chapter 6 and Chapter 7, a year-round control strategy for the experimental EDAC system at

both ADO and EDAC modes was developed. The control strategy enabled the operation of the EDAC system over a wide range of operating conditions so as to maintain an improved indoor humidity level all year round. Extensive experimental work has been carried out to examine both the operation of the experimental EDAC system and the controllability of the control strategy.

Finally, the Conclusions of the Thesis and the proposed future work are given in Chapter 8.

Chapter 2

Literature review

2.1 Introduction

For buildings located in hot and humid climates, air conditioning is normally required for up to 7 months in a year. Direct expansion (DX) air conditioning (A/C) systems are widely used in buildings, in particular in small-to medium-scale buildings. Compared to central chilled water-based A/C systems, DX A/C systems are simpler, more energy efficient and cost less to own and maintain [Chen, 2005; Xia et al., 2017]. However, when using DX A/C systems, appropriately controlling indoor air humidity level is as important as controlling indoor air temperature, since air humidity directly affects building occupants' thermal comfort, indoor air quality (IAQ) and the operating efficiency of building A/C systems.

A conventional single evaporator DX A/C system is schematically shown in Fig. 2.1. However, using such a system to appropriately control indoor humidity is problematic, since air cooling and dehumidification is a coupled process. Usually, a DX A/C system does not control directly but indirectly indoor humidity. Therefore, inadequate dehumidification can be often found when using a conventional DX A/C system. Adding humidity as a control target in addition to temperature necessitates providing extra equipment or suitable control methods [Xu et al., 2017].

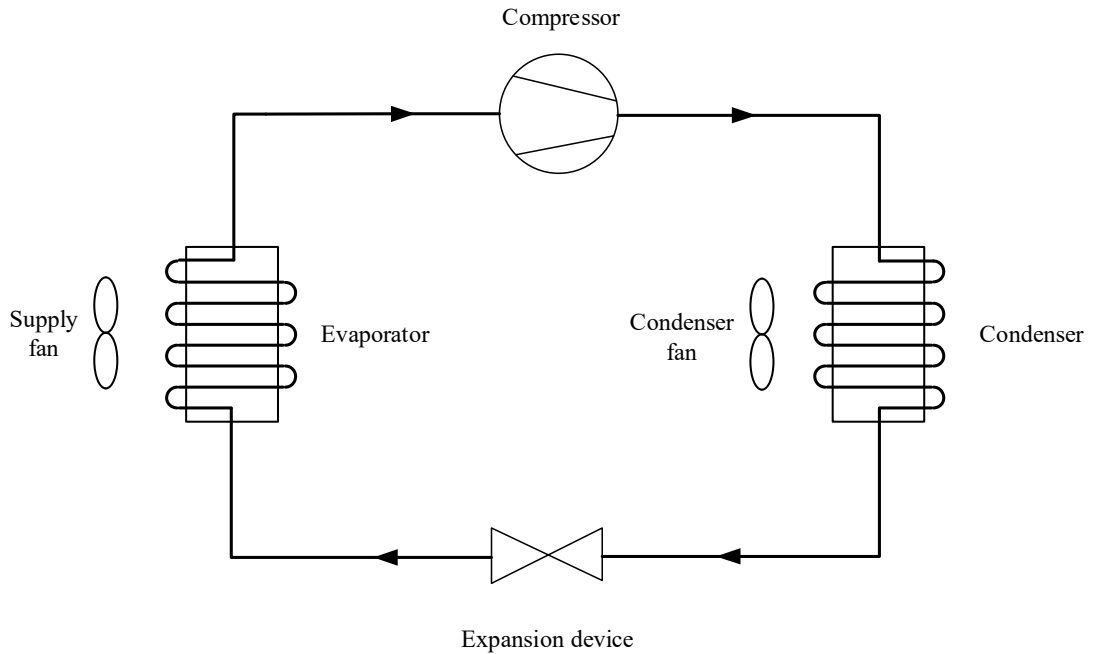


Fig. 2.1 Schematic diagram of a typical DX A/C system

Although there have previous efforts on improving the dehumidification ability for DX A/C systems, further studies are considered necessary in order to reduce equipment cost or to develop more suitable control methods for DX A/C systems. A comprehensive literature review on a number of issues related to indoor air humidity control using DX A/C systems has been conducted and the review outcomes are presented in this Chapter. Firstly, the fundamental issues about indoor air humidity control including the source of indoor moisture and the importance of indoor humidity control are presented. Secondly, the reasons for inadequate dehumidification encountered in hot and humid climates when using DX A/C systems are discussed. This is followed by reviewing the measures to deal with inadequate dehumidification at different seasonal space cooling load situations. Fourthly, the previous studies on the modeling of DX A/C systems and their major components are reviewed. Finally, the conclusions of the literature review are presented.

2.2 The fundamental issues about indoor humidity level

In this Section, the following two fundamental issues on indoor air humidity level are reviewed.

2.2.1 Source of indoor moisture

The sources of indoor moisture can be grouped into external and internal. External sources may include outdoor air ventilation and infiltration. Most residential buildings require the ASHRAE-recommended minimum ventilation rate to ensure IAQ and occupants' thermal comfort [McGahey, 1998]. The effects on indoor air humidity level due to ventilation and infiltration are significantly dependent on the moisture content of outdoor air. Generally, the higher the moisture content of outdoor air, the higher the indoor latent cooling load an A/C system would have to deal with. In particular, during part load conditions in hot and humid climates, the latent cooling load from ventilation air would have greater influences on indoor air humidity than that at full load conditions [Aynur et al., 2008a], and therefore should receive more attentions. On the other hand, internal sources for indoor moisture load mainly include the moisture gains from occupants and other indoor activities, such as washing and cooking.

2.2.2 The importance of indoor air humidity control

Indoor humidity control is equally important to indoor temperature control for the following reasons:

The first and the most important reason is that indoor thermal comfort can be

significantly influenced by indoor humidity level [Fanger, 1970]. It was found in previous studies [Toftum and Fanger, 1999] that indoor humidity level could affect the skin humidity and respiratory comfort of a human being. Low indoor humidity level ($RH < 30\%$) in inhabited dwellings is associated with dryness of mucous membrane and the dryness of eyes and skin. Indoor air humidity is closely related to human health as well as the problem of static electricity [Paasi et al., 2001]. Reinikainen and Jaakkola [2003] conducted a study on assessing the effects of absolute humidity and RH on skin and upper airway symptoms. On-site investigation results showed that skin and nasal symptoms were deteriorated when air dry-bulb temperature rose, but improved when air RH was increased. Dryness in a heated space could be alleviated by lowering room temperature or through humidification. Sunwoo et al. [2006] studied the physiological and the subjective responses to low RH, and showed that eyes and skin became dry at 30% RH, whereas nasal cavity became dry at 10% RH. On the other hand, high indoor RH level ($RH > 60\%$) would also cause discomfort for occupants since it would lead to a high level of skin humidity and insufficient cooling of the mucous membranes in the upper respiratory tract by inhalation of humid or warm air [Toftum and Fanger, 1999].

The second reason is that it can affect indoor air quality (IAQ). Related studies [Toftum et al., 1998a, b] showed that there should be an upper limit for indoor RH since a high humidity environment directly influenced the perceived IAQ and also induced the growth of mold, leading to respiratory discomfort and allergies. Kishi et al. [2009] carried out a survey in various climate regions and concluded that the risk of sick building syndrome was increased when several dampness indicators were observed concurrently.

The third reason was that an increased moisture level of indoor air in buildings would also deteriorate building materials and impact energy use performance in buildings [Osanyintola and Simonson, 2006], leading to either oversized HVAC equipment in dry climates or underestimated the energy consumption in humid regions.

Therefore, ASHRAE Standard [ASHRAE, 2002] recommends that an optimum indoor air humidity zone be maintained between 30% and 60% RH to minimize the growth of allergenic or pathogenic organisms and avoid respiratory difficulties.

2.3 The reasons for inadequate dehumidification encountered when using DX A/C systems

In hot and humid climates, an A/C system will have to deal with both sensible and latent loads in a space, and in many cases, to deal with space latent cooling load using a DX A/C system is more challenging and difficult [Li et al., 2006]. The reasons for inadequate dehumidification when using DX A/C systems included the design and selection of DX A/C systems, variations in indoor latent loads in conditioned space and existing control strategies for DX A/C systems, as follows:

2.3.1 The design and selection of a DX A/C system

The current trend in designing a conventional DX A/C system is to have a smaller moisture removal capacity in an attempt to boost its energy efficiency ratings (EER) and Coefficient of Performance (COP) [Kittler, 1996]. The method used to raise EER is to increase the surface area of heat exchangers in a DX A/C system. Such a strategy allows a DX A/C system to run at a higher refrigerant temperature in its evaporator

and a lower refrigerant temperature in its condenser, resulting in however a lower dehumidification capacity of the DX A/C system. This could therefore potentially lead to a situation where a DX A/C system will provide a desired temperature control but not a desired indoor humidity control [Murphy, 2002; Shirey, 1993; Westphalen, 2004]. Furthermore, it was previously shown [Kurtz, 2003] that as homeowners were more informed and aware of energy conservation and high energy costs, they would raise their thermostat set points in summer. As a result, some residences suffered from poor IAQ, high indoor moisture levels and mold growth.

Therefore, the first step in addressing inadequate dehumidification when using DX A/C systems is to properly undertake system design. This entails conducting appropriate design analysis to ensure that a DX A/C system can deal with not only sensible load but also latent load. Hourahan [2004] and Komor [1997] summarized the key steps in properly both sizing HVAC equipment and performing a rigorous heat gain/heat loss procedure. Considering the high demand of dehumidification in subtropical regions, Lin and Deng [2006] suggested that the sizing of a DX based room air conditioner (RAC) used in a sleeping environment in the subtropics should preferably be based on 70-80% of the peak load in the sleeping environment, since this could help enhance its dehumidification capacity by prolonging the running time of its compressor. However, this method may lead to a higher room temperature when the indoor sensible load in the sleep environment was high.

2.3.2 Space cooling load characteristics

Even with a correctly sized conventional DX A/C system, inadequate dehumidification may still be encountered due to variation in indoor space latent load.

Total cooling capacity (TCC) and sensible heat ratio (SHR) are two key parameters in studying the characteristics of space cooling load and the ability of a DX A/C system to cool and dehumidify air. There are two different but related SHRs, Equipment SHR (E SHR) and Application SHR (A SHR). E SHR is defined as the ratio of the output sensible cooling capacity to the output TCC of a piece of A/C equipment, which is a property of equipment. A SHR is defined as the ratio of the space sensible cooling load to the total space cooling load, which is a property of space. For an air conditioned space served by a DX A/C system, to maintain its indoor air temperature and humidity settings should match not only the system's output TCC with the total space cooling load, but also system's E SHR with space's A SHR [Li and Deng, 2007b]. However, A SHRs for residential buildings located in hot and humid climates normally ranged between 0.6 and 0.7, which were lower than an E SHR of 0.7-0.8 for standard DX RACs extensively used in the subtropics [Lin and Deng, 2004]. A number of other studies [Amrane et al., 2003; Andrade and Bullard, 2002; Harriman III, 2002; Hourahan, 2004; Lam, 1993; Lstiburek, 2002; Murphy, 2002; Shirey III and Henderson Jr, 2004] also reported mismatching between an A SHR and an E SHR when using DX A/C systems.

In hot and humid climates, such as Hong Kong, A/C is usually required for up to 7 months from April to October in a year [Lam, 1993]. At different time period within the 7 months, however, A SHR, or space latent load in an indoor space that directly affects indoor air humidity level can vary significantly.

A previous study [Li et al., 2006] suggested that in a bedroom in a residential flat in Hong Kong, the share of the latent part in the total space cooling load was at 53%, i.e., at an A SHR value of 0.47 (or 1-53%) in April, but only 28% in October and stayed

from 30% to 40% between April and October, as shown in Fig. 2.2. Therefore, in hot and humid climates in different seasons in a year, different cooling and dehumidification requirements in an air conditioned space can be encountered, as follows:

- In April to early May (Period I), at a low A SHR value, with a moderate outdoor air temperature usually lower than 25 °C but a higher moisture content, space air conditioning is dominated by dehumidification;
- From mid-May to mid-September (Period II), both outdoor air temperature and moisture content stay high, and therefore both air cooling and dehumidification are required;
- In mid-September to October (Period III), outdoor air temperature may still be high, but outdoor air is drier and space air conditioning dominated by air cooling, demanding less dehumidification.

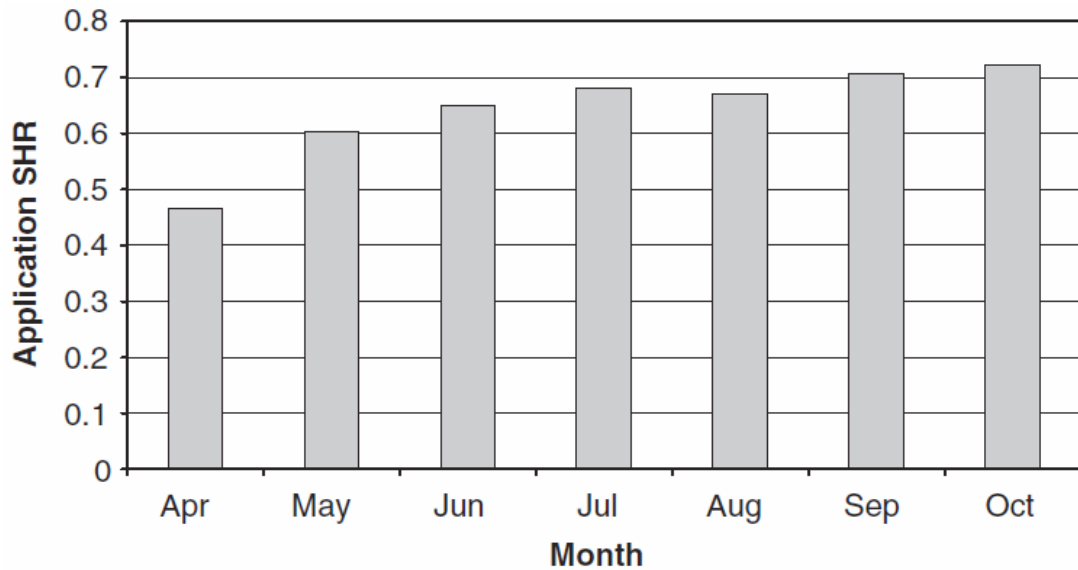


Fig. 2.2 Averaged monthly application SHRs between April and October in a master bedroom in Hong Kong [Li et al., 2006].

Therefore, when a conventional On-Off controlled DX A/C system is used at such a variable indoor latent load condition in the three different Periods, inadequate dehumidification is often encountered due to its poor moisture removal capacity, leading to a higher equilibrium indoor air humidity.

2.3.3 Existing control strategies for DX A/C systems

Most DX A/C systems are equipped with a single speed compressor and supply fan, relying on On-Off cycling of the compressor as a low cost approach to maintaining only indoor air temperature, whereas indoor air humidity is not controlled directly. Dehumidification is usually the by-product of a cooling process. When a preset air temperature is reached, compressor is stopped, and dehumidification is also stopped. Therefore, indoor air humidity may remain at a high level in the space served by an On-Off controlled DX A/C system. The situation may become worse when the supply fan in a DX A/C system runs continuously while its compressor is On-Off operated.

A portion of the moisture on the wet surface of a cooling coil and a drain pan may evaporate back into air stream during an Off-period, resulting in a high indoor humidity level [Amrane et al., 2003; Shirey III and Henderson Jr, 2004]. A further inadequacy of the above space temperature control method is when indoor sensible loads are low, the compressor does not run long enough to allow the condensed moisture actually to drip off the coil and into the drain [Harriman III, 2002].

However, if the operation of a DX A/C system is controlled based on indoor humidity level, indoor temperature may be too low and reheating to maintain indoor comfort conditions [Huh and Brandemuehl, 2008] may be required. Therefore, there is a cost penalty for overcooling the air and then reheating it.

2.4 Measures to deal with inadequate dehumidification at different load conditions

In Section 2.3, the reasons for inadequate dehumidification encountered when using DX A/C system are briefly summarized. Therefore, when a conventional On-Off controlled DX A/C system is operated during at three respective periods shown in Section 2.3.2, inadequate dehumidification may be encountered, resulting in different levels of indoor thermal environmental control. However, various measures can be taken in the three respective periods to achieve the desired indoor thermal environment, as follows:

2.4.1 Measures in Period I

During Period I, a conventional On-Off controlled DX AC system deals with a high indoor latent load and a relatively low sensible load, and space overcooling is therefore common, unless reheating is provided. However, reheating is obviously energy inefficient and is prohibited in many building energy codes. Furthermore, it is difficult to include a re-heater in certain DX AC systems such as a room air conditioner.

To address the problem of space overcooling, an additional standalone dehumidifier, either desiccant based or vapor compression based, may be employed. However, heat generated by a solid desiccant dehumidifier or rejected from the condenser of a vapor compression based dehumidifier can cause thermal discomfort for occupants [Alpuche et al., 2005]. On the other hand, a DX AC system may be modified , so that the heat rejected from its condenser which is usually air cooled, or the hot refrigerant gas discharged from its compressor may be used for reheating air [Alsenz, 2002; Fan et al., 2014; Fye et al., 2012; Knight et al., 2008; Trent, 2003], as shown in Fig. 2.3 and Fig. 2.4, respectively.

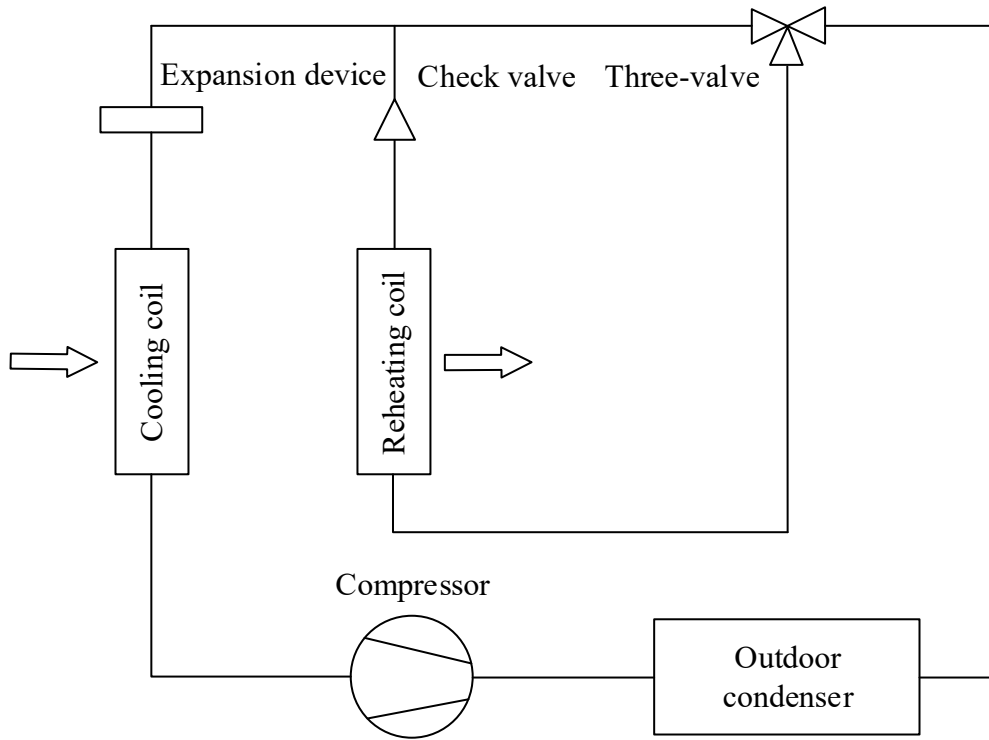


Fig. 2.3 Using the heat rejected from condenser for reheating air [Alsenz, 2002]

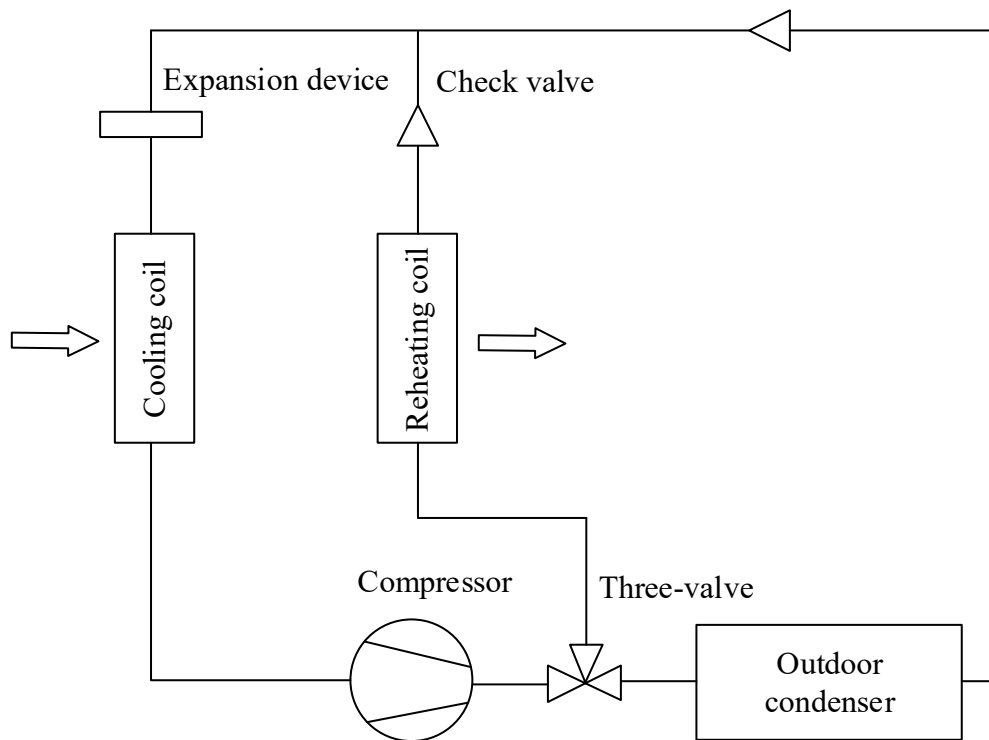


Fig. 2.4 Using the heat rejected from compressor for reheating air [Knight et al., 2008]

Recently, an isothermal dehumidifier [Han et al., 2013] was proposed, where its DX cooling coil was split into two parts, as shown in Fig. 2.5. The dehumidifier can be operated at a cooling and a dehumidification mode. At the cooling mode, both parts of the evaporator acted as a cooling coil by opening Valve 2 and Valve 3, and closing Valve 1 and Valve 4. However, at the dehumidification mode, one part acted as a cooling coil and the other a refrigerant sub-cooler to reheat the dehumidified air by closing Valve 2 and Valve 3, and opening Valve 1 and Valve 4, respectively. The common problems resulting from these modifications, however, included complicated refrigerant circuits and increased air flow resistance due to the addition of a re-heater which is redundant when not in use. In addition, these modifications only addressed the issue of space overcooling in this particular period of relatively short duration.

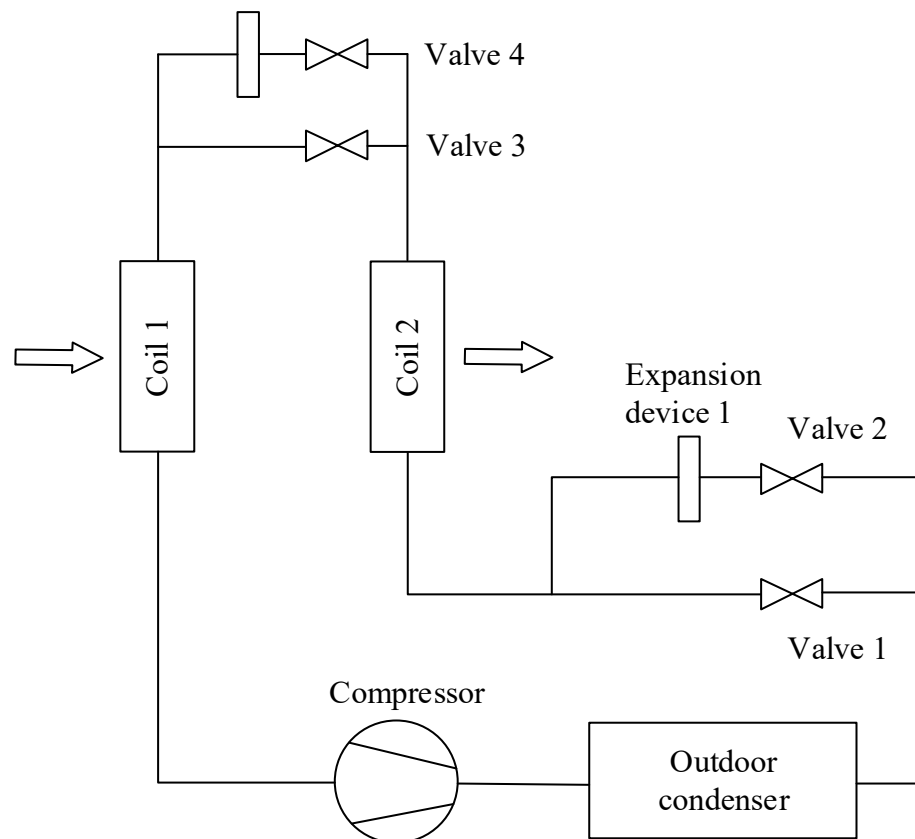


Fig. 2.5 Schematics of the novel isothermal dehumidifier [Han et al., 2013]

2.4.2 Measures in Period II

During this Period, the demands for both air cooling and dehumidification are high. To address inadequate dehumidification when using DX A/C systems in this Period, there can be two major measures for achieving better indoor humidity control, as follows:

2.4.2.1 DX based separated sensible and latent cooling (SSLC) technology

The first was DX based separate sensible and latent cooling (SSLC) technology to provide variable dehumidification ability. There are reported studies on the development of various SSLC technologies, which can be further divided into the following three types.

1) The first type was to use chilled ceilings / radiant panels assisted SSLC systems, where a DX A/C system was used to directly cool and dehumidify the air while a supplementary chilled ceiling or a radiant panel was employed to deal with the sensible load in a conditioned space [Ge et al., 2011; Li et al., 2018; Seo et al., 2014; Song et al., 2008]. The chilled water to the chilled ceiling / radiant panel was often produced by exchanging heat with the refrigerant [Han and Zhang, 2011] or using ground-source heat pumps [Villarino et al., 2017]. In these reported studies, these systems were proved to have a higher energy saving potential and can provide variable dehumidification ability. For example, a radiant panel assisted SSLC system as shown in Fig. 2.6 was experimentally studied by Han and Zhang [2011]. The experimental results showed that such a system could provide a variable dehumidification capacity ranging from 0 to 4.02 kg/h, and save about 15.6% of the cooling energy consumption against a traditional residential cooling-only air-conditioner. However, the use of supplementary radiant chilled ceilings / radiant panels would not only increase the

initial and maintenance costs but also have a high risk of condensation on panel / ceiling surface in hot and humid climates where the dew-point of indoor air was often high [Lee et al., 2012; Niu et al., 2002].

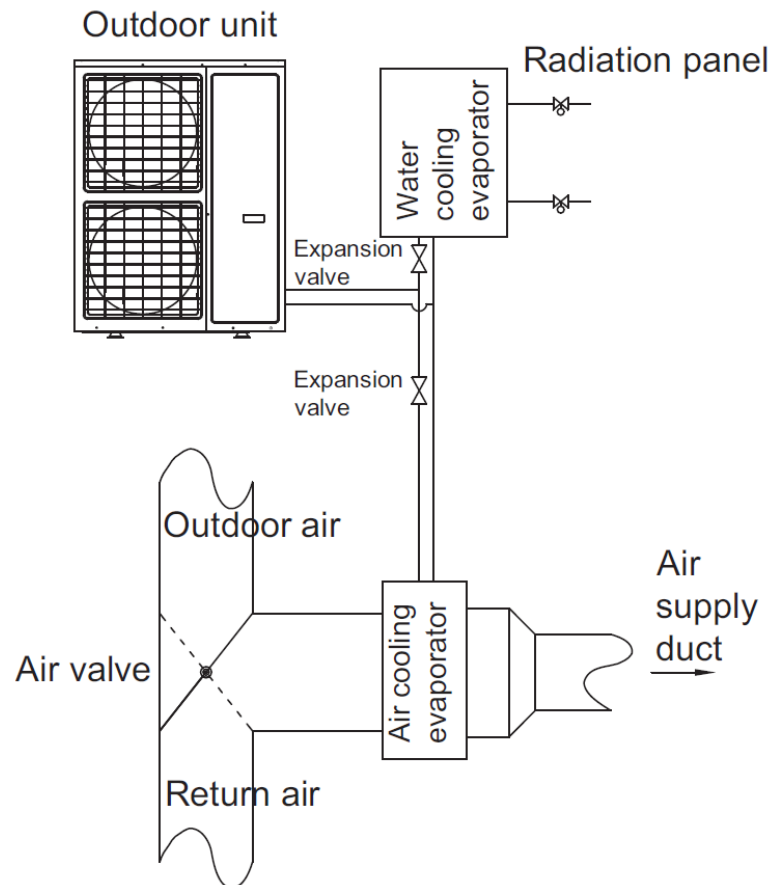
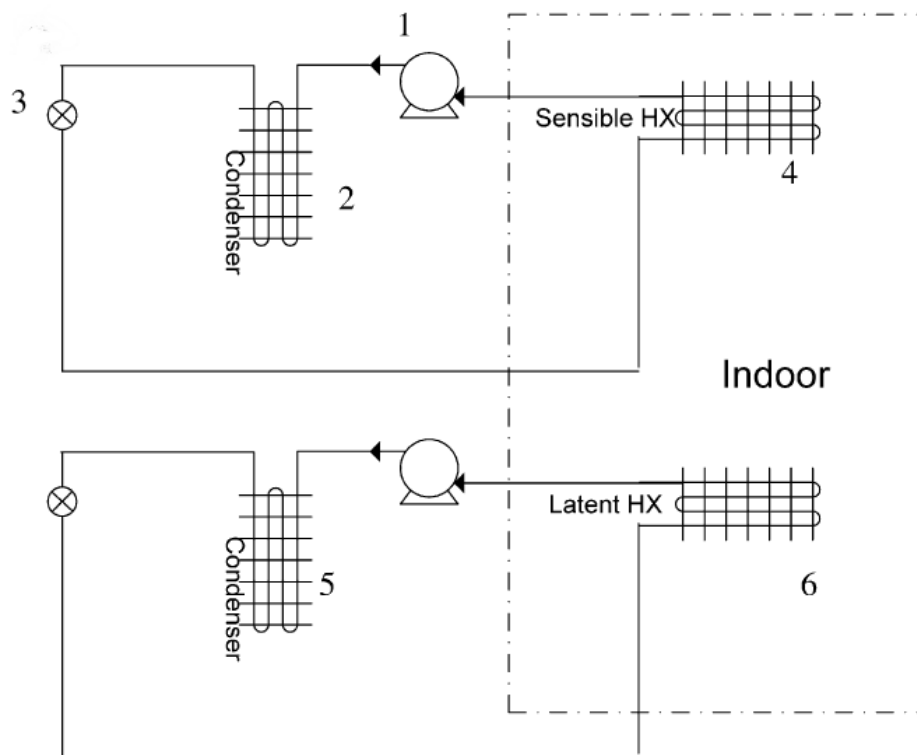


Fig. 2.6 The schematic diagram of a radiant panel assisted SSLC system [Han and Zhang, 2011]

2) The second type was to modify a traditional DX A/C system to provide variable dehumidification ability without using chilled ceilings / radiant panels. For example, Ling et al. [2010] theoretically studied the pertinent characteristics of a SSLC system using two parallel compression cycles, one for sensible cooling and the other latent cooling. Its schematic diagram is shown in Fig. 2.7. 30% energy savings were estimated for this SSLC system as compared to a conventional DX A/C system. However, the study was simulation based without any experimental validation. On the

other hand, Cao et al. [2017] experimentally validated that if two or more independent refrigerant subcycles with stepped pressures were used, the irreversible losses in the heat exchange processes could be reduced, thus providing high energy saving potentials. However, it was understandable that the use of two or more refrigeration cycles would inevitably lead to a complicated system configuration and a higher initial cost.



(a) Refrigerant side schematics

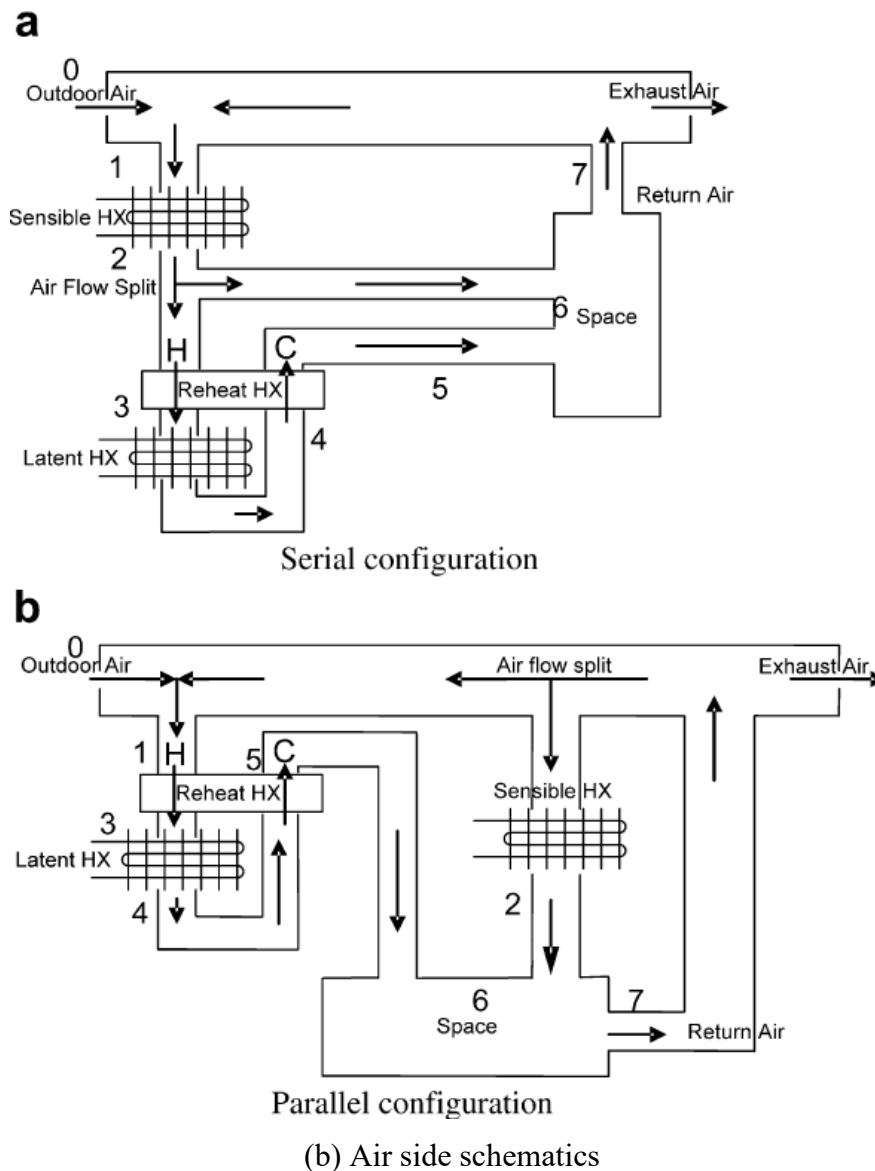


Fig. 2.7 Schematic diagram of the SSLC system using two parallel compression cycles [Ling et al., 2010]

3) The third type was to incorporate thermally activated solid / liquid desiccant units into a DX A/C system to provide variable dehumidification capacity. These measures were experimentally [Aynur et al., 2008b; Aynur et al., 2008c; Aynur et al., 2010a; Aynur et al., 2010b, c; Ge et al., 2010; Jiang et al., 2014a, b; Tu et al., 2017] or theoretically [Aynur et al., 2008d; Jiang et al., 2013] proved effective to provide sufficient variable dehumidification ability for achieving the desired indoor humidity level.

For example, Wang et al. [2013] studied an A/C system employing a solid desiccant wheel and found that the maximum difference between the actual indoor air relative humidity and its set point was 4.13%, suggesting an improved indoor thermal environment. However, such an improved humidity control was achieved with the help of a complicated model predictive control (MPC) strategy, inevitably increasing its development cost. Similarly, Subramanyam et al. [2004] found that incorporating a solid-based desiccant wheel into a DX A/C system could enhance the dehumidification of supply air, thereby increasing the scope for low humidity air-conditioning, but the COP of the A/C system was marginally lower by about 5% compared to that of a conventional A/C system without the desiccant wheel incorporated. The schematics of the experimental setup is shown in Fig. 2.8. However, the direct contact of air with desiccant material may cause health and corrosion problems, such as the entrainment of hazardous salts into a ventilation system [Keniar et al., 2015].

A further point to note was that employing desiccant to provide variable dehumidification ability required external heat sources for its regeneration which may come from either solar heat [Davanagere et al., 1999; Eicker et al., 2010; Fong et al., 2011; Ge et al., 2012] or the heat rejected from a condenser in a vapor compression refrigeration cycle [Dai et al., 2001; Ling et al., 2011, 2013; Zhao et al., 2011]. Keniar et al. [2015] studied a solar-regenerated liquid desiccant membrane system and found that it could result in a 10% decrease in indoor relative humidity. However, the payback period of the system was about 7 years, which was long due to the high initial cost of solar panels. Tu et al. [2017] proposed and experimentally studied a DX based A/C system with desiccant coatings on its heat exchangers as shown in Fig. 2.9. Such a system could independently and simultaneously handle sensible and latent loads at

the same time. However, the control of the thickness of the desiccant-coated layer was very critical, thus increasing the development cost of the system. Therefore, as seen, these desiccant assisted SSLC A/C systems were inevitably complicated, with higher initial and operational / maintenance costs, thus usually suitable for large-scaled applications.

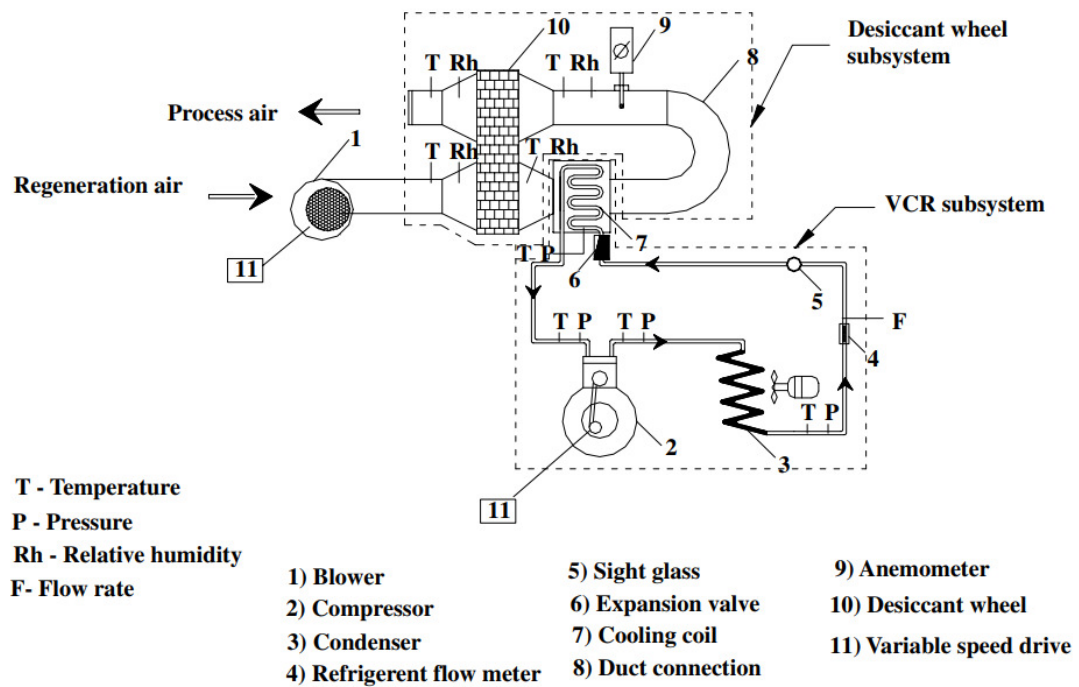


Fig. 2.8 Schematics of an experimental setup for a desiccant assisted SSLC A/C system [Subramanyam et al., 2004]

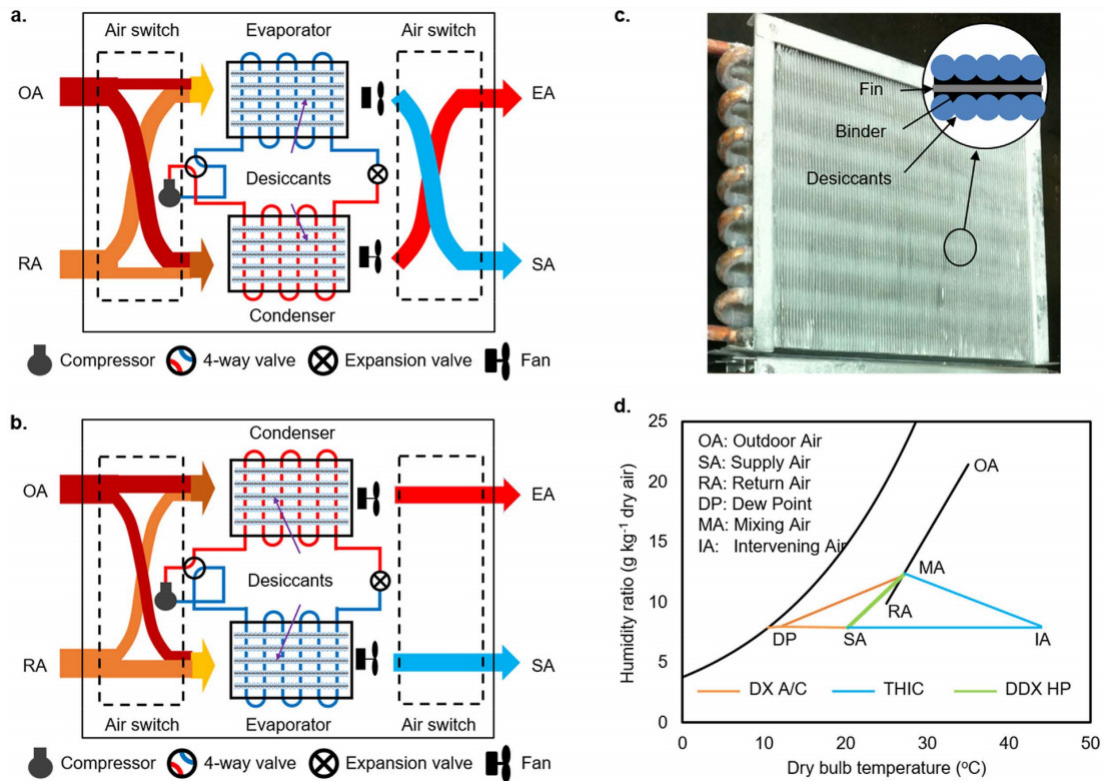
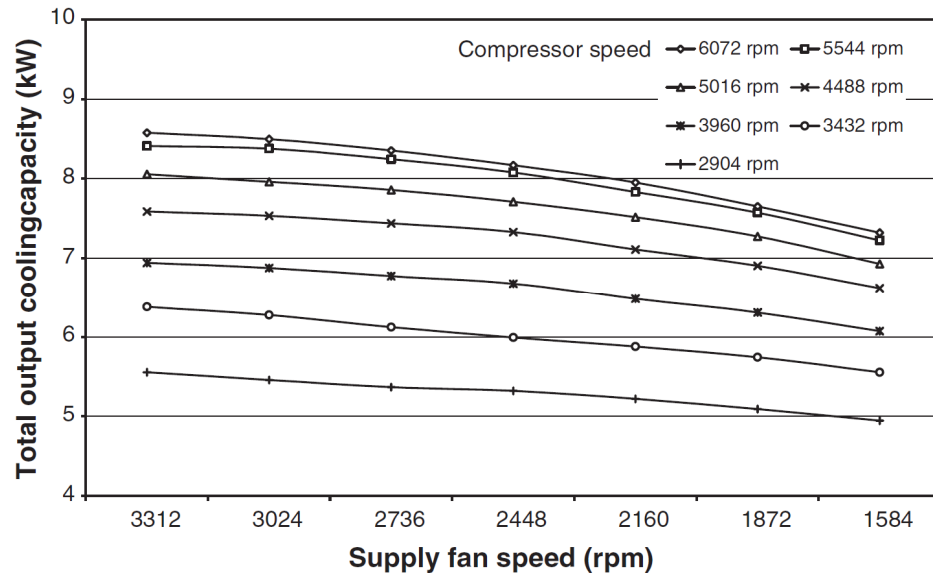


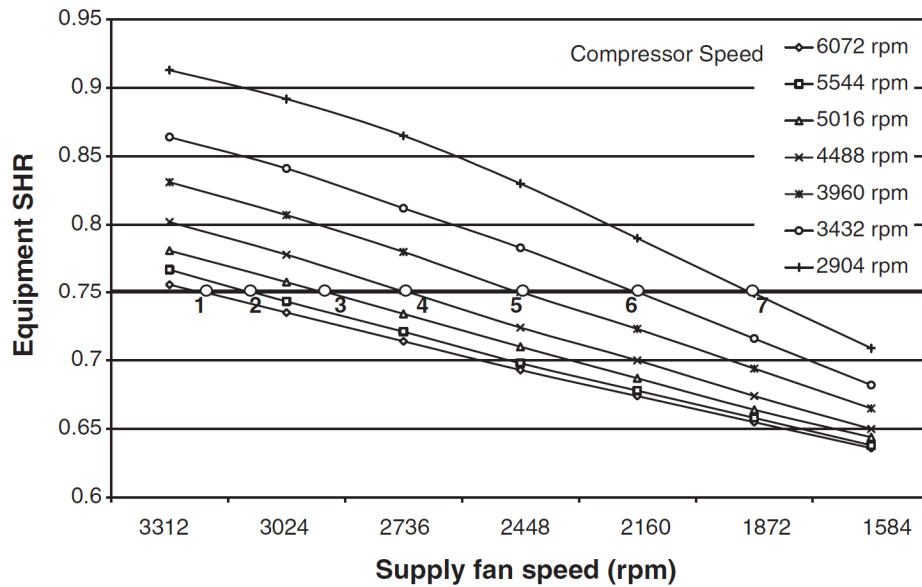
Fig. 2.9 Schematics of the structure and operational modes of a novel concept for a desiccant-enhanced DX A/C system [Tu et al., 2017]

2.4.2.2 Variable speed (VS) technology

The other major measure was to simultaneously vary the compressor and supply fan speeds in a DX A/C system so as to obtain different system output total cooling capacity (TCC) and sensible heat ratio (E SHR) to deal with different space sensible and latent loads [Krakow et al., 1995]. The introduction of variable-frequency inverts has made it more achievable for varying the compressor and supply fan speeds. Over the years, in order to achieve simultaneous control over indoor air temperature and humidity using a DX A/C system, there have been extensive detailed studies on the operational characteristics of a DX A/C system under variable speed (VS) operation [Li and Deng, 2007b; Li et al., 2014; Xia et al., 2017; Xu et al., 2010].



(a)



(b)

Fig. 2.10 The variations in TCC and E SHR at different combinations of compressor and supply fan speeds [Li and Deng, 2007b]

The operational characteristics of an experimental DX A/C system under VS operation were firstly studied by Li and Deng [2007b]. The obtained experimental results of the variations in TCC and E SHR at different combinations of compressor and supply fan speeds are shown in Fig. 2.10. As seen, the changes in output TCC from the DX A/C system were predominately affected by changing compressor speed, although at a

given compressor speed, reducing supply fan speed would also reduce, but less significantly, the output TCC. On the other hand, at a higher compressor speed, further increasing compressor speed would not significantly increase the output TCC, as compared to the increases at lower compressor speeds. In addition, at a given compressor speed, although there were not significant changes in the output TCC with varying supply fan speed, there were significant changes in the sensible to the latent components of the output TCC, with a lower supply fan speed or smaller airflow rate leading to a larger latent heat removal, thus a lower E SHR.

Therefore, Xu et al. [2010] presented inherent correlations (ICs) between the output TCC and E SHR at different speed combinations of compressor and supply fan of the experimental system using a TCC - E SHR diagram as shown in Fig. 2.12. As seen from the diagram, for a VS DX A/C system, its output TCC and output E SHR under VS operation were strongly coupled but mutually constrained within a trapezoid. It was impossible for the experimental VS DX A/C system to output those E SHR / TCC combinations represented by those points outside the trapezoids when varying its compressor speed from the lowest of 2904 rpm to the highest of 6072 rpm and its supply fan speed from the lowest of 1584 rpm to the highest 3312 rpm.

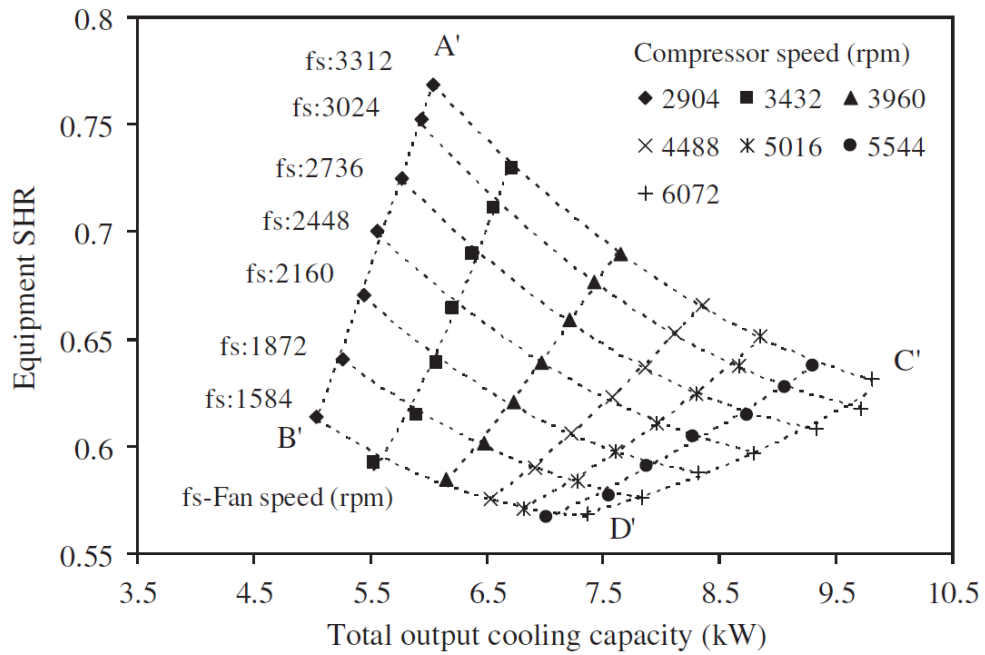


Fig. 2.11 The inherent correlation between TCC and E SHR at different speed combinations of compressor and supply fan for a VS DX A/C system [Xu et al., 2010]

In 2014, Li et al. [2014] further studied the inherent operational characteristics of the same experimental VS DX A/C system used by Li and Deng [2007b] and Xu et al. [2010], but at different inlet air states. The experimental results shown in Figs. 2.12 and 2.13 demonstrated that both inlet air temperature and RH level would significantly influence the operational characteristics of the experimental DX A/C system. At a constant inlet RH, varying inlet air temperature would cause the position shifting of a TCC - E SHR trapezoid, but its shapes remained unchanged. On the other hand, varying inlet RH level would however result in both position shifting and the changes in trapezoid shapes.

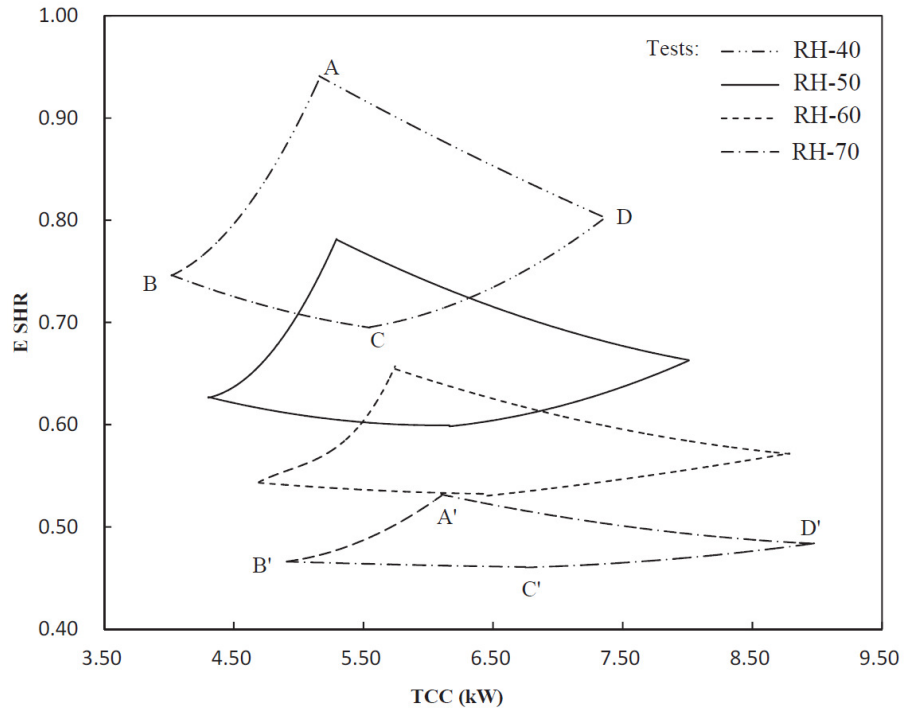


Fig. 2.12 Inherent correlations between output TCC and equipment SHR of the experimental VS DX A/C system at constant temperature group [Li et al., 2014]

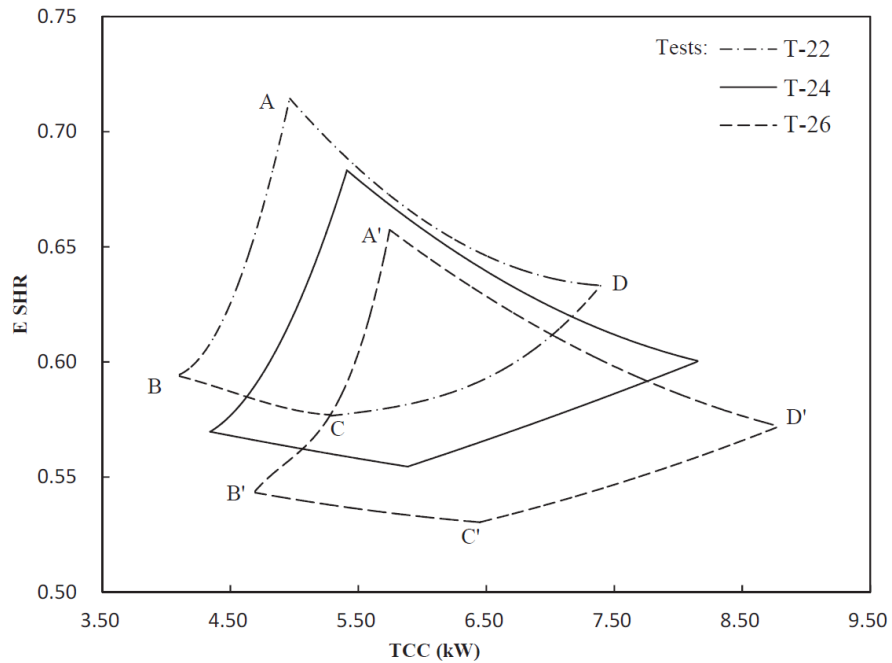


Fig. 2.13 Inherent correlations between output TCC and Equipment SHR of the experimental VS DX A/C system at constant RH group [Li et al., 2014]

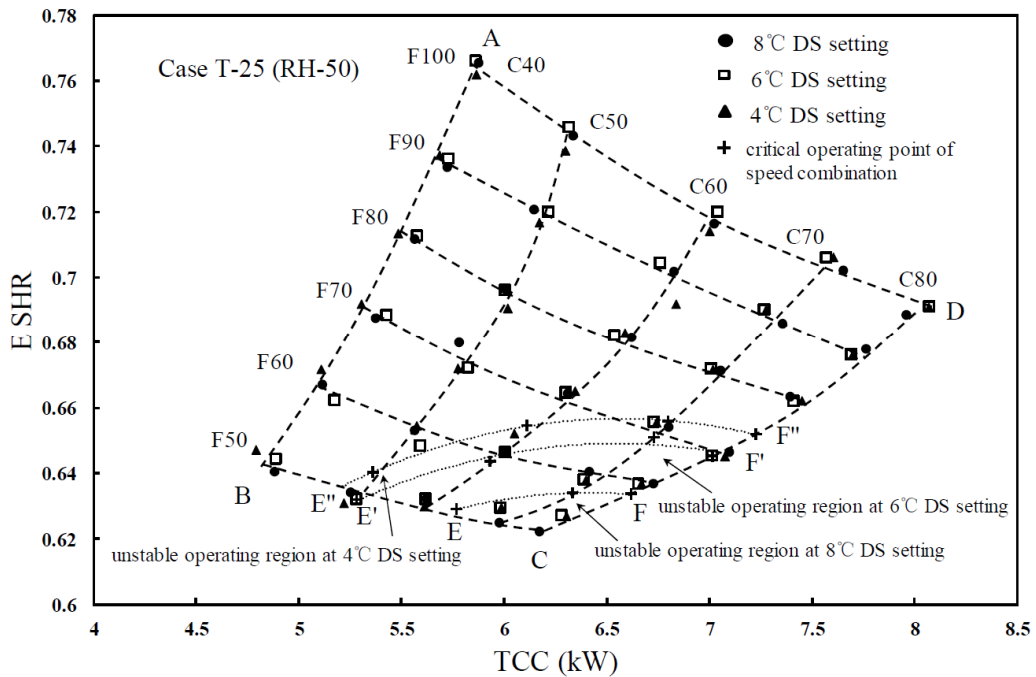


Fig. 2.14 The inherent correlation of the experimental VS DX A/C system at three different DS settings [Xia et al., 2017]

Lastly, Xia et al. [2017] experimentally studied the inherent correlations between its TCC and E SHR of an experimental DX A/C system using R410A as working fluid at different combinations of compressor speed and supply fan speed, and identified the unstable operating points of speed combinations under different degree of refrigerant superheat (DS) settings and inlet air states. The experimental results at an inlet air state of 25 °C and 50% RH are shown in Fig. 2.12. As seen, different DS settings may not significantly influence the inherent correlations between TCC and E SHR, but did impact the operational stability. A lower DS setting would result in a larger unstable operating region in a TCC - E SHR trapezoid. In addition, it was also shown that the operational conditions of the DX A/C system including VS operation and inlet air states also significantly impacted the system operational stability. A higher compressor speed or a lower supply fan speed, and a lower inlet air temperature or RH

would result in a higher possibility for the experimental VS DX A/C system to be unstably operated.

These studies [Li and Deng, 2007b; Li et al., 2014; Xia et al., 2017; Xu et al., 2010] have provided detailed insights into the operational characteristics of DX A/C system, as well as the constraints of applying these characteristics to developing appropriate control strategies, so as to better design, operate and control DX A/C systems for improved indoor humidity and thus thermal environmental control. Generally, it was observed that when a VS DX A/C system was operated at a high compressor speed but a low fan speed, a lower evaporating temperature and thus better dehumidification can be achieved, at however the expenses of both a lower system efficiency and a higher risk of unstable operation.

Based on the obtained operational characteristics of VS DX A/C systems, a number of novel controllers, either model based [Li et al., 2012, 2013; Li and Deng, 2007a; Muñoz et al., 2017; Qi and Deng, 2009] or black-box based [Li et al., 2015a, b; Xu and Deng, 2012; Yan et al., 2018] have been developed. For example, based on the obtained ICs between TCC and E SHR at different inlet air states, an artificial neural network (ANN) model for an experimental VS DX A/C system was trained and tested to predict the compressor and supply fan speeds when the experimental VS DX A/C system was operated at different combinations of sensible and latent cooling loads. Consequently, a novel neural network aided fuzzy logic controller was successfully implemented in the experimental VS DX A/C system for simultaneously controlling indoor air temperature and humidity [Li et al., 2015a]. Furthermore, according to the previous study by Xia et al. [2017], Xia et al. [2018] developed a new capacity controller that can not only simultaneously control indoor air temperature and

humidity, but also select an optimized DS setting to properly balance the operational safety and efficiency. The controllability test results showed that the new capacity controller could be applied to DX A/C systems for indoor thermal control with a higher operational safety and energy efficiency. Recently, Yan et al. [2018] developed a fuzzy logic controller, which for the first time, directly use the inherent operational characteristics of a VS DX A/C system. The experimental results demonstrated that such an inherent operational characteristics aided fuzzy logic controller can achieve the simultaneous control over indoor air temperature and humidity, with a reasonable control accuracy and sensitivity.

As seen, VS technology could also be a useful measure to enable DX A/C systems to provide variable dehumidification ability. However, with the use of VS technology, there were two associated concerns. Firstly, the corresponding control logics and hardware were both complicated and costly, often requiring a complicated mathematical model to support their developments such as artificial neural network (ANN) and fuzzy logic. Secondly, in many cases, adequate air circulation was required for better IAQ in a conditioned space. Running a supply fan at a low speed would however deteriorate indoor air-distribution performances [Xu et al., 2010], and can be counterproductive to better IAQ.

2.4.3 Measures in Period III

During this Period, the moisture content of outdoor air is generally low, so that the space latent load is relatively small and air conditioning is dominated by sensible cooling. Operating a conventional On-Off controlled DX A/C system will in general be sufficient to meet the requirements of both indoor sensible and latent loads removal. While indoor air temperature may be suitably controlled close to its setting, indoor air

RH, although not directly controlled, may also be expected to stay within a comfort range of 40-60%.

2.5 Modeling of DX A/C systems

More and more research attention has been paid on studying A/C systems using modeling approach because of its cost effectiveness compared to using experimental approach [Choi and Kim, 2003]. Mathematical modeling has been hence extensively used to investigate the operational performance of an A/C system, to exam the controllability of a control strategy, to verify the optimization design of a configuration and to detect and diagnose system faults, etc. [Qi, 2009].

A large number of published studies in open literature are available on modeling both steady-state and dynamic behaviors of A/C systems. The models available can be classified into two types: physical and empirical. A physical model, which can reflect the physical insight of a real system, is built based on physical principles and expressed using mathematical equations. However, an empirical model can be established using different methods such as regression analysis, polynomial curve fit, artificial neural networks (ANN) and system identification, with possibly high adaptability. There exist however some unsolvable problems in an empirical modeling method because of the imperfection of the method itself and the limitation of a model developer's understandings [Diaz et al., 1999; Ding, 2007; Pacheco-Vega et al., 2001; Singh et al., 2006].

Graph Theory, which has been used in many subject areas, such as electric circuit network and fluid network, is a modeling approach different from either a physical or

an empirical modeling approach. It converts a specific problem into a graph of nodes and verges. A refrigeration cycle can be usually depicted on a p-h diagram. When applying Graph Theory modeling approach to A/C or refrigeration systems, the refrigerant flow direction must be added in order to truly reflect the refrigeration cycle, and a complete refrigeration cycle will become a directed graph composed of multiple nodes [Ding, 2007; Liu et al., 2004]. Comparing with other modeling approach, Graph Theory modeling is flexible in describing complicated refrigerant circuit arrangement [Liu et al., 2004].

To develop a high quality model for an engineering system, the requirements for modeling at least include: (1) accuracy, (2) rapidness and (3) stability. These three requirements may conflict with one another, and then a compromise has to be made [Ding, 2007]. Generally, to achieve a high modeling accuracy for key system components, such as a heat exchanger, distributed-parameter modeling approach may be used, which can reflect well the distributed nature of the operational parameters in such a component [Chen, 2005; Qi, 2009]. However, because of distributed nature, using such a modeling approach is time-consuming with potential poor calculation stability. On the other hand, for the purpose of testing control strategies and studying dynamic response of a complete engineering system, a full understanding of the details of certain system components may not be necessary. Therefore, lumped-parameter modeling approach may be used. Although it is relative simple and difficult to reflect the detailed distribution of parameters along the dimension of a system component, it is more useful in studying the overall performance of a system, and consequently usually more effective in carrying out research work related to system control [Ding, 2007]. A partial-lumped parameter modeling approach is a compromise between the distributed- and lumped-parameter modeling approaches [Deng, 2000; Domanski,

1991]. With this approach, a system component, e.g., evaporator or condenser, is divided into several zones but lumped parameter modeling is adopted in each zone. For a condenser, usually three zones, i.e., a superheated zone, a two-phase zone and a sub-cooling zone, are assumed. For an evaporator, two zones, i.e., a two-phase zone and a superheated zone, are usually designated. Both the accuracy and the computational speed for a partial-lumped parameter modeling approach are between those of the distributed- and lumped-parameter modeling approaches. There can be some difference in the prediction accuracy between using a partial-lumped parameter modeling approach and using a distributed-parameter modeling approach, but the computational speed when using a partial lumped parameter modeling approach is obviously faster than that when using a distributed-parameter modeling approach, so a partial-lumped parameter modeling approach is suitable for system modeling when the accuracy requirement is not too high [Qi, 2009].

A DX A/C system usually consists of a DX refrigeration plant and an air-distribution sub-system. There have been previously reported studies on developing separate mathematical models for the two constituent parts [Chen, 2005; Chen et al., 2005; Xu et al., 1996]. The previous extensive modeling studies for single-, dual- and multi-evaporator DX A/C systems [Elliott and Rasmussen, 2008, 2013; Shah et al., 2004; Tuo et al., 2012; Yan et al., 2016; Yan et al., 2012] showed that using mathematical models was feasible to predict the performances of DX based A/C systems with reasonable accuracy. In this section, modeling studies for the refrigerant-side and the air-side of DX A/C systems are separately reviewed.

2.5.1 Sub-models for the refrigerant-side of a DX A/C system

The refrigerant-side of a DX based A/C system, a multi-evaporator A/C system is operated based on vapor compression refrigeration cycle, and consists of four key cycle components, i.e., a compressor, one or more evaporators in case of an multi-evaporator A/C system, the same number of expansion valves as that of evaporators and finally a condenser. Hence, the modeling for the refrigerant-side of a DX A/C system is usually modular-based. By linking the modules for the key cycle components and the connecting piping, a sub-model for the refrigeration-side of a DX A/C system may therefore be derived, and expressed by a set of ordinary differential equations and algebraic correlations. Hence, the modeling for the key components in the refrigerant-side of a DX A/C system is separately reviewed as follows.

2.5.1.1 Compressor modeling

The modeling of compressor plays an important role in the simulation of A/C and refrigeration systems. Typically, a compressor module calculates the refrigerant mass flow being circulated in a vapor compression cycle. Compressor speed is taken into consideration in modeling a variable-compressor [Deng, 2000]. Compressor modules have been reviewed and categorized. Compared to heat exchangers, the dynamics of a compressor may be negligible so that quasi-steady modeling is usually adopted [Rasmussen and Alleyne, 2004]. This is achieved by assuming that a compressor reaches its specified operating speed instantly. A compressor may also be represented dynamically, where the changes in compression chamber volume and refrigerant properties are described as continuous functions of time. A parametric analytical module for a centrifugal compressor was developed to predict the compressor performance from geometric information [Jiang et al., 2006]. Generally, a polytropic

compression process is assumed and a mathematical module for a compressor can be established by using the traditional thermodynamic approach. It assumes that a polytropic compression could represent all the processes from suction to discharge in a compressor.

On the other hand, a compressor may also be represented by an empirical correlation using the actual performance data with the aid of curve fitting or regression analysis. This approach can achieve a better approximation but a set of detailed tested compressor performance data from manufacturers or in-situ test is required. Li [2013b] proposed a semi-empirical compressor module, which was suitable for both single speed compressor and variable speed compressor. The method required an integration of physical based modeling and experimental data.

2.5.1.2 Heat exchanger modeling

Heat exchanger modeling has always been in the spotlight of simulation-based research work for DX A/C systems. Extensive investigations on heat exchangers modeling have been carried out using lumped-parameter modeling approach [Chi and Didion, 1982; Vargas and Parise, 1995], distributed-parameter modeling approach [Jia et al., 1995; Wang and Touber, 1991; Zhang and Zhang, 2006] and partial-lumped parameter modeling approach [Deng, 2000; Domanski, 1991], where an evaporator was divided into two zones, i.e., two-phase, and superheated zone and a condenser three zones, i.e., two-phase, superheated and sub-cooling zone. Graph Theory modeling approach can also be used to describe detailed structures of an evaporator. A practical way was to number each tube and refrigerant flow direction within a single tube first, so that a directed graph was created, then an adjacent matrix was built [Liu et al., 2004], With the help of the concepts of directed graph and graph-based search

algorithms in Graph Theory, Liu et al. [2004] developed a general steady-state distributed-parameter model for a fin-and-tube heat exchanger. This model made it possible to analyze the operational performance of an evaporator with complex refrigerant circuits.

2.5.1.3 EEV modeling

An expansion device in a refrigeration system controls the refrigerant mass flow and balances the system pressure. Commonly, an expansion valve can be represented by a steady-state model due to its small thermal inertia. Refrigerant expansion is generally treated as an isenthalpic process so that an expansion valve can be modeled by using an isenthalpic orifice equation [MacArthur and Grald, 1987]. One representative model for EEVs was developed by Damasceno et al. [1990], based on the specifications given by EEVs' manufacturers and the empirical fittings for one set of distributor nozzle and tube size. Although the throttling mechanism in an EEV is identical to that of a short orifice valve, the flow coefficient is much more complex for an EEV than an orifice because the opening area of the EEV is dynamically adjusted. The characteristics of EEVs are usually obtained experimentally for different refrigerant fluids. Park et al. [2007] developed an empirical correlation for predicting the mass flow rate passing through an EEV by modifying a single-phase orifice equation with consideration of EEV's geometries parameters and operating conditions. Li [2013a] modified the Bernoulli equation for a short orifice to develop a mass flow coefficient correlation for an EEV by introducing an expansion factor. Only two key parameters (EEV opening and the degree of subcooling) were used to develop the coefficient correlation. Experimental analysis showed that the mass flow coefficient

correlation could well describe the refrigerant flow behavior through the EEV with negligible errors.

2.5.1.4 Refrigerant pipework modeling

Fluid resistance in the connecting pipes in a single evaporator air conditioning (SEAC) system was usually ignored in previous studies. However, in a dual-evaporator A/C (DEAC) or multi-evaporator A/C (MEAC) system, since the connecting pipework is actually more complex, the fluid resistance cannot be simply ignored. Pan et al. [2012] reported a numerical study of the effects of refrigerant pipeline length differences on the operational performance of a DEAC system. Similar to that by Lu et al. [2009], refrigerant pipelines were divided into single-phase and two-phase types according to the refrigerant state and the two type were separately analyzed using fluid network theory. The famous Darcy-Weisbach Equation was applied to calculating pressure losses. For a two-phase pipeline, pressure drops were evaluated not only based on friction losses similar to that in single-phase pipelines, but also the kinetic energy change caused by refrigerant phase change. Other refrigerant pipeline models assumed that the liquid line and suction line were adiabatic, while the significant heat loss between the hot gas line and surroundings was modeled using the effectiveness-NTU method [Cheung and Braun, 2014].

2.5.2 Sub-models for the air-side of a DX A/C system

On the air-side of a DX A/C system, the major components are usually a supply air fan, air control dampers, air duct and the air side of a DX evaporator, and their models are reviewed as follows:

2.5.2.1 Fan modeling

Supply fans move air by forced convection through conditioned spaces in order to control indoor air temperature, humidity, air speed and air distribution. In HVAC systems, the pressure-volume flow characteristics of a fan can be presented in many different ways. In general, they are described by a set of constant-speed curves for pressure rise versus volume flow rate. As to a variable speed air blower, its characteristics at different speeds are obtained through using the performance data from manufacturers or the fan performance law (fan pressure rises being proportional to the square of the change in fan speed). In order to get a better approximation with the experimental performance data, Mei and Levermore [2002] used a ten-neuron sigmoid artificial neural network (ANN) model to represent the characteristics of a variable speed fan.

2.5.2.2 Air control damper modeling

For the air control dampers in a DX A/C systems, a large percentage of existing models simply treated an air damper as a variable flow resistance, with its pressure loss coefficient being a function of the inclination angle of damper blades. Such simplifications were believed to have little effect on the investigation of energy use performance of a DX A/C system [Lebrun, 1995]. On the other hand, Legg [1986] established a series of experimentally validated mathematical expressions for different types of dampers.

2.5.2.3 Modeling an air handling process on the air side of a DX evaporator

For a refrigerant-to-air heat exchanger using various inside micro-fin tube for heat transfer enhancement, its air-side heat transfer resistance may account for over 80% of the total heat transfer resistance. Hence, the correlations of air-side heat transfer coefficients would significantly affect the modeling accuracy for the overall heat transfer. A set of relatively simple correlations for an average heat transfer coefficient for different heat exchangers, such as plate-finned tube, flat fins or wavy and louvered fins, have been developed [Corberán and Melon, 1998; Gray and Webb, 1986; Turaga et al., 1988; Webb, 1990]. Currently, the most commonly enhanced heat transfer surface used in DX A/C systems is of louvered fin type that can provide a higher average heat transfer coefficient. Wang et al. [1999 and 2000] proposed general heat transfer correlations for louvered fin geometry having round tube configuration under dry and wet conditions, respectively. A total of 49 samples of louvered fin-and-tube heat exchangers with different geometric parameters, including louver pitch, louver height, longitudinal tube pitch, transverse tube pitch, tube diameter, and fin pitch were included in the correlations developed.

2.5.2.4 Air pressure drop across the air side of a DX evaporator

For a DX A/C system, when it is operated in hot and humid climates, the air-flow may interact with the water vapour condensated on the surface of its DX evaporator. This makes the flow pattern very complicated. As a result, significant changes in the heat transfer and friction characteristics are likely to occur under dehumidifying conditions. The friction characteristics of louvered fin-and-tube heat exchangers in dry-cooling and wet-cooling conditions have been studied by Wang et al. [1999 and 2000] and the

friction correlations recommended could be used to evaluate the air pressure drops across the air side of a DX evaporator under both dry cooling and wet cooling conditions.

2.5.2.5 Air duct modeling

Modeling of the air ductwork in an A/C system should also be given adequate attention because not only it plays a significant role in the energy balance of the system, but also the transport behavior of the working fluid inside the ductwork influences system's operating characteristics. A lumped-parameter model for air ductwork should be the first choice to be integrated into the complete model for an A/C system. Jakob et al. [1987] divided the whole air ductwork into a number of segments and assumed the air distribution to be linear and the duct wall temperature to be uniform along each duct segment. The duct wall temperature varied however from segment to segment.

2.5.3 Solving DX A/C system models

For solving a component-based model for a DX A/C system, there are two main methods: (1) simultaneous solving method and (2) sequential solving method.

For the first method, all the model equations, often of non-linear nature, and initial and boundary conditions, are solved simultaneously using the Euler Method or the Newton-Raphson Method, or the Runge-Kutta Method. Commercial software packages have been developed to help solve these non-linear equations [Klein and Alvarado, 2002; Masy, 2006]. Very often it can be difficult to find out the cause if divergence occurs during solving model equations, and thus calculation stability is not

easily ensured. On the other hand, when applying this method to a developed system model whose structure is normally fixed, additional component sub-model cannot be easily inserted into the system model, and thus the flexibility of system simulation might be compromised [Ding, 2007; Winkler et al., 2008]. Therefore, as far as A DX A/C system simulation is concerned, this solving method has not been popular.

The second method can be more conveniently used since the component models are established first and treated as “black-box” objects. Only the knowledge of how the component sub-models are connected is required when using this method to solve a complete model. A set of initial values for model inputs are assumed. If the convergence criterion is not satisfied, the assumed initial values would be updated and then the iteration has to be repeated. Winkler et al. [2008] studied the influence of setting initial values for the inputs to an A/C system model on computational speed. Component sub-models were run several times prior to solving the system model and it was shown that better initial values can help reduce the required computational time. The sequential solving method has clear physical meaning in solving a system model and is easy to debug to ensure the calculation stability [Ding, 2007].

2.6 Conclusions

A number of previous studies showed that increased interests in maintaining a proper indoor humidity level is highly necessary to achieve good occupants’ comfort, acceptable indoor air quality, and to minimizing energy use. In hot and humid climates, DX A/C systems are widely used for indoor thermal environmental control in all climates due to a number of advantages. However, it is often difficult and challenging for a conventional DX A/C system to provide desired humidity control in hot and

humid climates, and inadequate dehumidification could hence be found in various buildings. Three reasons for inadequate dehumidification have been identified as the current system design trends for DX A/C systems to have a small moisture removal capacity to boost their EERs, highly variable space load conditions throughout a year and commonly used On-Off control strategies for single speed DX A/C systems.

Tremendous efforts have been taken to address inadequate dehumidification in different buildings when using DX A/C systems through employing supplementary measures to provide variable dehumidification ability to deal with variable space sensible and latent loads. SSLC using desiccants or variable speed operation for DX A/C systems were the two measures to provide dehumidification capacity. Although these measures proved effective in addressing inadequate latent cooling capacity provided by a conventional On-Off DX A/C system for better indoor humidity control, there existed a number of associated problems such as complicated system configurations, higher initial and operational costs and complicated development processes often requiring mathematical modeling support. On the other hand, there have been extensive studies on the modeling of DX A/C systems. The available DX A/C system models can be used to assist the developments of both novel DX based systems for improved indoor thermal environment control and new controllers for better control accuracy and energy efficiency of DX A/C system.

The literature review presented in this Section has identified that a DX based standalone enhanced dehumidification air conditioning (EDAC) system for improved year-round indoor humidity level in buildings in hot and humid climates, without the need to employing supplementary measures such as SSLC or VS technologies, to

provide variable dehumidification capacity, should be developed. This is expected to be the main target of the research project presented in this Thesis.

Chapter 3

Proposition

3.1 Background

The literature review presented in Chapter 2 has identified a number of the causes for inadequate dehumidification in buildings in hot and humid climates when using DX A/C systems. It can be seen that so far there has been not a DX based standalone A/C system that can be satisfactorily operated in the three Periods mentioned in Section 2.3.2 to adequately deal with indoor sensible and latent loads at all times, without employing supplementary measures such as variable speed operation and the use of desiccants, which may only be good at a particular Period but redundant at others.

Therefore, to reduce the complexity and the initial and operational costs for DX based air conditioning installations while still being able to maintain indoor air temperature and relative humidity (RH) within the comfort range for all the three Periods in hot and humid climates such as Hong Kong, it becomes highly necessary to develop a DX based standalone enhanced dehumidification air conditioning (EDAC) system having two evaporators, for improved year-round indoor humidity level in hot and humid climates, without the need of employing supplementary measures to provide variable dehumidification ability.

3.2 Project title

This Thesis focuses on the following major issues related to the development of an EDAC system:

- 1) proposing a novel DX based EDAC system without any supplementary measures to supply variable dehumidification capacity;
- 2) setting up an prototype experimental EDAC system to experimentally study its operational performances in terms of year-round thermal environmental control and energy efficiency;
- 3) building up and experimentally validating a complete steady-state mathematical model for the experimental EDAC system.

The research project is therefore entitled “ Development of a novel direct expansion based standalone enhanced dehumidification air conditioning system for improved year-round indoor humidity control ”.

3.3 Aims and objectives

The project has the following objectives:

- 1) To develop a novel standalone EDAC system that can be used in different seasons for improved year round indoor humidity control in hot and humid climates, without requiring supplementary measures to provide variable dehumidification ability;
- 2) To build an experimental prototype of the EDAC system to experimentally evaluate its operational performance in terms of indoor air temperature and humidity control and operational energy efficiency, at different seasonal cooling load conditions;

- 3) To develop a steady-state mathematical model of the EDAC system and to experimentally validate the model using the data from the experimental prototype, and to further optimize the configuration and design of the EDAC system using the validated mathematical model;
- 4) To develop a control strategy for the EDAC system so that it can be operated year-round for improved indoor humidity control.

3.4 Research methodologies

Both experimental and mathematical modeling approaches will be employed in this research project. Firstly, a prototype experimental EDAC system will be set up in a laboratory with two environmental chambers, one indoor chamber and the other outdoor chamber, where the required experimental indoor and outdoor air conditions could be created and maintained, respectively, by an existing air conditioning system and load generation units (LGUs). The experimental EDAC system will be fully instrumented and all of its operating parameters can be real-time measured and recorded.

Secondly, with the availability of the prototype experimental EDAC system, extensive experimental work to obtain the operational characteristics of the EDAC system when both evaporators in the EDAC system are operated will be carried out.

Thirdly, a steady-state physical-based mathematical model for the prototype EDAC system will be developed, taking reference to a previously developed model for a dual-evaporator A/C (DEAC) system. The model will be physical based and made of sub-

models for both its refrigeration-side and air-side. The developed EDAC model will be experimentally validated using the experimental EDAC system.

Finally, a year-round control strategy will be developed to enable the EDAC system to be operated over a wide range of operating conditions so as to maintain an improved indoor humidity level all year round. Controllability tests for the control strategy will be carried out to verify if the EDAC system is operational in different seasons to adequately deal with indoor sensible and latent loads, and to evaluate the operating performances of the developed control strategy.

Chapter 4

The prototype experimental EDAC system

4.1 Introduction

A novel standalone enhanced dehumidification A/C (EDAC) system was proposed based on multi-evaporator air conditioning technology. A prototype experimental EDAC system has been purposely set up to facilitate carrying out the research work proposed in Chapter 3, including experimentally evaluating the operational characteristics of an EDAC system, validating the developed EDAC model, and finally testing the operating performances of the developed control strategy for the EDAC system.

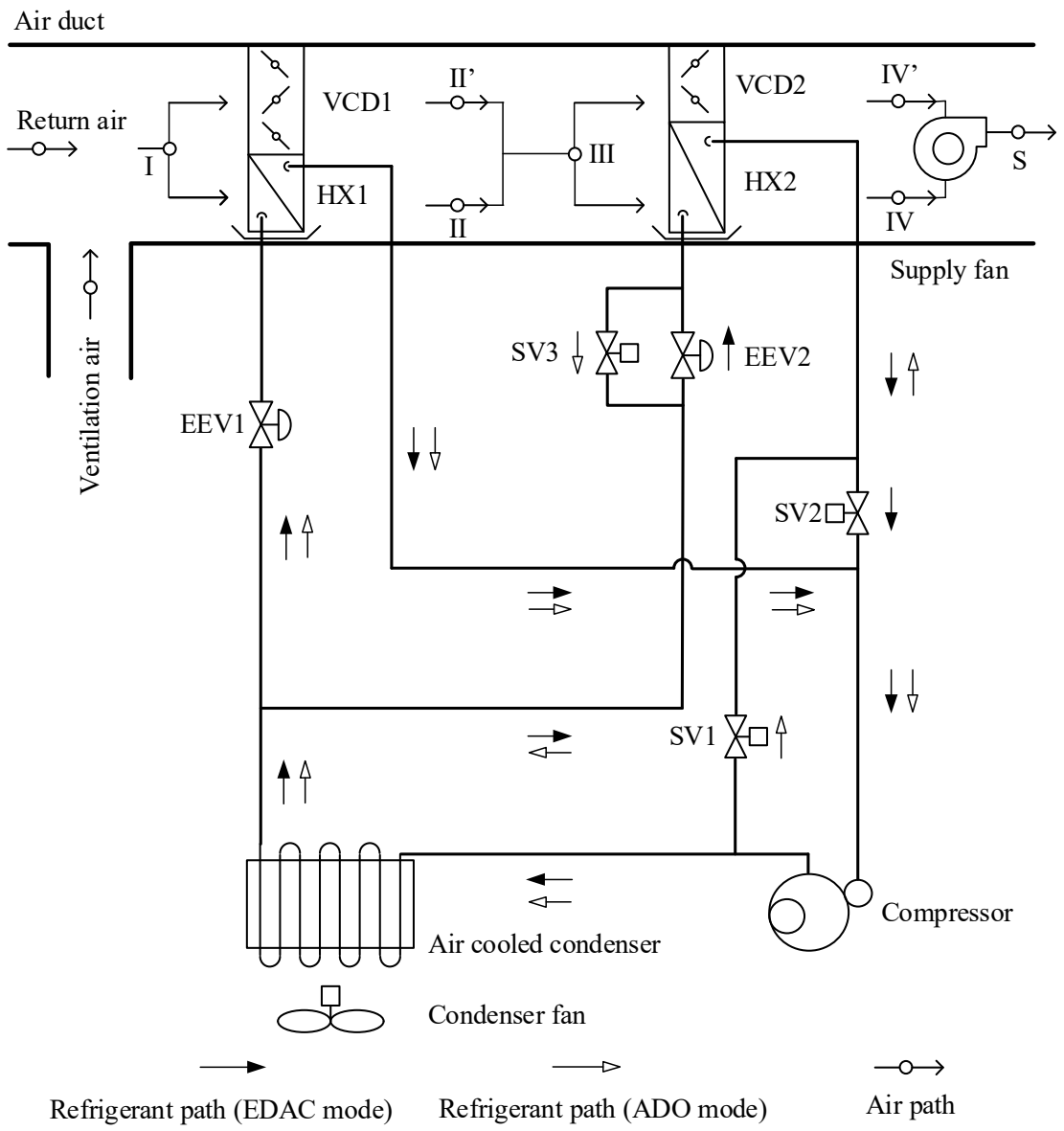
Advanced technologies such as variable-speed compressor, electric expansion valves (EEVs), as well as a computerized data measuring, logging and control system have been incorporated into the prototype experimental EDAC system.

This Chapter reports on the details of the prototype experimental EDAC system. The detailed configuration of the proposed EDAC system is firstly described. Then, detailed descriptions of the prototype experimental EDAC system and its major components are presented, followed by describing the computerized sensors / measuring devices for temperatures, pressures and flow rates. Finally, a computer supervisory program used to operate and control the experimental EDAC system is detailed.

4.2 Detailed configurations of the proposed EDAC system

The proposed EDAC system is shown schematically in Fig. 4.1. As seen, there were two parallel-connected evaporators, HX1 and HX2. Correspondingly, there were two electronic expansion valves (EEVs), with EEV1 connected to HX1 and EEV2 to HX2. Three modulating valves (SV1 to SV3) were installed on the refrigerant pipeline to allow different refrigerant flow arrangements when needed. To reduce the initial cost, instead of using a variable speed compressor and fan, a two-speed (capacity) compressor and a two-speed supply fan may be used. In addition, two air volume control dampers (VCDs) were included for adjusting air flow passing through the two evaporators, and reducing air flow resistance when either HX1 or HX2 was not in use. Consequently, the EDAC system can be operated in two different modes: Air dehumidification only (ADO) and Enhanced dehumidification air conditioning (EDAC), respectively.

At ADO mode, SV1 and SV3 were opened, while SV2, VCD1 and VCD2 closed. HX1 acted as an evaporator to cool and dehumidify air and HX2 a condenser to reheat the air to a suitable temperature. On the other hand, at EDAC mode, SV1 and SV3 were closed and SV2 opened. Therefore, HX2 was intended to be a main cooling and dehumidifying coil in the EDAC system and HX1 a supplementary one to provide variable latent cooling capacity when needed.



HX1 - the first heat exchanger	SV - solenoid valve	III - inlet air of HX2
HX2 - the second heat exchanger	I - mixed air	IV - outlet air of HX2
EEV - electronic expansion valve	II - outlet air of HX1	IV' - bypassed air from VCD2
VCD - volume control damper	II' - bypassed air from VCD1	S - supply air

Fig. 4.1 Schematics of the detailed configuration for the proposed EDAC system

4.3 Descriptions of the experimental EDAC system and its major components

The prototype experimental EDAC system was purposely established in a laboratory, in accordance with the schematics shown in Fig. 4.1. In the laboratory, there were two environmental chambers each measuring at 5 m (L) × 3 m (W) × 2.5 m (H). One of the chambers was used as a simulated indoor space and the other a simulated outdoor space. The two chambers were conditioned by two existing air conditioning systems as shown in Fig. 4.3. Each existing A/C system consisted of a DX cooling coil (CC) and a load generation unit (LGU). Two microprocessor-based PID controllers were used to maintain required experimental conditions in each chamber, with the following P-I-D parameters of 13-90-5 for the controller of the indoor chamber and of 10-110-5 for that of the outdoor chamber, respectively.

The prototype experimental EDAC system was composed of two parts, i.e., a DX refrigeration plant (refrigerant side) and an air-distribution sub-system (air side). To allow greater flexibility in outputting variable cooling capacities and air flow rates during experiments for possible further studies, a variable speed (VS) compressor, VS supply fan and VS condenser fan were used, although during the current experimental study, fixed speeds for compressor, supply fan and condenser fan were employed. The schematic diagrams for both the DX refrigeration plant and the air side of the experimental EDAC system are shown in Figs. 4.2 and 4.3, respectively, with their details described as follows.

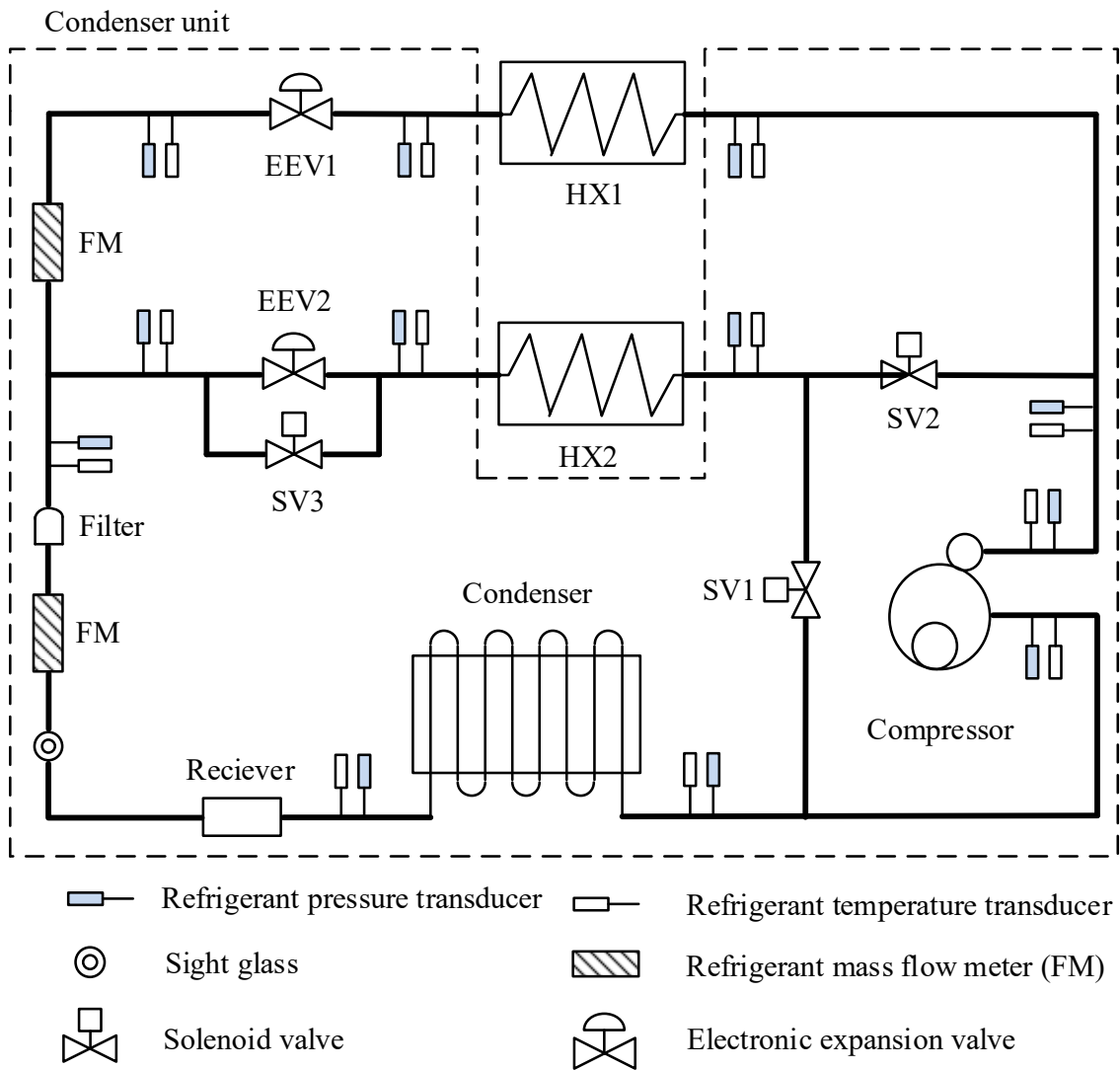


Fig. 4.2 The schematic diagram of the DX refrigeration plant in the prototype experimental EDAC system

output cooling capacity from the compressor was 5 kW. R410A was used as the working fluid, with a total charge of 4.3 kg.

On the other hand, as seen in Fig. 4.3, the air-distribution sub-system system included an air duct with two VCDs, a VS centrifugal supply air fan and an air flow rate measuring apparatus (FRMA). Except for the air cooled outdoor condenser which was placed in the outdoor chamber, the entire prototype experimental EDAC system was installed inside the indoor chamber. Furthermore, EEVs, solenoid valves and compressor on the refrigerant-side and VCDs, supply air fan and condenser fan on the air-side of the EDAC system were all connected to a control unit (C7) for manual or programmed control.

For a cooling coil, its total surface area was determined based on the peak cooling load it handled. Since there were two evaporators in the proposed EDAC system and each was assigned with its distinguished cooling / dehumidifying function, the relative size of the two evaporators in terms of their surface area can affect the overall operational characteristics of the EDAC system. However, in the current study, the surface ratio of HX1 to HX2 was initially set at 1:2. The detailed specifications for the major components used in the prototype experimental EDAC system are listed in Table 4.1.

Table 4.1 Specifications of the main components used in the prototype
experimental EDAC system

Components	Specifications	
Compressor	Type	Rotary
	Number of cylinder / Polarity	2 / 6
	Pressure ratio	≤ 6
	Allowable frequency range	10-120 Hz
	Cooling capacity at 70Hz	5 kW
	Displacement	14 mL/rev
EEV1	Pulse range	0-500 pulse
	Rated capacity	2.5 kW
	Port diameter	1.3 mm
EEV2	Pulse range	0-500 pulse
	Rated capacity:	3.5 kW
	Port diameter:	1.65 mm
HX1	Fin type	Louver
	Transverse / Longitude tube pitch	21 / 12.7 mm
	Fin pitch / thickness	1.2 / 0.115 mm
	Internal/external tube diameter	6.4 / 7 mm
	Coil width / height	450 / 200 mm
	Number of the tube row	4
	Number of refrigerant loop	2
	Total coil surface area	6.5 m ²
Rated cooling capacity	2 kW	
HX2	Fin type	Louver
	Transverse / Longitude tube pitch	21 / 12.7 mm
	Fin pitch / thickness	1.2 / 0.115 mm
	Internal/external tube diameter	6.4 / 7 mm
	Coil width / height	450 / 300 mm
	Number of the tube row /	5
	Number of refrigerant loop	3
	Total coil surface area	12.5 m ²
Rated cooling capacity	3 kW	
Condenser	Fin type	Louver
	Internal/external tube diameter	8.82 / 9.52 mm
	Total coil surface area	25 m ²
Supply air fan	Type	Centrifugal fan
	Input signal	Direct voltage
	Rated speed	1600 rpm
	Air flow rate	0.1-0.3 m ³ /s
Condenser fan	Type	Axial fan
	Input signal	Direct voltage
	Rated speed	2800 rpm
	Air flow rate	0.1-0.6 m ³ /s

4.4 Computerized instrumentation and data acquisition system

4.4.1 Sensors/ measuring devices for temperatures, pressures and flow rates

For the measurements in the DX refrigeration plant, the pressures in various locations of the refrigerant pipeline were measured using pressure transmitters with an accuracy of $\pm 0.3\%$ of full scale reading, while the sensors for refrigerant temperatures were of platinum Resistance Temperature Device (RTD) type with a pre-calibrated accuracy of $0.1\text{ }^{\circ}\text{C}$. Furthermore, there were two refrigerant mass flow meters based on the coriolis force effect with a high accuracy of $\pm 0.15\%$ of full scale reading. One was installed downstream of the air-cooled condenser while the other upstream of EEV1.

For the measurements in the air-distribution sub-system, the air states in the two chambers were measured using the sampling devices with an ANSI/ASHRAE Standard 41.1 [ASHRAE, 1986] specified tree and aspirating psychrometer, and the air dry and wet bulb temperature sensors in the psychrometer were also of platinum resistance (PT100) type. However, the air states at the inlets to HX1 and HX2, the outlets from HX1 and HX2, and condenser inlet and outlet were measured by totally six pairs of temperature and humidity probes integrated with air duct due to the limited space available.

The total air volumetric flow rate for the experimental EDAC system was measured by the airflow rate measuring apparatus (FRMA) constructed in accordance with ANSI / ASHRAE Standard 41.2 [ASHRAE, 1987], consisting of a set of nozzles of

different sizes, diffusion baffles and a differential pressure transducer with a measuring accuracy of $\pm 0.1\%$ of the full scale reading.

Furthermore, to obtain the air mass flow rate passing through HX1, a short air duct of 400 mm connected to its inlet was added. Air velocities inside the air duct at three evenly distributed points were measured using three hot wire anemometers. The averaged air velocity was obtained by averaging the three measured air velocities and the air flow rate evaluated by multiplying the averaged air velocity by the cross-section area of the short air duct. The uncertainty of air flow rate measurement was evaluated at about 1.5%.

Finally, the energy consumption of the compressor was obtained from its variable speed drive (VSD) and the total energy consumption of the experimental EDAC system including the compressor and the two fans by using a power meter.

Details of instrumentation and sensors used in the experimental EDAC system are listed in Table 4.2.

Table 4.2 Details of instrumentation and sensors used in the experimental EDAC system.

Measurement parameter	Instrument Type	Range	Accuracy
Average space air dry- and wet-bulb temperature	Tree and aspirating psychrometer	-50-100 °C	±0.1 °C
Air dry-bulb temperature	T&RH probe	-40-60 °C	±0.3 °C
Air relative humidity	T&RH probe	10-95%	±2% RH
Air velocity	Hot film anemometer	0-10 m/s	±0.1 m/s
Air flow rate	FRMA	0-1 kg/s	±1.2%
Refrigerant temperature	Platinum RTD	-50-100 °C	±0.1 °C
Refrigerant pressure	Pressure transducer	-1-34 bar	±0.3%
Refrigerant pressure	Pressure transducer	-1-20 bar	±0.3%
Refrigerant mass flow rate	Coriolis mass flow meter	0.3-18 kg/min	±0.15%
Power consumption	Single-phase power meter	1-40 A	±0.1%

4.4.2 The data acquisition system

A data acquisition unit was used in this experimental EDAC system. It provided up to 60 channels for monitoring various types of system operating parameters. The direct current signal from various measuring devices / sensors can be scaled into their real physical values of the measured parameters using a logging & control supervisory program which was developed using LabVIEW programming platform. The minimum data sampling interval was two seconds.

4.5 LabVIEW logging & control supervisory program

A computer supervisory program which was capable of performing simultaneously data-logging and parameter-controlling was necessary. It needed to communicate with not only the data acquisition unit, but also the control unit for the EDAC system, as shown in Photo 1 in Appendix A. A commercially available programming package, LabVIEW, provided a powerful programming and graphical platform for data acquisition and analysis, as well as for control application.

A data logging & control supervisory program was therefore developed using LabVIEW, with all measured parameters real-time monitored, curve-data displayed, recorded and processed. The program can also perform the retrieval, query and trend-log graphing of historical data for measured parameters. The program ran on a personal computer, as shown in Photos 11 and 12 in Appendix A. The LabVIEW-based logging & control supervisory program enabled the computer to act as a central supervisory control unit for both data logging and low-level control loops in the experimental EDAC system.

4.6 Summary

A prototype experimental EDAC system was made available for carrying out the research project reported in this Thesis. The system consisted of two parts: a DX refrigeration plant and an air-distribution sub-system.

The experimental EDAC system was fully instrumented using high quality sensors / measuring devices. Totally sixty operating parameters in the system can be measured and monitored simultaneously. One set of airflow rate measuring apparatus was

constructed in accordance with ANSI/ASHRAE Standard 41.2. Two sets of air dry-bulb and wet-bulb temperature sensors were placed in the air-sampling devices for evaluating the enthalpy of the air entering and leaving the prototype EDAC system, and two Coriolis mass flow meters were used for measuring the refrigerant flow rate being circulated in HX1 and the DX refrigerant plant, respectively.

A logging & control supervisory program was developed specifically for this experimental VS DX A/C system using LabVIEW programming platform. All parameters can be real-time measured, monitored, curve-data displayed, recorded and processed by the logging & control program.

The availability of such a prototype experimental EDAC system is expected to be extremely useful in investigating the operational characteristics of the EDAC system, validating the developed EDAC model, and developing a year-round control strategy for EDAC system. Therefore, the research project proposed in Chapter 3 can be carried out using the prototype experimental EDAC system, with the details to be reported in Chapters 5-7 in this Thesis.

Photos showing the prototype experimental EDAC system are given in Appendix.

Chapter 5

Operational characteristics of the experimental EDAC system

5.1 Introduction

With the availability of the prototype experimental EDAC system described in Chapter 4, the research project proposed in Chapter 3 can be carried out, and the project details are respectively reported in Chapters 5 to 7. In this Chapter, an experimental study on the operational characteristics of the experimental EDAC system at the EDAC mode is firstly presented to establish if such an EDAC system can provide variable latent cooling capacity when both refrigerant and air mass flow rates passing through the two evaporators in the EDAC system, HX1 and HX2, were varied.

The schematic diagram of the experimental EDAC systems is shown in Fig. 4.1, and is described in details in Chapter 4. In this Chapter, firstly, the experimental cases and conditions are specified. Then the experimental results and their related analysis and discussions are presented. Finally, conclusions are given.

5.2 Experimental procedures and data interpretation

When an EDAC system was operated with two evaporators at the EDAC mode, its compressor and supply fan were both constant speed operated. In this Chapter, therefore, the speeds of the VS compressor and supply fan were fixed at their maximum values, 4800 rpm for compressor and 1400 rpm for supply fan, respectively. Hence, the factors influencing the operational characteristics of the EDAC system at

the EDAC mode in terms of the relationship between its output total cooling capacity (TCC) and its equipment sensible heat ratio (E SHR) were as follows:

The first one was the ratio of the refrigerant mass flow rate through HX1, m_{rHX1} , to the total mass flow rate, m_{rcom} , or:

$$R_r = \frac{m_{rHX1}}{m_{rcom}} \quad (5.1)$$

R_r could be varied by adjusting the opening degrees of EEV1, while EEV2 can respond accordingly to maintain the degree of refrigerant superheat (DS) at the compressor suction.

The other was the ratio of the air mass flow rate passing through HX1, m_{aHX1} , to the total air mass flow rate of the EDAC system, m_a , or:

$$R_a = \frac{m_{aHX1}}{m_a} \quad (5.2)$$

R_a could be varied by adjusting the opening degree of VCD1.

Given that the inlet air states to an EDAC system may also impact on its operational characteristics, in this Chapter, five experimental cases at five different inlet air states were designed, as shown in Table 5.1. These five inlet air states correspond to typical indoor air settings for comfort air conditioning, which were often used in the studies related to the operational characteristics of DX based A/C systems [Li et al., 2014; Xia et al., 2017; Xu et al., 2010]. In each experimental case, for the experimental EDAC

system, the operational characteristics at different combinations of R_a and R_r shown in Table 5.2 were obtained.

Table 5.1 Five experimental cases with different inlet air settings

Group	Case	T_{ai} (°C)	T_{awI} (°C)	RH_{ai} (%)
T constant	RH-40	26	17	40
	RH-50*	26	18.7	50
	RH-60	26	20.3	60
RH constant	T-22	22	15.4	50
	T-24	24	17.1	50
	T-26*	26	18.7	50

* The same case.

Table 5.2 The combinations of R_a and R_r used in the five experimental cases

R_a					
No.	1	2	3		
%	30	45	60		
R_r					
No.	1	2	3	4	5
%	14	25	38	53	67

In order to simplify the experimental procedure, no fresh air was introduced to the experimental EDAC system in each case. When the experimental EDAC system was operated at a steady state condition, air parameters inside the indoor chamber were considered to be the same as those at the inlet to the experimental EDAC system. When the variations for indoor air dry-bulb and wet-bulb temperatures were both less than 0.1 °C, respectively, a steady state of operation for the experimental EDAC

system was arrived. Then the operating parameters of the experimental EDAC system were recorded continuously for 15 min at an interval of 1 min and the averaged measured data were used for evaluating the operational characteristics of the experimental EDAC system.

During all tests, the condenser fan ran at its maximum speed of 2800 rpm and the air states in the outdoor chamber were maintained at 33 °C and 68% RH, in accordance with the maximum coincident air dry bulb temperature and RH in Hong Kong [ASHRAE, 2009]. The DS at compressor suction was set at 7 °C.

For all the five cases, using the measured operating parameters, the output sensible cooling capacity of the EDAC system was evaluated as,

$$Q_s = m_a C_{pa} (T_{al} - T_{as}) \quad (5.3)$$

Where m_a is the total air mass flow rate of the EDAC system, T_{as} the supply air temperature from the EDAC system and T_{al} the inlet air temperature to the EDAC system.

The TCC of the EDAC system was

$$TCC = m_a (h_{al} - h_{as}) \quad (5.4)$$

Where h_{as} is the specific enthalpy of the supply air from the EDAC system and h_{al} that of the inlet air to the EDAC system.

Therefore, E SHR was evaluated by

$$E \text{ SHR} = \frac{Q_s}{TCC} = \frac{C_{pa}(T_{aS} - T_{aI})}{h_{aS} - h_{aI}} \quad (5.5)$$

The uncertainties of these calculated parameters were evaluated by using the classic root-sum-square formula [Holman and Gajda, 2001] and are shown in Table 5.3.

Table 5.3 Measurement/calculation uncertainty of system operating parameters

Operating parameter	Uncertainty	Unit
R_a	$\pm 1.12\%$	—
R_r	$\pm 0.3\%$	—
TCC	1.05%-1.58%	kW
E SHR	0.81%-1.33%	—

5.3 The measured operational characteristics of the EDAC system

Extensive experimental work was carried out on the operational characteristics of the prototype experimental EDAC system, with the two evaporators operated, to examine if by varying R_a and R_r , variable output latent cooling can be obtained, as compared to a single evaporator On-Off controlled DX A/C system, both with a constant speed compressor and supply fan. In this Section, firstly, the measured operational characteristics at one of the five cases, Case T-26 or RH-50, where the inlet air state to the experimental EDAC system corresponding to the typical indoor air settings for air conditioning, i.e., 26 °C and 50% RH, are detailed. Secondly, the measured operational characteristics in all the cases are presented, to demonstrate the influences of different inlet air states on the operational characteristics of the prototype experimental EDAC system.

5.3.1 The measured operational characteristics of the experimental EDAC system at Case T-26 or RH-50

Fig. 5.1 illustrates the experimental results for Case T-26 / RH-50 by X-Y plotting the experimental data of total cooling capacity (TCC) and equipment sensible heat ratio (E SHR) at different values of R_a and R_r . As seen, TCC and E SHR were correlated but mutually constrained within an irregular area of ABCDEF shown in Fig. 5.1. Clearly, varying both R_a from 30% to 60% and R_r from 14% to 67% at the fixed inlet air state of 26 °C and 50% RH can only produce those E SHR / TCC relationships represented by the points inside the area of ABCDEF.

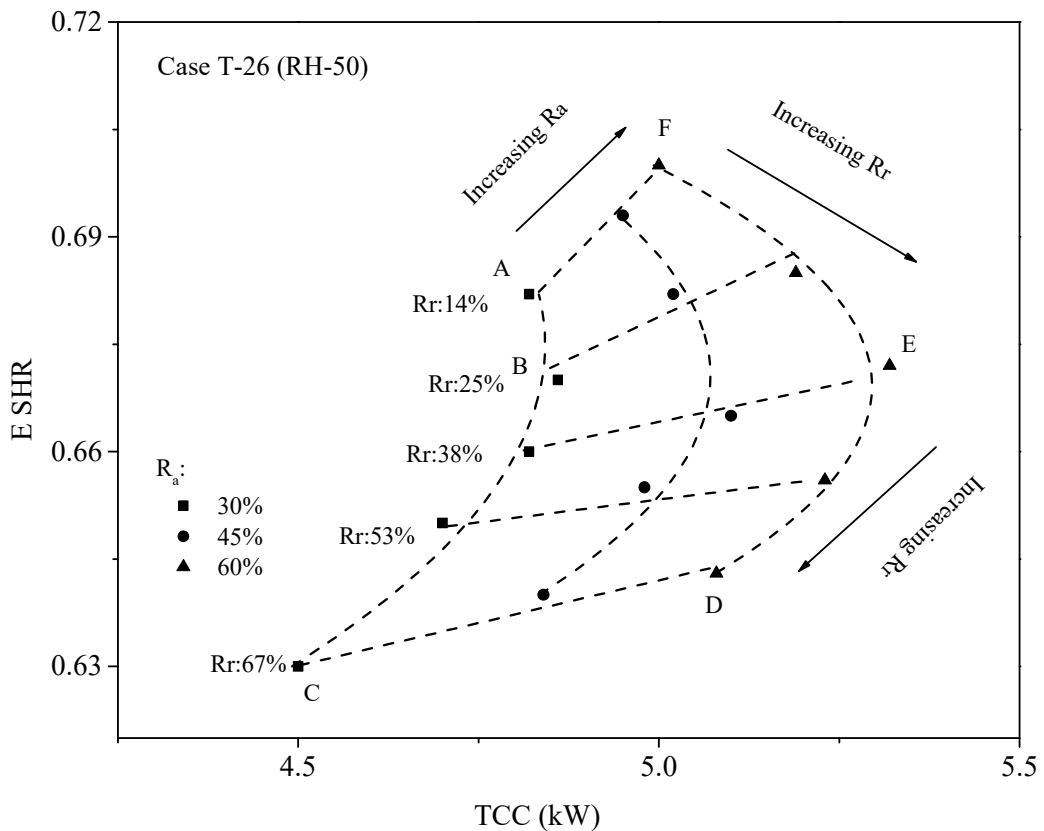


Fig. 5.1 The measured operational characteristics of the prototype experimental EDAC system under various R_r and R_a (Case T-26)

In Fig. 5.1, Points A and C correspond to the TCC / E SHR relationship when the experimental EDAC system was operated at its lowest and highest R_r values of 14% and 67%, respectively, while R_a was fixed at its lowest level of 30%. Similarly, Points F and D correspond to the TCC / E SHR relationships when the EDAC system was operated at its lowest and highest R_r values of 14% and 67%, respectively, while R_a was maintained at its highest level of 60%. Points B and E correspond to the TCC / E SHR relationships with the maximum TCC on the borderlines ABC and DEF, respectively.

Furthermore, for the area of ABCDEF, its borderline AF represents the relationship between TCC and E SHR when varying R_a from 30% to 60%, at a fixed R_r of 14%, and its borderline CD the same relationship, but at a fixed R_r of 67%. Similarly, borderlines ABC and DEF are for the relationship between TCC and E SHR when varying R_r values from 14% to 67%, at two fixed R_a values of 30% and 60%, respectively. Therefore, as demonstrated in Fig. 5.1, at a fixed compressor and fan speed, varying R_a and R_r values could result in significant variations in the output TCC / E SHR values, between 4.5 kW and 5.32 kW for TCC and between 0.64 and 0.7 for E SHR respectively. It should be mentioned that the maximum output TCC was about 6.4 % greater than the rated output cooling capacity of the VS compressor operated at its maximum speed of 4800 rpm, at point E, when the EDAC system was not operated at compressor's nominal working condition.

The influences of varying R_a and R_r on the operational characteristics in terms of the relationship between TCC and E SHR of the prototype experimental EDAC system are separately detailed with their physical reasons as follows:

5.3.1.1 The influence of varying R_r on the variation of the relationship between TCC and E SHR, at a constant R_a

From Fig. 5.1, it can be seen that for all R_a values from 30% to 60%, at a constant R_a value, an increase in R_r would lead to a decrease in equipment sensible heat ratio (E SHR). However, an increase in R_r would lead to an increase in total cooling capacity (TCC) at a lower R_r values, but a decrease in TCC at higher R_r values. Using the line DEF in Fig. 5.1 as an example, i.e., at a R_a value of 60% when R_r varied from 14% to 67%, the variation trend in E SHR / TCC relationship is explained based on the key operating parameters of the experimental EDAC system as shown in Figs. 5.1-5.7.

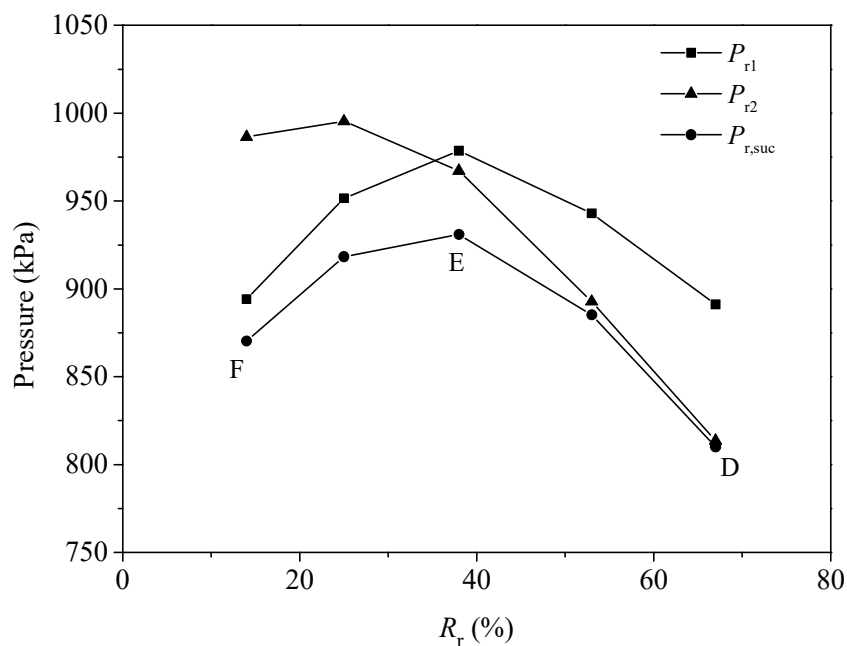


Fig. 5.2 The influences of R_r on the evaporating pressures in HX1 and HX2, and the compressor suction pressure

As seen from Fig. 5.2, compressor suction pressure of the experimental EDAC system was increased with an increase in R_r from 14% to 38%, peaked at about 931 kPa when R_r was at 38%, but decreased as R_r continued to increase from 38% to 67%. The

evaporating pressures in HX1 and HX2 experienced similar variation trends of increasing, peaking and decreasing but with different magnitudes as R_f was increased from 14% to 67%. Such variation trends were largely due to the joint effect of the variations in EEV1 and EEV2 openings, refrigerant mass flow rate distribution to, and the inlet air states to HX1 and HX2 as follows:

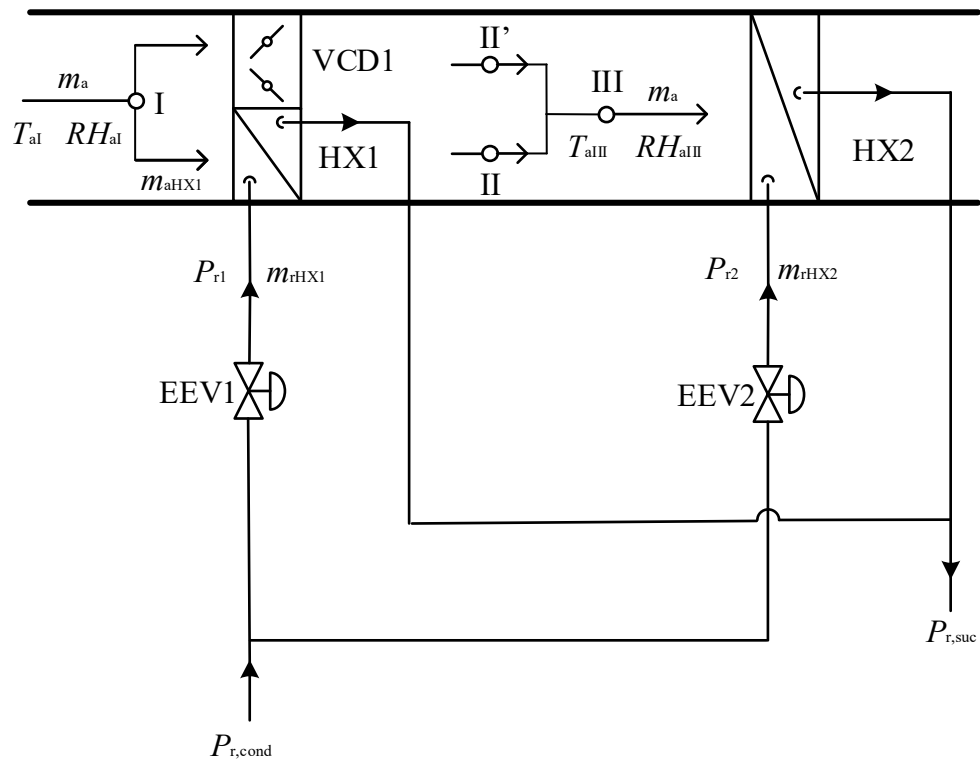


Fig. 5.3 The factors affecting the evaporating pressures in HX1 and HX2, and compressor suction pressure

As seen from Fig. 5.3, for HX1, its evaporating pressure was jointly affected by EEV1 opening, refrigerant mass flow rate, m_{rHX1} , and its inlet air state and air flow rate, which remained unchanged at a fixed R_a value and inlet air state. In the experimental EDAC system, as mentioned in Section 5.2, EEV1 acted as a modulating valve to control m_{rHX1} . Hence, as R_f was increased, EEV1 opening was increased, so that the pressure drop across EEV1 was reduced. This would lead to a higher P_{r1} . On the other hand, more refrigerant mass flowing into HX1, at a fixed inlet air state and air flow

rate, would however lead to a lower evaporating pressure. Consequently, the actual evaporating pressure P_{r1} was determined by the net effect of a larger EEV1 opening and an increased refrigerant mass flow. Hence, at a smaller R_r value from 14% to 38%, the impact of a larger EEV1 opening on P_{r1} was greater than that of a greater refrigerant mass flow rate on P_{r1} , leading to an increased P_{r1} . However, as R_r value continued to increase from 38% to 67%, the impact of increased refrigerant mass flow on P_{r1} would be greater than that of a larger EEV1 opening, leading to a decreased P_{r1} .

For HX2, its evaporating pressure, P_{r2} , was jointly affected by not only EEV2 opening, and refrigerant mass flow rate, m_{rHX2} , but also its inlet air state and air flow rate. As HX2 was placed downstream of HX1, its inlet air state was therefore not constant, but variable due to the changes in the output capacity of HX1. During experiments, EEV2 was operated in response to the changes in DS at compressor suction. Therefore, as seen from Fig. 5.4, as R_r was increased, DS at HX1 exit was decreased, which called for an increase in DS at HX2 exit to maintain a stable DS at compressor suction. Hence, EEV2 opening was reduced, and thus with less refrigerant flowing into HX2. A smaller EEV2 opening would lead to a lower P_{r2} , but a smaller refrigerant mass flow rate a higher P_{r2} . However, for HX2, a reduced inlet air temperature and humidity due to the increased output cooling capacity from HX1 as R_r was increased would also lead to a lower evaporating temperature in HX2. Therefore, as seen in Fig. 5.2, when R_r was increased from 14% to 25%, P_{r2} was slightly increased, as the impact of smaller refrigerant mass flow rate was greater than the combined impacts from both reduced EEV2 opening and reduced inlet air temperature and humidity. However, as R_r was further increased from 25% to 67%, the combined impacts significantly overtook that of smaller m_{rHX2} on P_{r2} , so that P_{r2} started to quickly decrease and reached its lowest level of 814 kPa at $R_r = 68\%$.

For compressor suction pressure, it would be determined by the lower one of P_{r1} and P_{r2} , since HX1 and HX2 were connected in parallel to a common compressor. Consequently, with the change of R_r from 14% to 67%, the variation in the compressor suction pressure shown in Fig. 5.2 was resulted in.

Furthermore, as seen in Fig. 5.4, increasing R_r would lead to a lower degree of refrigerant superheat (DS) at HX1 exit from 28 °C to 2 °C as more and more refrigerant flowed in, while the DS at HX2 exit was zero at lower R_r values but increased to 18 °C at the highest R_r of 67% as less and less refrigerant flowed in. These variation trends for the evaporating pressures in HX1 and HX2, compressor suction pressure and DSs were similar to those previously reported by Zhou et al. [2002], where a dual-evaporator A/C system was simulated at a constant compressor speed and fixed DS.

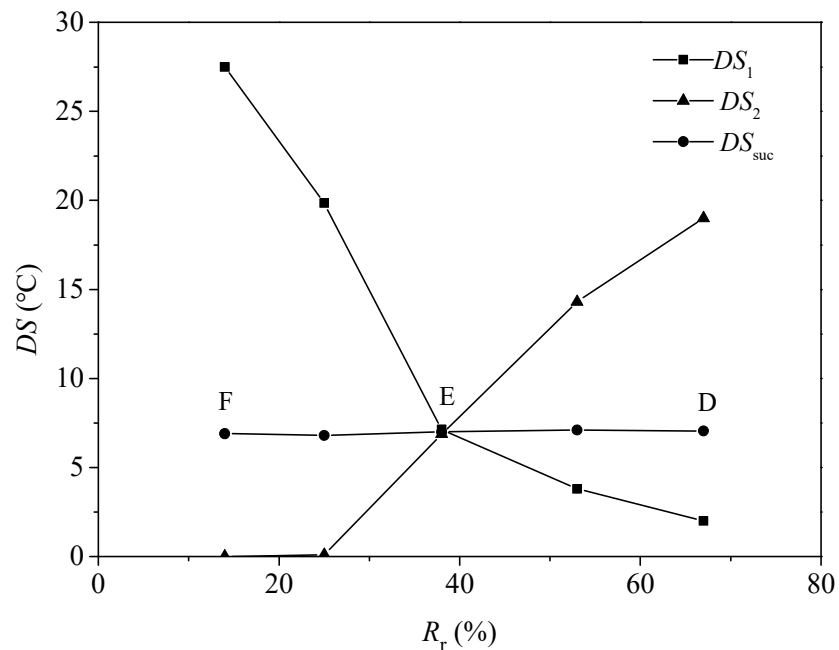


Fig. 5.4 The influences of varying R_r on the DSs at exits of HX1, HX2 and the compressor suction

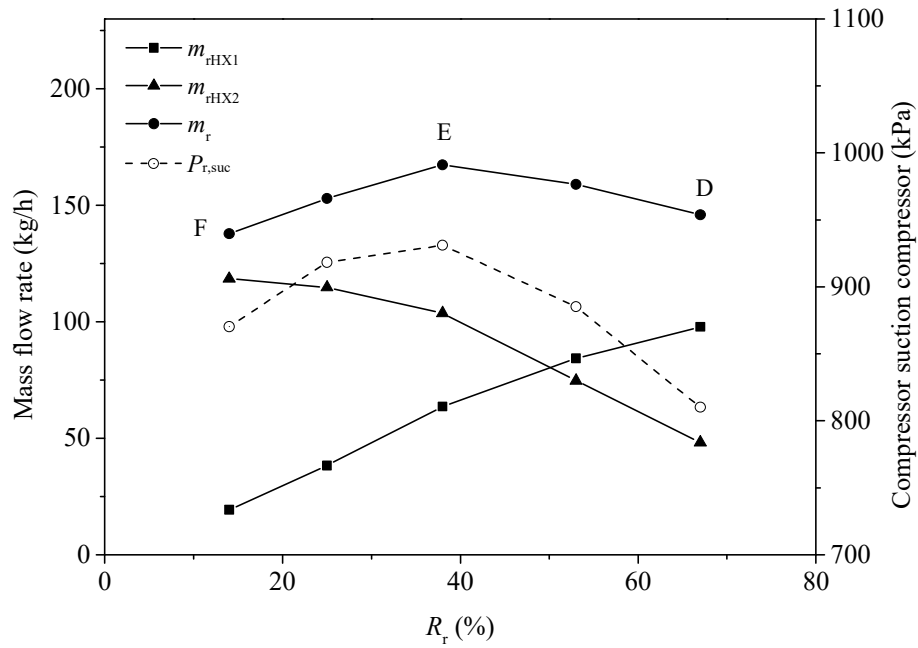


Fig. 5.5 The influences of R_r on the mass flow rates through HX1, HX2 and compressor of the EDAC system (Points D, E, F correspond to the same shown in Fig. 5.1)

The influences of varying R_r on the TCC of the EDAC system:

As R_r was increased, more refrigerant flowed into HX1, but less into HX2, as shown in Fig. 5.5. However, the refrigerant mass flow rate at compressor suction, which was the sum of those into HX1 and HX2, experienced an increasing, peaking and decreasing trend, similar to that of compressor suction pressure. As it can be understood, when other conditions in a DX cooling coil remained unchanged, an increase in refrigerant mass flow rate would result in an increase in its cooling capacity. Therefore, the changes in TCC of the EDAC system would follow that in compressor refrigerant mass flow rate, experiencing an increasing, peaking and decreasing trend, as R_r was increased from 14% to 67%, shown in Fig. 5.5. It is further noted from both Fig. 5.1 and Fig. 5.5 that compressor refrigerant mass flow rate and the TCC at point F, i.e., $R_r = 14\%$, were lower than those at Point D, i.e., $R_r = 67\%$. With respect to the

output cooling capacity from HX1 and HX2, as R_r was increased, the cooling capacity from HX1 was gradually increased, but that from HX2 reduced, similar to the variation trends for m_{rHX1} and m_{rHX2} , respectively shown in Fig. 5.5.

The influences of varying R_r on the E SHR of the EDAC system:

For a DX cooling coil, its surface temperatures and the coil surface areas where dehumidification could take place would jointly determine its dehumidification ability or E SHR. A lower surface temperature was clearly desirable for achieving better dehumidification [Li and Deng, 2007b; Xia et al., 2017; Xu et al., 2010], but a larger dehumidifying surface area could also result in better dehumidification. However, it was difficult to know the exact dehumidifying area on a DX cooling coil. Given that dehumidification usually takes place at the two-phase region of the DX coil, the DS at coil exit could therefore be used to indicate the extent of dehumidifying surface area on a DX coil. A larger DS usually suggests a smaller dehumidifying surface area, and vice versa.

Therefore, for R_r values from 14% to 38%, as shown in Fig. 5.2, a higher R_r would lead to a higher evaporating pressure and thus a higher evaporating temperature in HX1. Hence, a poor dehumidification ability on per unit coil surface area was resulted in. However, a significant decrease in the DS at HX1 exit as R_r was increased from 14% to 38% as shown in Fig. 5.4 indicated a considerable increase in its two-phase heat transfer region or a larger dehumidifying surface area. This would offset the poor dehumidification ability due to a higher evaporating temperature in HX1, and its net dehumidifying ability was increased. For HX2, as R_r was increased for 14% to 38%, the variation in its evaporating pressure was slightly increased first but moderately decreased thereafter. This suggested that the changes in its evaporating temperature

were insignificant. Furthermore, as shown in Fig. 5.4, the DS at HX2 exit stayed at zero when R_r was increased from 14% to 25%, indicating that the entire HX2 remained in two-phase region. When R_r was further increased to 38%, the DS at HX2 exit was moderately increased to 7 °C when its evaporating pressure was actually moderately decreased from the highest value of 995 kPa. Hence, the impacts on dehumidification ability from both reduced evaporating pressure and reduced two-phase surface areas cancelled each other, leading to a fairly constant dehumidification ability of HX2. Overall speaking, as R_r was increased from 14% to 38%, the dehumidification ability of the EDAC system was mainly affected by that of HX1, which was actually enhanced, so that a lower E SHR of the EDAC system was resulted in.

On the other hand, at higher R_r values of 38% to 67%, a higher R_r , or more refrigerant mass flow rate, would lead to a lower evaporating pressure and thus a lower evaporating temperature in HX1. Together with the continued increase in two-phase heat transfer surface area in HX1 as the DS at its exit continued to decrease, the dehumidification ability in HX1 was further enhanced. For HX2, as the DS at its exit was increased, its two-phase surface area and inlet air moisture content due to a better dehumidification effect in HX1, were decreased, leading to a poor dehumidification effect. However, a significant decrease in the evaporating temperature in HX2 would compensate the poor dehumidification effect. Thus, a better overall dehumidification ability for the experimental EDAC system would be still resulted in mainly due to the enhanced dehumidification in HX1. Hence as R_r was increased from 38% to 67%, a lower E SHR was resulted in.

5.3.1.2 The influence of varying R_a on the variation of the relationship between TCC and E SHR, at a constant R_r

As seen in Fig. 5.1, for all R_r values from 14% to 67%, at a fixed R_r , increasing R_a would increase both TCC and E SHR. This suggested that, at a fixed R_r , running the EDAC system at a lower R_a would lead to a lower E SHR, which was beneficial to dehumidification, but also a lower TCC. Given the fixed R_r or the fixed openings of EEV1 and EEV2, such a variation trend was due to the changes in both air flow rate passing through HX1 and inlet air state to HX2, respectively. Using the line CD in Fig. 5.1 as an example, i.e., at a R_r value of 67% when R_a was varied from 30% to 60%, the variation trend in E SHR / TCC relationship is explained based on the operating parameters of the experimental EDAC system as shown in Fig. 5.6 and 5.7.

For HX1, at a fixed inlet air state, increasing air flow rate would lead to an increase in its evaporating pressure or evaporating temperature, as shown in Fig. 5.6. As seen from Fig. 5.7, the DS at HX1 exit was only slightly increased, indicating that its dehumidifying area did not change much. As the evaporating temperature in HX1 was increased, the difference between the evaporating temperature and inlet air temperature was also reduced. However, as the rate of increase in air mass flow rate was much higher than that of evaporating temperature, the TCC of HX1 was increased. Furthermore, at a reduced difference between evaporating temperature and inlet air temperature, the rate of increase in the sensible component of the TCC was much higher than that in the latent component of TCC, leading to an increased E SHR. With an increased E SHR at a higher R_a , although the absolute amount of latent capacity may be increased due to an increased air flow rate, the actual dehumidification ability

per unit air flow rate was in fact reduced. Therefore, as R_a was increased, at HX2 inlet, air temperature was reduced, but air moisture content was on the contrary increased.

For HX2, as R_a was increased, its total air mass flow rate remained unchanged, but inlet air state was changed due to the changes in HX1's output cooling capacity. As explained earlier, its inlet air temperature was reduced, but its moisture content was increased. From Fig. 5.6, it can be seen that the evaporating pressure in HX2 was also slightly increased as R_a was increased. This suggested that the total load imposed on HX2 was also increased, because the rate of reduction in the sensible load due to the increased sensible heat transfer in HX1 was smaller than the rate of increase in the latent load due to a higher E SHR from HX1. Consequently, the evaporating temperature in HX2 was increased. Also from Fig. 5.7, the DS at HX2 exit was slightly decreased, leading to a slightly increased dehumidifying surface area. Consequently, due to the cancelling effects from increased evaporating temperature, increased dehumidifying surface area and increased moisture content of inlet air to HX2, the changes in the latent cooling capacity from HX2 were not significant. With regard to the output sensible cooling capacity from HX2, since its inlet air temperature was reduced, at an increased evaporating temperature, the difference between evaporating temperature and inlet air temperature was reduced, leading to a reduced output sensible cooling capacity from HX2. Therefore, as R_a was increased, its sensible cooling capacity was reduced.

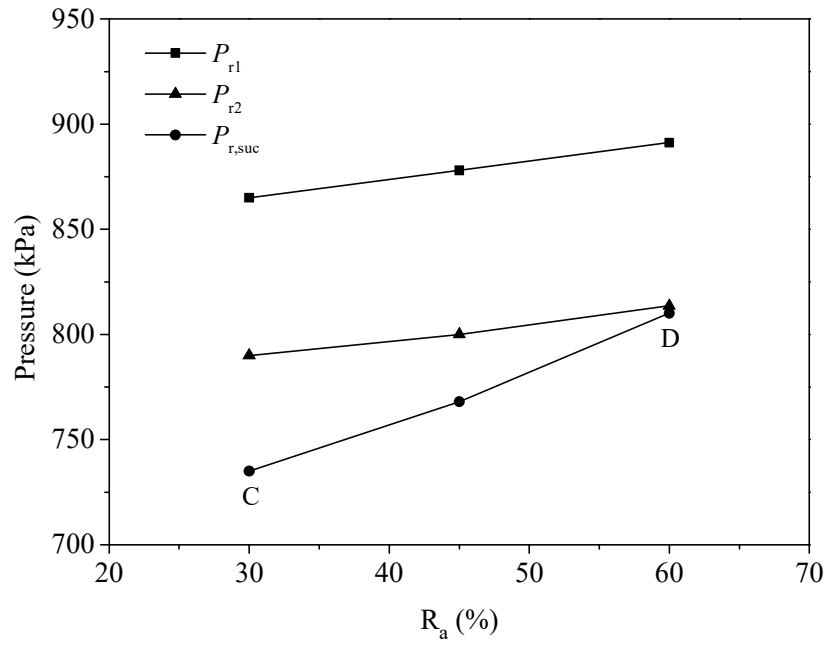


Fig. 5.6 The influences of varying R_a on the evaporating pressures in HX1 and HX2, and compressor suction pressure, at a fixed R_r

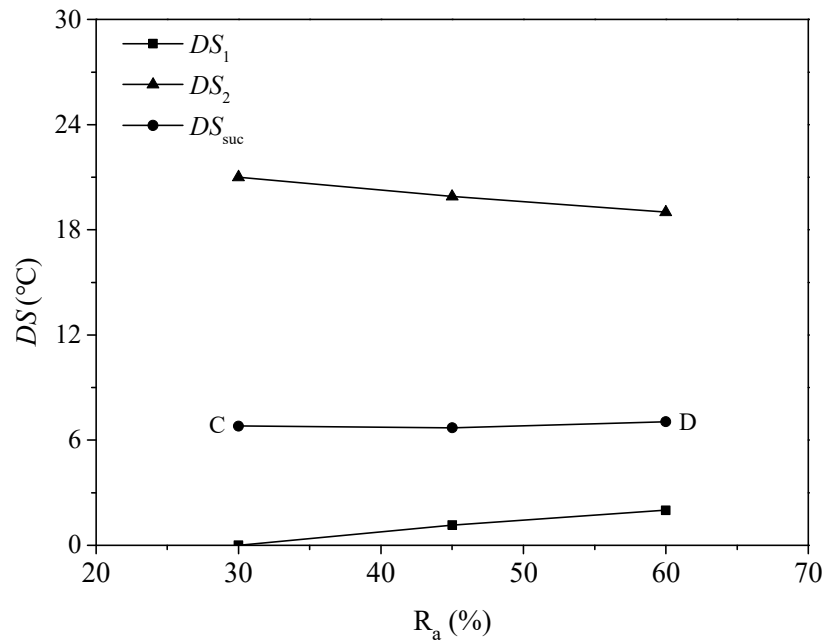


Fig. 5.7 The influences of varying R_a on the DSs at exits of HX1 and HX2, and the compressor suction

The influences of varying R_a on the TCC of the EDAC system:

As R_a was increased from 30% to 60%, its TCC was increased. As discussed earlier, for HX1, its TCC was increased. However, for HX2, while its sensible capacity was reduced, its latent capacity did not change much. Since more air was treated in HX1, the increase in the TCC of HX1 would dominate the change in TCC of the EDAC system, leading to an overall increase in the TCC of the EDAC system.

The influences of varying R_a on the E SHR of the EDAC system:

Also as discussed earlier, increasing R_a would lead to an increase E SHR in HX1. For HX2, actually, its latent cooling capacity was not significantly changed, resulting in a net increase in E SHR of the EDAC system.

5.3.2 The influence of different inlet air states on the operational characteristics of the experimental EDAC system (all the cases)

Fig. 5.8 shows the experimental results from Test Cases of RH-40, RH-50 and RH-60, at Constant T Group and Fig. 5.9 those from Test Cases of T-22, T-24 and T-26, at Constant RH Group. Detailed discussions for these results are as follows:

As seen from Figs. 5.8 and 5.9, different inlet air states would impact not only the high-low limits of TCC and E SHR but also the ranges between these limits. However, the extents of the impacts at different inlet air states appeared different.

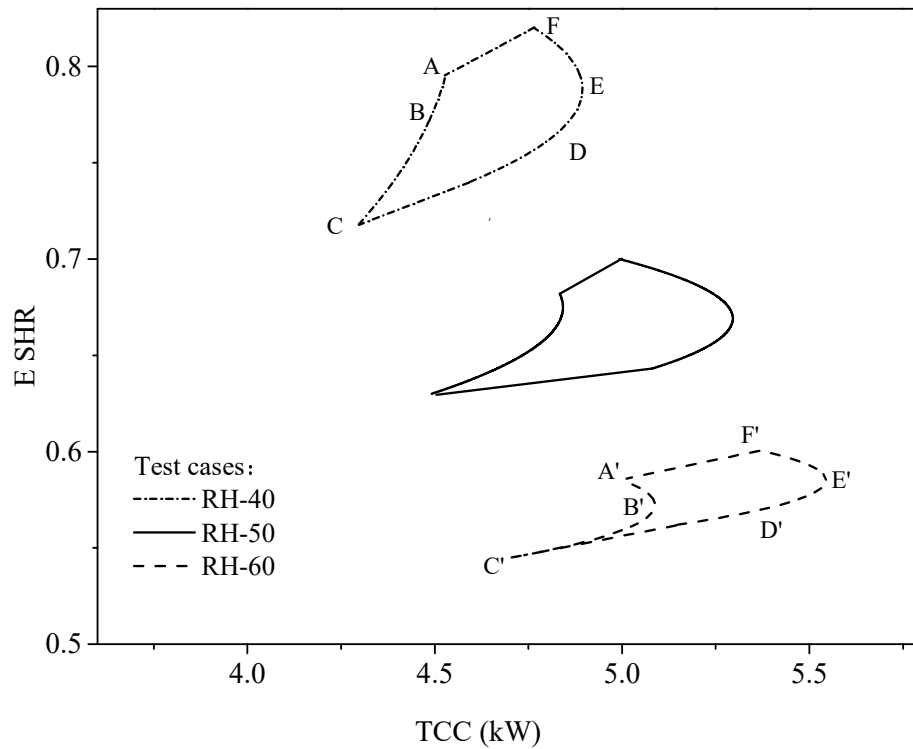


Fig. 5.8 The measured operational characteristics of the experimental EDAC system at the Constant T Group (Cases RH-40, RH-50 and RH-60)

At a constant inlet air temperature of 26 °C, with an increase in RH level, the high-low limits of TCC were increased and those of E SHR decreased, as shown in Fig. 5.8. When inlet air RH was at 40%, the high-low limits for TCC were 4.9 kW and 4.3 kW, and those for E SHR 0.82 and 0.72, respectively. When the RH was increased to 60%, these limits for TCC were changed to 5.6 kW and 4.7 kW and for E SHR, 0.59 and 0.54, respectively. These suggested that a wider operational range for TCC, but a narrower operational range for E SHR at a higher RH level, and vice versa, may be resulted in. Furthermore, as inlet air RH was increased, the slope of borderlines AF and CD was decreased, suggesting that increasing R_a would lead to a larger increase in TCC but a smaller increase in E SHR. For borderlines ABC and DEF, their curvatures became more obvious, meaning that at a higher RH level, increasing R_r would influence more on TCC than on E SHR. Therefore, the changes in inlet air RH, at a constant air temperature, would not only shift the position of the irregular area of

ADCDEF from top-left to down-right in Fig. 5.8, but also flatten it. Position shifting and the change in shape for these irregular areas in the diagram suggested an obvious influence caused by increased inlet air RH level on the operational characteristics of the EDAC system at a constant inlet air temperature.

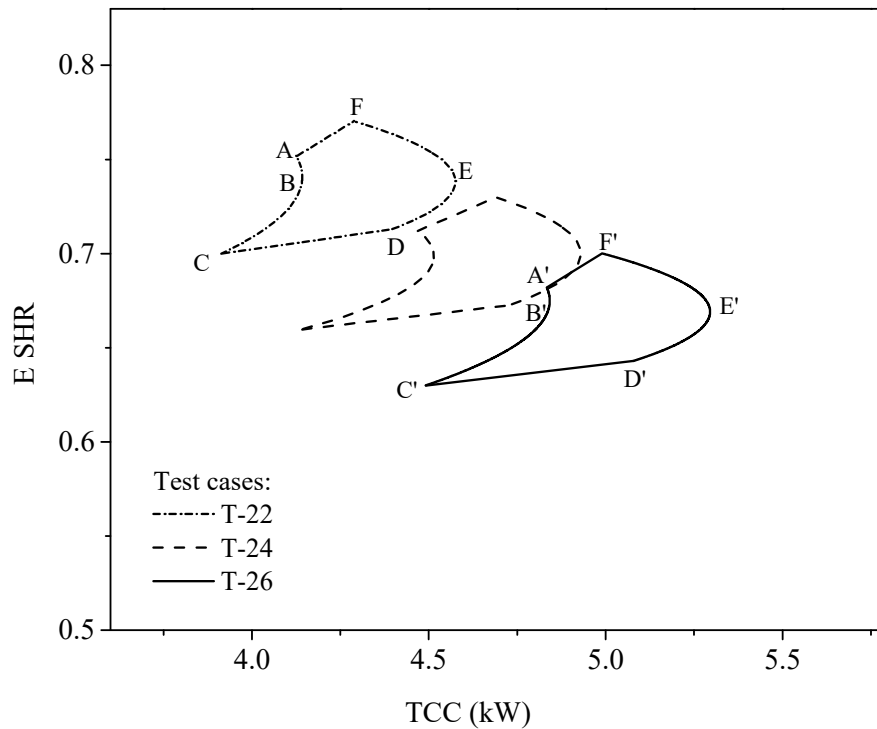


Fig. 5.9 The operational characteristics of the EDAC system at the Constant RH Group (Cases T-22, T-24 and T-26)

However, the measured results from the Constant RH Group presented in Fig. 5.9 suggest something different. At a constant inlet air RH of 50%, when inlet air temperature was 22 °C, the high-low limits for TCC were 4.6 kW and 3.9 kW, and for E SHR 0.77 and 0.7, respectively. As inlet air temperature was increased to 26 °C, the high-low limit for TCC were changed to 5.32 kW and 4.5 kW and for E SHR, 0.7 and 0.63, respectively. However, unlike that the ranges between the limits for both TCC and E SHR experienced a considerable change in the Constant RH Group, the changes in the ranges between the limits in the Constant T group were not significant.

Furthermore, all the borderlines appeared parallel to each other. This indicated that the changes in TCC and E SHR would not be considerable at constant inlet air RH but at varying inlet air temperature, when R_r and R_a were varied. Therefore, at a constant RH, varying inlet air temperature would only shift the positions of the irregular areas of ABCDEF but not change their shapes in Fig. 5.9. This suggested that increasing the inlet air temperature at constant RH level would not pose much impact on the output ranges of TCC and E SHR of the EDAC system.

5.3.3 Discussion

From the experimental results presented in Sections 5.3.1 and 5.3.2, it is obvious that unlike a conventional On-Off controlled single evaporator DX A/C system that can only provide a fixed TCC / E SHR combination at a constant inlet air state, the proposed EDAC system was able to produce variable output sensible and latent capacity, enabling the EDAC system to deal with varying sensible and latent space loads. In other words, when an EDAC system was operated at part load conditions, its compressor and the supply fan would not stop, but by varying R_r and R_a , a new TCC and E SHR relationship to deal with the variable sensible and latent loads in a conditioned space can be obtained. Thus, a better humidity control could be achieved by using the EDAC system, as compared to using a conventional On-Off controlled DX A/C system which was impossible to output variable TCC and E SHR at varying indoor latent load conditions. For example, for the experimental Case T-26, through varying R_r and R_a , a variation from 4.5 kW to 5.32 kW for TCC and that from 0.63 to 0.7 for E SHR could be provided by the EDAC system.

Furthermore, as mentioned in Chapter 4, HX1 was intended as a supplementary cooling coil to provide variable latent cooling capacity. The experimental results

presented in this Chapter demonstrated that allowing more refrigerant or less air flow to HX1, i.e., a higher R_r or lower R_a , would lead to a lower E SHR for the EDAC system, which was beneficial to dehumidification. This provided a simple and direct approach to adjusting the latent cooling capacity output from the EDAC system. However, varying E SHR through varying both R_r and R_a would be constrained by the required TCC from the EDAC system. From the results shown in Sections 5.3.1 and 5.3.2, decreasing R_a to obtain a lower E SHR would however lead to a lower TCC at the same time. On the other hand, care should be exercised when increasing R_r to obtain a lower E SHR, since TCC would experience a unique variation trend of increasing, peaking and decreasing when R_r was increased. In addition, the experimentally obtained relationships between TCC and E SHR of the EDAC system at different inlet air conditions could clearly reflect the influences of inlet air temperature and RH on the operational characteristics of the EDAC system. These would help the system designers better understand the inherent operational characteristics of the EDAC system, so as to further determine its actual application and suitable control strategy.

5.4 Conclusions

In this Chapter, an experimental study on the operational characteristics of the EDAC system when both evaporators were operated at the EDAC mode is reported. Experimental work was carried out at a constant compressor speed and supply air fan speed but at different inlet air conditions. At each inlet air condition, refrigerant mass flow rate and air mass flow rate to the two evaporators were varied, by varying the degrees of opening of EEVs and VCDs. Based on the experimental results, the following conclusions can be obtained:

- 1) Varying relationships between TCC and E SHR of the EDAC system could be obtained through varying R_a and R_r , and TCC and E SHR were mutually constrained with an irregular area in a TCC - E SHR diagram, thus providing variable dehumidification ability to deal with variable space latent load.

- 2) Inlet air temperature and relative humidity would significantly influence the operational characteristics of the EDAC system, resulting in shifted position of, and varied shape of an irregular area of TCC - E SHR relationship on a TCC - E SHR diagram.

The experimental results reported in this Chapter have provided detailed insights into the operational characteristics of the proposed novel EDAC system, as well as the constraints of applying these characteristics to developing appropriate control strategies, so as to better design, operate and control EDAC systems for improved indoor humidity and thus thermal environmental control. With these insights, it was possible to further develop a steady-state mathematical model for the experimental DX A/C system and year-round control strategy for the satisfactory operation of the EDAC system at different seasons of a year. These will be reported in Chapters 6 and 7, respectively.

Chapter 6

Development of a steady-state mathematical model for the experimental EDAC system at the EDAC mode

6.1 Introduction

An experimental study on the operational characteristics of the experimental EDAC system at the EDAC mode was carried out and the experimental results are presented in Chapter 5. In order to fully comprehend the operational characteristics of an EDAC system operated at different operating conditions and with different system configurations, which was difficult and costly to realize by using a prototype experimental EDAC system of a fixed configuration, it was highly necessary to develop a steady-state physical-based mathematical model for the experimental EDAC system.

This Chapter reports the development of a steady-state physical-based model for the experimental EDAC system with reference to some of the existing DX A/C models reviewed in Section 2.5. Firstly, the development and experimental validation of the steady-state model for EDAC system are reported. Secondly, using the validated model, a modeling study for an EDAC system was carried out to further demonstrate its ability to provide variable dehumidification ability and to optimize the sizing of the two evaporators used in the EDAC system and the modeling study results are presented. Finally, conclusions are given.

6.2 Development of a steady-state mathematical model for the EDAC system at the EDAC mode

For the proposed EDAC system, as mentioned, it can be operated at both ADO and EDAC modes. However, the current model development only covered the mode of enhanced dehumidification (EDAC), i.e., with both HX1 and HX2 operated. This Section reports the development of a steady-state mathematical model for the EDAC system at the EDAC mode, taking reference to an existing dual-evaporator air conditioning (DEAC) model [Pan et al., 2012]. The thermal properties of R410A were obtained from Refprop [Lemmon et al., 2013] and the State Equations for humid air from ASHRAE Handbook [ASHRAE, 2009].

The following assumptions were made in the model development:

On the refrigerant-side of the EDAC system:

- Refrigerant: R410A;
- A fixed setting of degree of refrigerant sub-cooling, T_{sc} , at 5 °C [Whitman et al., 2012];
- Isenthalpic expansion in the EEVs;
- The heat gain by or loss from the refrigerant lines on the refrigerant-side of the EDAC system was initially given fixed values, but subject to experimental verification later;
- The refrigerant at both inlet and outlet of receiver was isenthalpic;
- Isentropic efficiency and volumetric efficiency of the compressor were evaluated based on its pressure ratio (PR) [Hwang, 2004] ($\eta_{isen}=0.9-0.046 \cdot PR$, $\eta_{vol}=1-0.04 \cdot PR$);

- Compressor motor efficiency: 0.95 [ASHRAE, 2008].

On the air-side of the EDAC system:

- Pressure drops along the ducts and fittings: a constant value was initially given, but subject to experimental verification later;
- No ventilation air;
- The air streams passing through HX1 and VCD1 were well mixed;
- The air mixing process was adiabatic;
- Homogeneous and annular air flow;
- Counter-flow heat exchange between the air and refrigerant in HX1 and HX2;
- The heat gains from supply air fan and ductwork was represented by an increase in supply air temperature and its actual value varied linearly with the supply air flow rate between 1 and 2 °C.

6.2.1 Steady-state modeling of the experimental EDAC system at EDAC mode

A conceptual model of the EDAC system is shown in Fig. 6.1. It was made up of two sub-models for its refrigerant-side and air-side, respectively.

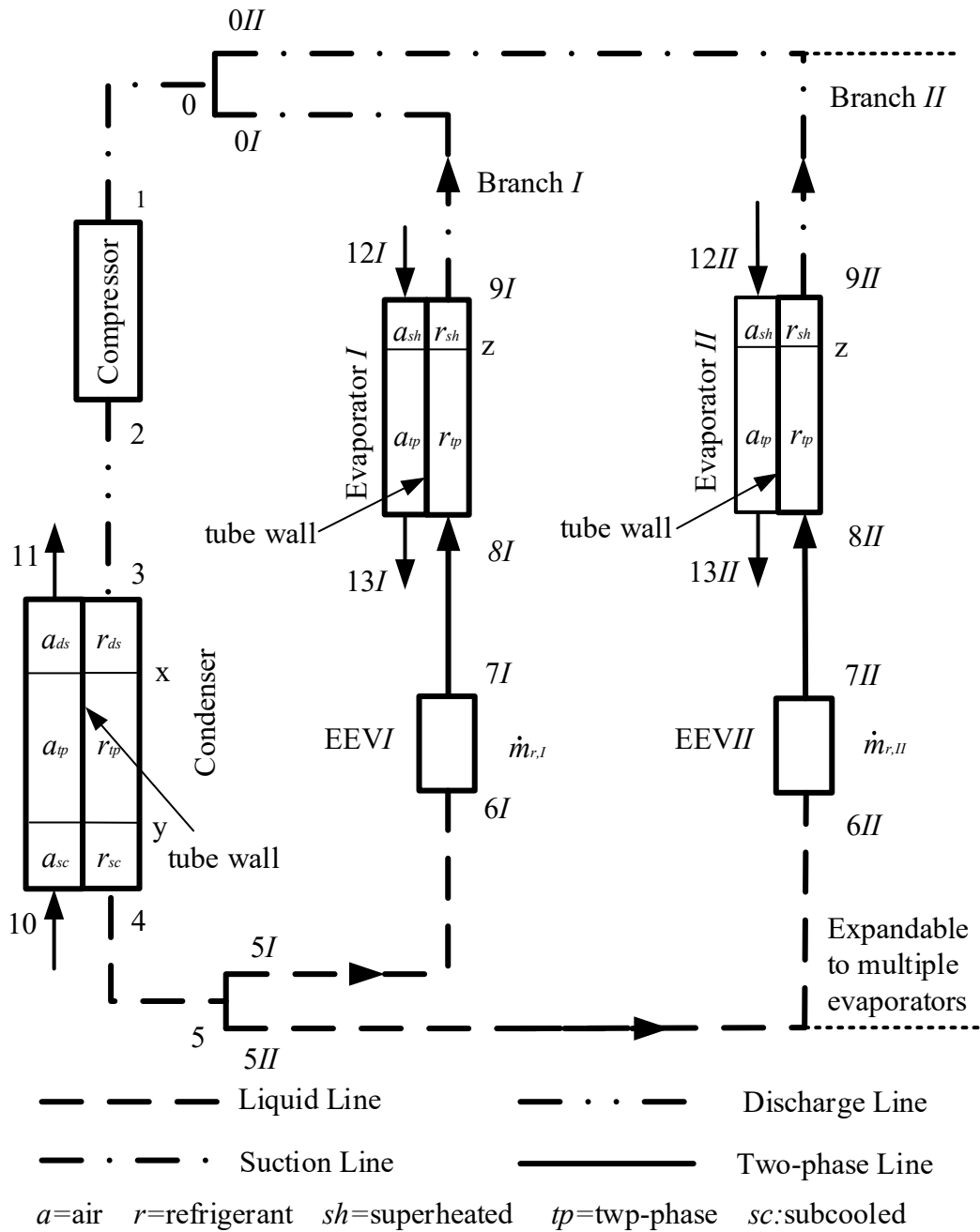


Fig. 6.2 An existing conceptual model for the DEAC system [Pan et al., 2012]

This experimental EDAC system was in fact similar to a DEAC system, and it was noted that a steady-state mathematical model for such a DEAC system was previously developed and reported by Pan et al. [2012], with its conceptual model shown in Fig. 6.2. The DEAC system model was also made of the sub-models for both refrigerant-side and air-side. As seen from both figures, the refrigerant-sides for both systems were exactly the same, so that the sub-model for the refrigerant-side of the DEAC

system was directly adopted without any modifications in modeling the experimental EDAC system for its refrigerant-side. However, the air-side in the EDAC system was different from that in the DEAC system as follows:

For the conceptual model for the EDAC system shown in Fig. 6.1, it can be seen that in its air-side, HX1 and HX2 were in series, and air flowed firstly through HX1 and VCD1, which were in parallel, and then through HX2, using only one supply fan. However, for the model for the DEAC system shown in Fig. 6.2, the air-sides for the two indoor cooling coils were not connected, with their own supply fans. Apart from these, all other processes including the heat and mass transfer taking place in the two coils were similar. Consequently, all the other equations in the sub-model for the air-side of the DEAC system may be adopted except that the following equations describing the hydraulic characteristics for the air-side of the EDAC system, as shown in Fig. 6.3 and its related energy and mass balances were added or replaced:

Hydraulic characteristics:

$$m_a = m_{aHX1} + m_{aVCD1} = m_{aHX2} \quad (6.1)$$

$$DP_{fan} - DP_{VCD1} - DP_{HX2} - DP_{duct} = P_S - P_I \quad (6.2)$$

$$P_S - P_I = 0 \quad (6.3)$$

$$DP_{VCD1} = DP_{HX1} \quad (6.4)$$

Energy and mass balances:

$$m_{aHX1} (h_{aI} - h_{aII}) = Q_{aHX1} \quad (6.5)$$

$$m_{aHX1} h_{aII} + m_{aVCD1} h_{aII'} = m_a h_{aIII} \quad (6.6)$$

$$m_{aHX1} d_{aII} + m_{aVCD1} d_{aII'} = m_a d_{aIII} \quad (6.7)$$

$$m_{aHX2} (h_{aIII} - h_{aIV}) = Q_{aHX2} \quad (6.8)$$

$$m_{aHX2} h_{aIV} + Q_{afan} = m_a h_{aS} \quad (6.9)$$

$$m_{aHX2} d_{aIV} = m_a d_{aS} \quad (6.10)$$

The final model for the proposed EDAC system was therefore made of the refrigerant-side sub-model of 18 equations and the air-side sub-model of 31 equations including Equations (6.1-6.10). Except for the 10 equations listed above, all the other 39 equations were available from Pan et al. [2012].

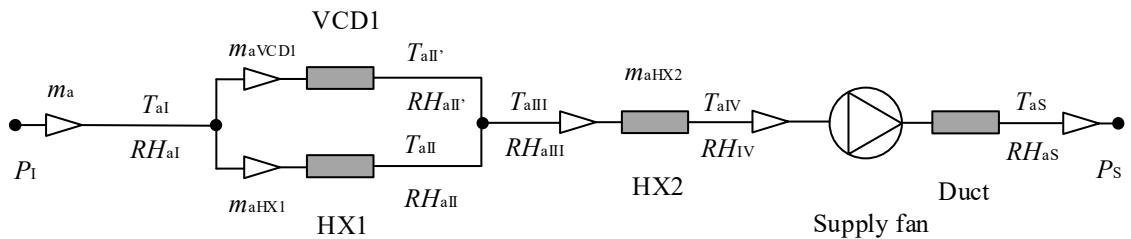


Fig. 6.3 Schematic diagram of the hydraulic network for the air-side in the proposed EDAC system

6.2.2 Numerical procedure for solving the EDAC model

The refrigerant-side sub-model and air-side sub-model were linked together via the metal temperatures of tube wall in both HX1 and HX2. The flow chart for solving the complete EDAC system model is shown in Fig. 6.4. The detailed explanations for the calculation procedures are given as follows:

There were five iteration loops when solving the model. The first one (Loop I) was for the evaluation of the compressor discharge pressure, P_{r2} . The second and third ones (Loop II and Loop III) were for evaluating the refrigerant mass flow rates passing through HX1 and HX2, m_{rHX1} and m_{rHX2} , respectively. Finally, the fourth and fifth ones (Loop IV and Loop V) were for obtaining the compressor suction pressure and temperature, P_{r1} and T_{r1} , respectively.

After the initial values of T_{r1} , P_{r1} , h_{r1} and P_{r2} were assumed, the refrigerant mass flow rate passing through the compressor, m_{rcom} , could be obtained by solving compressor module. Thus the refrigerant pressure at compressor suction, or point 0 in Fig. 6.1, P_{r0} , was evaluated by the pressure drop equations for the pipelines [Pan et al., 2012]. The degree of refrigerant sub-cooling at condenser outlet, $T_{sc,calc}$, which was calculated using condenser module, was used as an index for Loop I convergence. If a convergence was not reached, a new P_{r2} value was assumed, and the calculations in the Loop I would not stop until $T_{sc,calc}$ was equal to its assumed value of 5 °C.

After the calculations in Loop I were completed, the refrigerant state at condenser outlet was obtained. Then, the calculations in Loop II and III began. With the assumed m_{rHX1} and m_{rHX2} , the refrigerant pressures at the end of each branch for the HX1 and HX2, P_{r0_1} and P_{r0_2} , could be obtained by solving the modules for HX1 / HX2 and

their matching EEVs, and the pressure drop equations for the refrigerant pipelines. Since the two branches were connected in parallel to the suction of a common compressor, the values of P_{r0_1} and P_{r0_2} should be the same and further equal to P_{r0} . If this was not the case, m_{rHX1} and m_{rHX2} were respectively updated to ensure that both P_{r0_1} and P_{r0_2} were equal to P_{r0} . At the same time, key system parameters on the air-sides of HX1/HX2 such as supply air temperature and relative humidity, T_{aS} and RH_{aS} , could also be evaluated by solving the sub-model for the air-side of the EDAC system.

The evaluated m_{rcom} from Loop I, was used as a convergence criterion for Loop IV. If the convergence was not reached, a new P_{r1} value was assumed, and the calculations in the Loop IV would not stop until the sum of m_{rHX1} and m_{rHX2} , which was updated from Loops II and III, was equal to m_{rcom} .

After the calculations in Loop IV were finished, the enthalpy at compressor suction, $h_{r1,calc}$, was obtained by solving the equations for refrigerant mixing [Pan et al., 2012], and was used as a convergence index for Loop V. The assumed value of T_{r1} was therefore updated until $h_{r1,calc}$ was equal to the assumed enthalpy at compressor suction, h_{r1} .

When all the convergence requirements in the five iteration loops were satisfied, the calculation process for the EDAC model was ended.

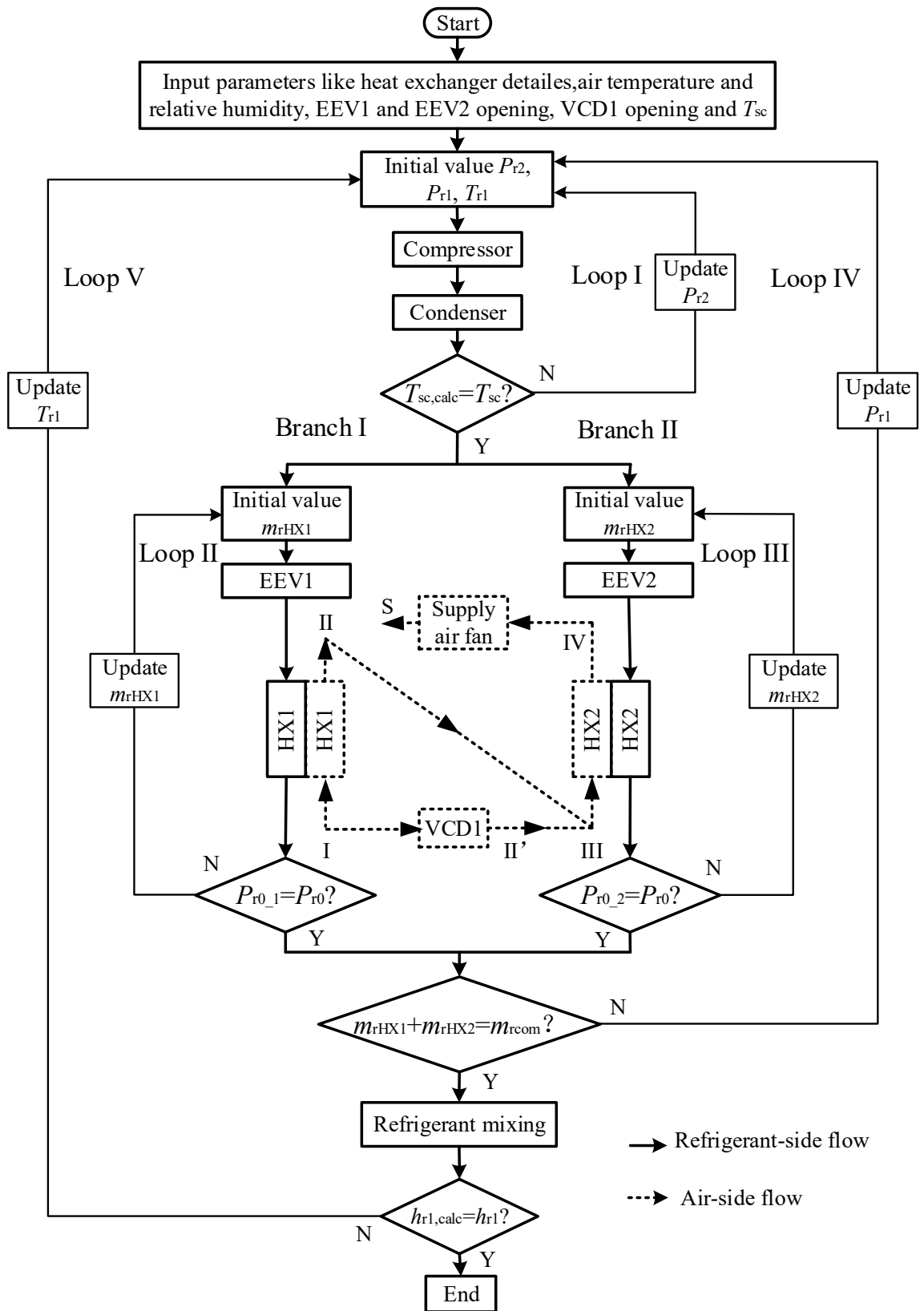


Fig. 6.4 Flow chart of the calculation procedure of the complete EDAC system model

6.3 Experimental validation of the EDAC model

The experimental results presented in Chapter 5 for the five experimental cases as shown in Tables 5.1 and 5.2, were used for model experimental validation.

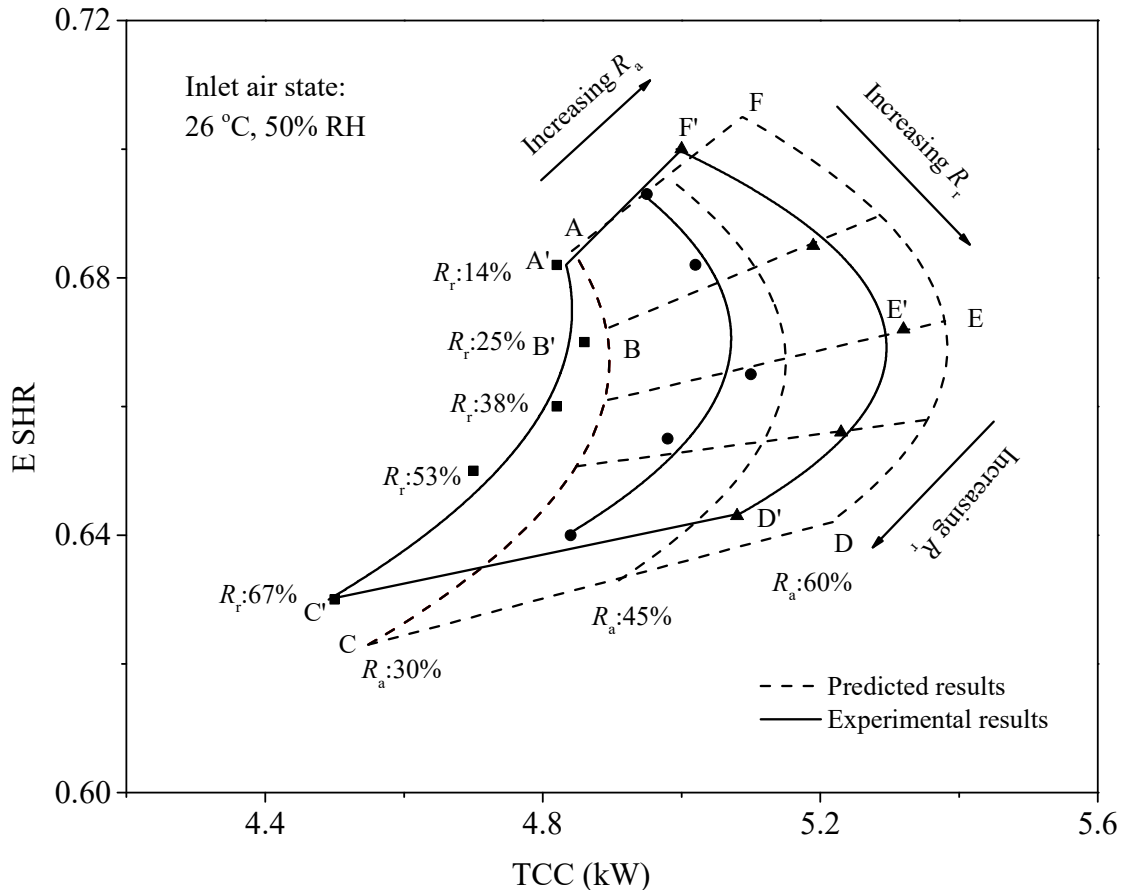


Fig. 6.5 Comparison of the predicted and experimental TCC and ESHR at the inlet air state of 26 °C and 50% RH (Case RH-50 or T-26)

As an example, the predicted and experimental results of TCC and ESHR at the inlet air state of 26 °C and 50% RH (Case RH-50 or T-26) were X (TCC) and Y (ESH) plotted in Fig. 6.5, as two irregular areas of ABCDEF and A'B'C'D'E'F', respectively. In the figure, Points A (A') and C (C') correspond to the predicted (experimental) TCC / ESHR values when the EDAC system was operated at its lowest and highest R_r values of 14% and 67%, respectively, while R_a was fixed at its lowest

level of 30%. Similarly, Points F (F') and D (D') correspond to the predicted (experimental) TCC / E SHR values when the system was operated at its lowest and highest R_r values of 14% and 67%, respectively, while R_a was maintained at its highest level of 60%. Points B (B') and E (E') correspond to the TCC / E SHR values with the maximum TCC on the borderlines ABC (A'B'C') and DEF (D'E'F'), respectively.

As seen from Fig. 6.5, the shapes of the two irregular areas, ABCDEF and A'B'C'D'E'F' were similar to each other. At a fixed R_a value, when R_r was increased from 14% to 67%, both the predicted and experimental TCC values experienced similar variation trends of increasing, peaking and decreasing, while both E SHR values were decreased. In addition, at a constant R_r value, when R_a was increased from 30% to 60%, both the predicted and experimental TCC / E SHR values were increased. Also seen from the figure, the maximum relative error between predicted and experimental TCC values at each R_a / R_r combination was only at 3.5% and that for E SHR value was at 2.5%. On the other hand, the accuracy of the developed model was further examined by comparing the predicted and experimental TCC / E SHR values at all the five experimental cases, as shown in Fig 6.6 for TCC values and Fig. 6.7 for E SHR values, respectively. As seen, the relative errors between predicted and experimental TCC values were all within 8%, but only 4% for 80% of the data sets, while the relative errors between predicted and experimental E SHR values within 4%.

The above comparisons demonstrated that the model developed can predict the operational characteristics of the EDAC system in terms of TCC and E SHR at different inlet air states, with an adequately high accuracy and therefore was used in a follow-up modeling study to demonstrate that the EDAC system was able to provide

variable dehumidification ability and to optimize the sizes of two evaporators, to be reported in Section 6.4.

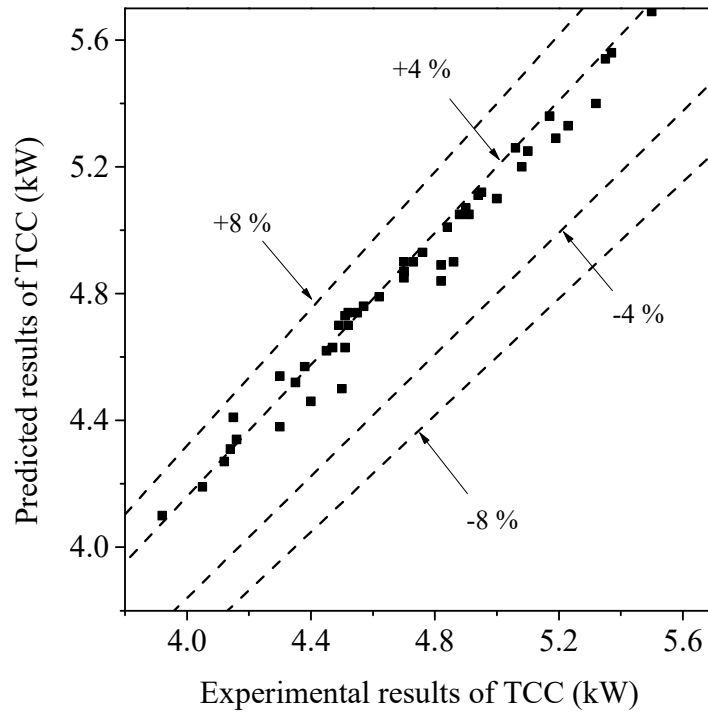


Fig. 6.6 Comparison of the predicted and experimental TCC values at all the five experimental cases

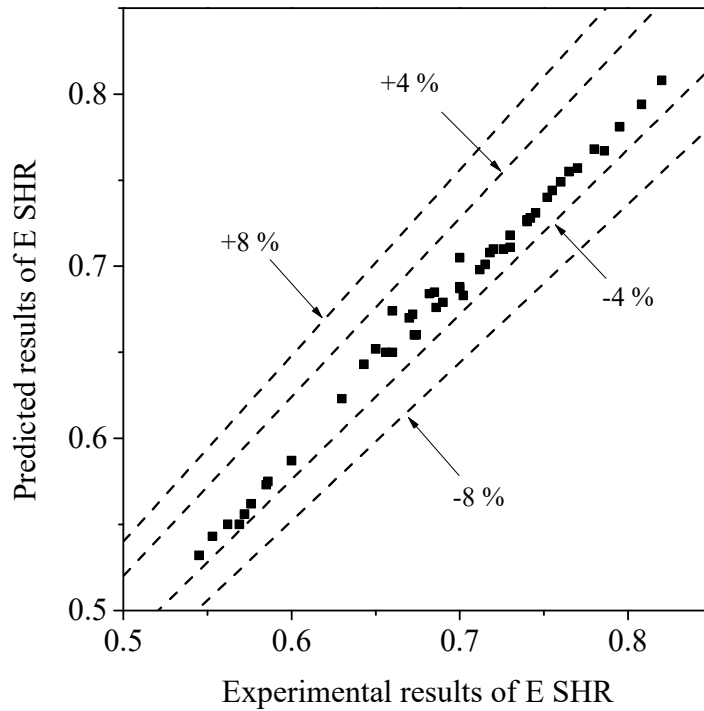


Fig. 6.7 Comparison of the predicted and experimental E SHR values at all the five experimental cases

6.4 The follow-up modeling study

Using the validated model for the EDAC system, a follow-up modeling study was carried out and the study results are presented in this Section.

6.4.1 EDAC system's ability to provide variable dehumidification ability

It was necessary to demonstrate that the EDAC system was able to provide variable dehumidification ability, as it was so intended. This was done by comparing its simulated operational characteristics with those of the other two commonly used DX A/C systems. The first one was a conventional On-Off controlled single evaporator DX A/C system and the second a variable speed (VS) DX A/C system.

For the On-Off controlled A/C system, at its full-load condition, its output TCC and E SHR value could be evaluated by using a previously developed single evaporator A/C (SEAC) system model [Chen and Deng, 2006]. However, at the part load conditions, when its compressor was cycled off, an existing cyclic model previously developed by Shirey III et al. [2006] was used to evaluate E SHR values. This cyclic model took into account the degradation of dehumidification when the moisture that was condensed on coil surfaces during an On-period of a compressor evaporated back into air steam when the compressor was off. On the other hand, the experimental operational characteristics of a VS A/C system in terms of the relationship between TCC and E SHR under different combinations of compressor and supply fan speed at various inlet air states previously reported by Xia et al. [2017] were used for comparison purpose.

For a fair comparison, while the sum of the surface areas of HX1 and HX2 was assumed to be equal to the surface area of the DX evaporator used in both the On-Off A/C system and the VS A/C system, all the other parameters related to system configurations, operational settings and the inlet air state were exactly the same for the three A/C systems: EDAC, On-Off controlled and VS. Furthermore, the area ratio of HX1 to HX2 in the simulated EDAC system was fixed at 1:2, in accordance with the experimental EDAC system described in Chapter 4.

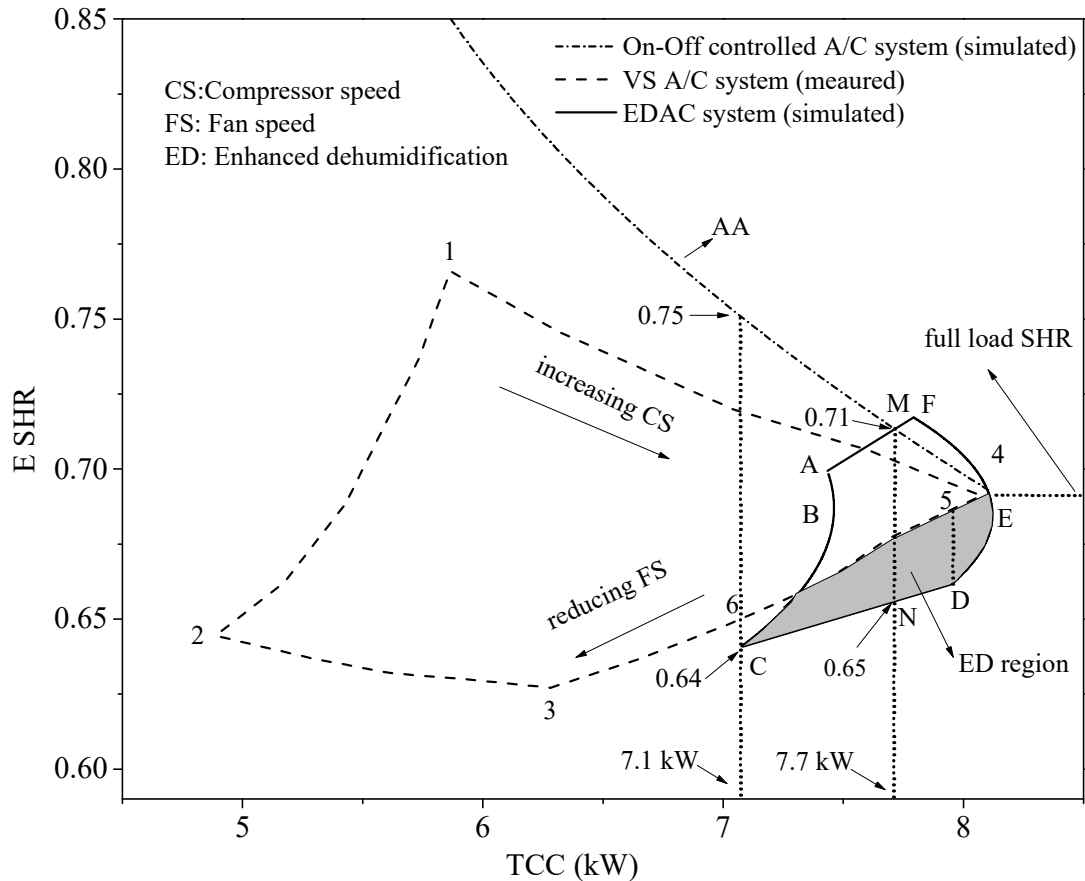


Fig. 6.8 The operational characteristics of different DX A/C systems at the same inlet air state of 25 °C and 50% RH

Using the validated model reported in this Chapter, the previous SEAC model and the cyclic model, the operational characteristics in terms of the relationship between TCC and E SHR of the EDAC system and On-Off controlled SEAC system were simulated and compared to the experimental data for the VS A/C system from Xia et al. [2017]. As an example, Fig. 6.8 shows the simulated and experimental results for the three systems at a fixed inlet air state at 25 °C and 50% RH. In Fig. 6.8, the trapezoid 1234 represents the experimental data from the VS DX A/C system, and the irregular shape ABCDEF and the curve AA the simulated data from the EDAC system and the On-Off controlled DX A/C system, respectively. As shown, when the three systems were operated at their respective full-load conditions, their TCC / E SHR values were

similar to one another. However, the situation became quite different when they were operated at part-load conditions, with details as follows:

From Fig. 6.8, it is seen that unlike the On-Off controlled A/C system that could only provide a fixed E SHR at a fixed TCC, the EDAC system was able to produce a relative wide range of E SHR, enabling its dealing with variable latent space loads. For example, as shown in Fig. 6.8, at a fixed TCC of 7.7 kW, the corresponding E SHR for the On-Off controlled A/C system was fixed at 0.71 (Point M). However, for the EDAC system, it could provide variable E SHR values from 0.65 to 0.71 (from Point N to Point M). Furthermore, for the On-Off controlled A/C system, when the required TCC was decreased at part-load conditions, its output E SHR was increased significantly or its dehumidification ability was deteriorated. However, the E SHR values of the EDAC system may even be decreased, which was beneficial to better dehumidification. For example, when the required TCC was at 7.1 kW, E SHR of the EDAC system was 0.64 (Point C), much lower than that of the On-Off controlled A/C system at 0.75, indicating a 43.7% increase in latent cooling capacity.

From Fig. 6.8, it can also be seen that similar to the VS A/C system, the EDAC system could produce several TCC / E SHR combinations to deal with sensible and latent space loads using fixed compressor and fan speeds. Although the ranges of TCC and E SHR values provided by the EDAC system were not as large as that produced by the VS system, it was understandable that if variable compressor and fan speeds were used in EDAC system, the EDAC system would have been able to produce many irregular areas, each corresponding to a compressor / fan speed combination, enlarging its range for the TCC and E SHR values. Furthermore, for the VS A/C system, lowering its supply air fan speed could effectively enhance its dehumidification ability.

However, this would also lead to a considerable decrease in its output TCC, especially at a higher compressor speed, i.e., represented by the borderline 3-4. Therefore, a so-called enhanced dehumidification (ED) region may be identified in Fig. 6.8, in which the EDAC system can have a better dehumidification ability by avoiding the negative impacts of lowering supply air fan speed on the output TCC. For example, the EDAC system could provide an 8.5% increase in latent cooling capacity at Point D and 3% at Point C, as compared to that from VS A/C system represented by Point 5 and Point 6, respectively.

6.4.2 Sizing optimization for the two evaporators in the EDAC system

Since there were two evaporators in an EDAC system and each had its distinguished cooling / dehumidifying function, the relative size of the two evaporators, in terms of their surface area ratio can affect the overall operational characteristics of the EDAC system. Hence, using the validated model, the impacts of different surface area ratios on the operational characteristics of the EDAC system were numerically studied and are reported in this Section.

For a cooling coil, its total surface area was determined based on the peak cooling load it handled. The ratio of surface area for the two evaporators (R_s) in an EDAC system, HX1 and HX2 was defined using Equation (6.11).

$$R_s = \frac{A_{HX1}}{A_{HX2}} \quad (6.11)$$

Where A_{HX1} is the total surface area of HX1 and A_{HX2} the total surface area of HX2.

At five different R_s values of 1:3, 2:5, 1:2, 2:3 and 1:1, the operational characteristics of the EDAC system in terms of relationship between TCC and E SHR at all the combinations of R_a and R_r shown in Table 5.2, at five different experimental cases shown in Table 5.1 were simulated using the validated model.

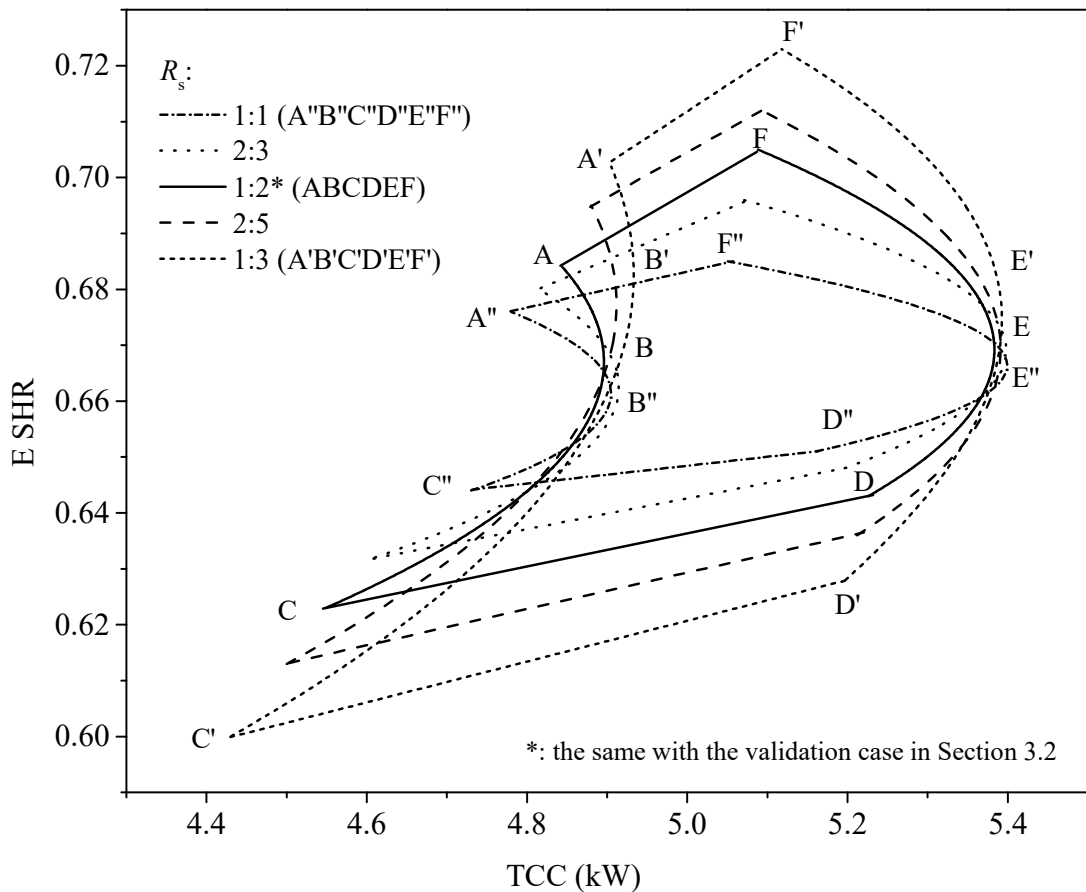


Fig. 6.9 The operational characteristics of the EDAC system with different R_s values at an inlet air state of 26 °C and 50% RH

As an example, Fig. 6.9 shows the simulated operational characteristics of the EDAC system at the fixed inlet air state of 26 °C and 50% RH. In Fig. 6.9, the irregular areas of A''B''C''D''E''F'', ABCDEF and A'B'C'D'E'F' represent the simulated results of the TCC / E SHR relationships for the EDAC system at R_s values of 1:1, 1:2 and 1:3, respectively. As shown, the variation in R_s value would significantly influence the shape of these irregular areas. When R_s was decreased from 1:1 to 1:3, the high limit

of TCC value stayed almost unchanged at 5.39 kW (at Point E'', E and E'), while the low limit of TCC value was decreased from 4.73 kW at Point C'' to 4.42 kW at Point C', leading to a 47% increase in the range between high-low limits for TCC from 0.66 kW at an R_s value of 1:1 to 0.97 kW at an R_s value of 1:3. On the other hand, the high limit of E SHR value was increased from 0.685 at Point F'' to 0.723 at Point F', while the low limit was decreased from 0.644 at Point C'' to 0.6 at Point C'. Thus, the range between high-low limits for E SHR was significantly increased from 0.041 at an R_s value of 1:1 to 0.123 at an R_s value of 1:3.

Furthermore, the influences of varying R_r and R_a on the operational characteristics in terms of the relationship between TCC and E SHR appeared different at different R_s values. As seen from Fig. 6.9, the curvatures of borderlines A''B''C'' and D''E''F'' was more obvious than those of borderlines A'B'C' and D'E'F', suggesting that increasing R_r at a higher R_s would impact more on TCC values than E SHR values, and the slopes of borderlines A''F'' and C''D'' were smaller than those of borderlines A'F' and C'D', indicating that the changes in R_a at a higher R_s influenced more on TCC values but less on E SHR values than those at a lower R_s .

Therefore, the simulated results suggested that using a lower R_s could lead to a larger variation range of TCC and E SHR, and the variation in R_s would influence E SHR more than TCC. It was noted that a further advantage of having two coils of a lower surface area ratio was that when HX1 or HX2 functioned separately, both can suitably meet the variations in the cooling and dehumidification requirements at different seasons.

For an EDAC system, the simulated results suggested that a lower R_s was beneficial to enlarging the variation range of output TCC and E SHR. However, care should be

exercised when using a lower R_s for the following two reasons. Firstly, when R_s was too small, the range of TCC may be enlarged due to a decrease in the low limit of TCC. However, this may also deteriorate the system efficiency when using a larger R_r . In such a case, HX1 is not able to provide enough heat to evaporate all refrigerant passing through it, so that the degree of refrigerant superheat at HX2's exit will be unreasonably large so as to maintain an appropriate degree of refrigerant superheat at the compressor suction. Secondly, as mentioned in Section 2.1, an EDAC system may also operate as a dehumidifier with HX1 functioning solely to cool and dehumidify air and HX2 as a condenser to reheat the cooled and dehumidified air. Therefore, there should be a minimum value of the surface area of HX1, thus guaranteeing a certain dehumidification capacity of the EDAC system when it is used as a dehumidifier.

6.4.3 Discussion

In this modeling study, it was verified that the EDAC system could provide variable dehumidification ability. However, there have two issues that should be considered in future studies, as follows:

The first is that in this modeling study, a simple lumped parameter counter flow evaporator model where an evaporator was divided into one single-phase zone and one two-phase zone was used. In each zone, constant air properties and heat and mass transfer coefficients were assumed. However, the actual temperature distribution on the surface of an evaporator was much more complicated, and the changes in the surface areas of both HX1 and HX2 would make the distribution even more complicated. It was therefore hard for the developed EDAC model to accurately reflect temperature variations. Hence, a distributed parameter model where the whole evaporator was divided into a number of control volumes and varying Lewis Number

[Xia et al., 2010] can be adopted to increase the predicting accuracy of the EDAC model. This would nonetheless result in an increased computational effort and thus a higher development cost. Therefore, in the future work, developing a hybrid EDAC model which would consist of a distributed sub-model for its evaporator and empirical modules for the other system components such as EEVs and compressor to save the development cost, should be considered [Xu et al., 2014].

The second is that, in the current study, an On-Off controlled solenoid valve SV2, with a fixed opening area was used in order to reduce the initial cost for an EDAC system. However, it was understandable that if the opening area of SV2 can be varied, a wider range for the evaporating pressure in HX2 can then be achieved, thus further enlarging the variation range of TCC and E SHR for the EDAC system at the EDAC mode.

6.5 Conclusions

In this Chapter, by referring a previously developed dual-evaporator A/C model, a physical-based steady-state model made of a total of 49 equations for the experimental EDAC system at EDAC mode, i.e., when both evaporators were operated was developed. The model was experimentally validated using the measured data from the experimental EDAC system, with an acceptable predicting accuracy. Using the validated EDAC model, a follow-up modeling study was carried out to demonstrate that the EDAC system was able to provide variable dehumidification ability and to optimize the sizing of the two evaporators used in the EDAC system. The modeling study results indicated that the EDAC system was able to provide variable dehumidification ability as compared to a conventional On-Off controlled single evaporator DX A/C system and a VS DX A/C system. The modeling study results also

suggested that using a lower ratio of surface area for the two evaporators in an EDAC system could enlarge the variation ranges in both TCC and E SHR at the EDAC mode, but at different magnitudes. Therefore, the model developed provided an effective platform in studying the operational characteristics of the EDAC system at different operating conditions and with different system configurations, so as to better design, operate and control the EDAC system for improved indoor thermal environmental control.

Chapter 7

Development of a control strategy for the EDAC system for its year-round operation

7.1 Introduction

To enable the EDAC system to be operated over a wide range of part-load conditions to maintain an improved year-round indoor humidity level, as one of the project objectives, a control strategy to operate an EDAC system on a year-round basis should be developed.

As mentioned in Chapter 4, the EDAC system is intended to be operated on a year-round basis, with two modes, an ADO mode and an EDAC mode. In Chapters 5 and 6, the operational characteristics of the experimental EDAC system operated at EDAC mode, were experimentally studied, and a steady-state mathematical model for the EDAC system at EDAC mode was developed. Therefore, in this Chapter, the development of a control strategy for the EDAC system for achieving improved year-round indoor air humidity level is presented. Firstly, the developed control strategy for the EDAC system is presented. Then using the prototype experimental EDAC system as described in Chapter 4, two set of experiments to verify if the EDAC system was operational in different seasons to adequately deal with indoor sensible and latent loads, and to evaluate the operating performances of the developed control strategy, were carried out, and the experimental results and related discussions are reported. Finally, conclusions are given.

7.2 Development of the year-round control strategy for the EDAC system

A complete year-round control strategy whose flow chart is shown in Fig. 7.1 was purposely developed. It was previously noted that the EEVs in the EDAC system were tasked with three different functions at different operating modes: to function as a stop valve to shut off the supply of refrigerant to the heat exchangers ($EEV_i=0, i=1, 2$), to control the degree of refrigerant superheat ($EEV_i=1, i=1, 2$) and to act as a modulating valve to regulate the refrigerant mass flow rate passing through heat exchangers ($EEV_i=2, i=1, 2$)

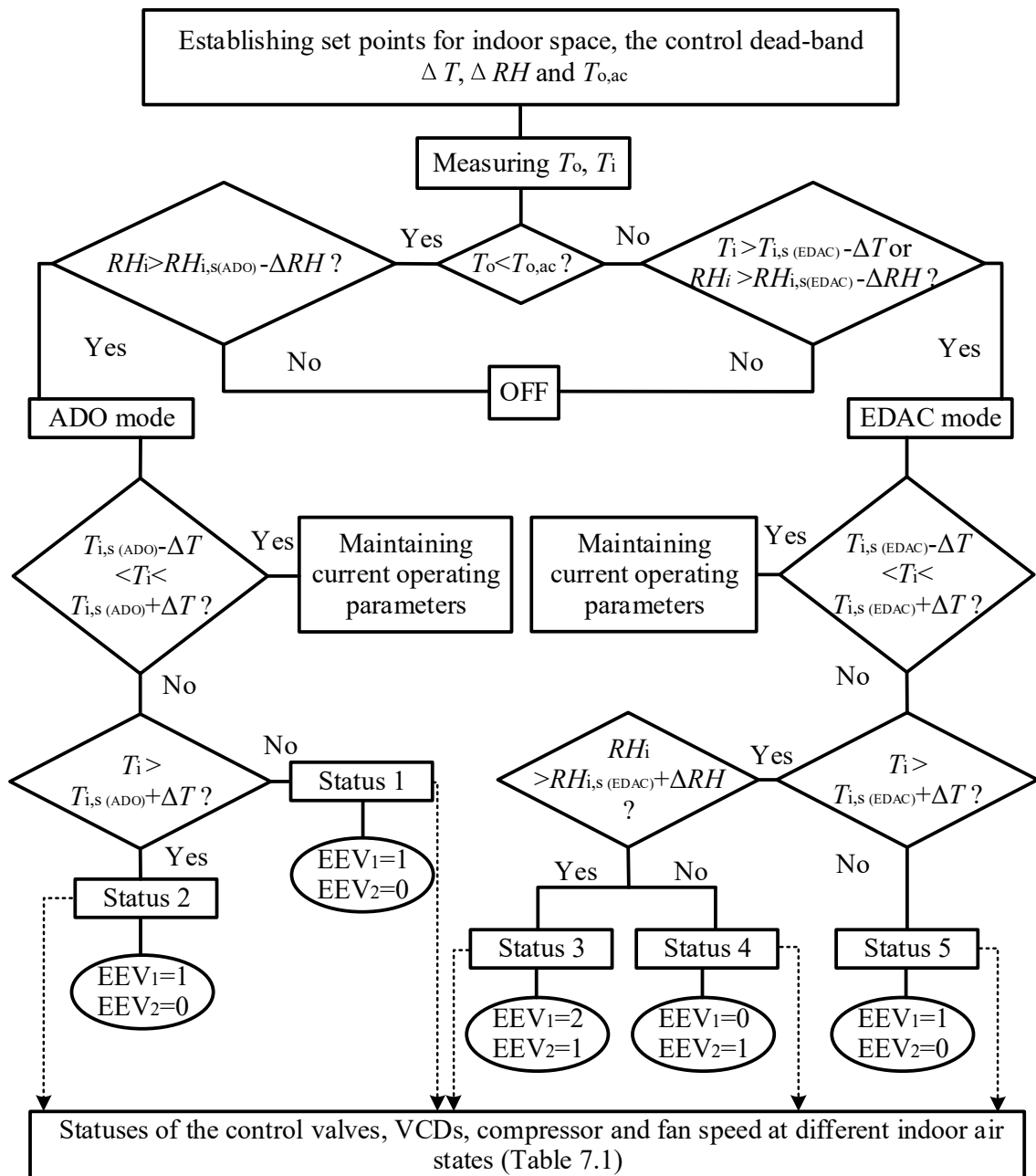


Fig. 7.1 Flow chart of the year-round control strategy for the EDAC system for improved indoor humidity level

Table 7.1 Statuses of the control valves and VCDs at different operating modes

Mode	Air dehumidification only (ADO)		Enhanced dehumidification Air Conditioning (EDAC)		
	1	2	3	4	5
SV1	O	O	C	C	C
SV2	C	C	O	O	O
SV3	O	O	C	C	C
VCD1	C	C	O*	O	C
VCD2	C	C	C	C	O
Compressor speed	L	L	H	H	L
Supply fan speed	L	L	H	H	L
Condenser fan speed	S	L	H	H	L
Note: O: fully open C: fully close O*: partially open H: high capacity/speed L: low capacity/speed S: shutdown					

ADO mode

The EDAC system is operated in ADO mode when $T_o \leq T_{o,ac}$ and $RH_i > RH_{i,s(ADO)} - \Delta RH$, where $T_{o,ac}$ is the outdoor air temperature above which air conditioning is required, $RH_{i,s(ADO)}$ indoor air relative humidity set point at ADO mode and ΔRH relative humidity control dead-band. Therefore, ADO mode usually occurs in Period I as specified in Section 2.3.2. At this mode, depending on indoor air state, there are two different combinations of open/close status for all valves and VCDs, and compressor and fan speeds, namely Status 1 and Status 2, as shown in Table 7.1.

At ADO mode, when indoor air temperature, T_i , is lower than $T_{i,s(\text{ADO})} - \Delta T$, where $T_{i,s(\text{ADO})}$ is indoor air temperature set point at ADO mode and ΔT temperature control dead-band, the EDAC system is operated at Status 1. At this Status, the condenser fan is stopped, so that HX2 acts as a main condenser to reheat the cooled and dehumidified air. If T_i is higher than $T_{i,s(\text{ADO})} + \Delta T$, the EDAC system is operated at Status 2, where the condenser fan runs at a low speed to allow more condensation heat being rejected to the air cooled condenser and less to HX2, thus lowering supply air temperature, T_s , for a lower T_i . However, when the indoor air temperature is within the dead-band, the current operational status remains unchanged. Therefore, at ADO mode, indoor air temperature control is realized by varying the operation durations between Status 1 and 2, while indoor air RH is indirectly controlled, depending on the dehumidification abilities of the EDAC system at the two statuses. At this operational mode, both compressor and supply fan operate at low speeds and both VCDs are fully closed.

EDAC mode

The EDAC system is operated in EDAC mode when $T_o > T_{o,ac}$ and $T_i > T_{i,s(\text{EDAC})} - \Delta T$ or $RH_i > RH_{i,s(\text{EDAC})} - \Delta RH$, where $T_{i,s(\text{EDAC})}$ and $RH_{i,s(\text{EDAC})}$ are the settings for indoor air temperature and RH in EDAC mode, respectively. Therefore, EDAC mode usually takes place during at Periods II and III as also specified in Section 2.3.2. At this mode, depending on indoor air state, there can be three different status of open/close positions for all valves and VCDs, and compressor and fan speeds, namely Status 3, 4 and 5, as shown also in Table 7.1. At Status 3, both HX1 and HX2 are put into operation, acting as two evaporators. However HX2 only operates at Status 4 and HX1 at Status 5.

At EDAC mode, firstly, the EDAC system will be operated at a default Status (Status 4), Once T_i is lower than the low boundary of the dead-band, instead of being completely shut down the compressor as in a conventional On-Off controlled DX A/C system, the operation of the EDAC system will move to Status 5. If both T_i and RH_i are higher than their respective high boundary of the dead-bands, the EDAC system will operated at Status 3. If indoor air temperature is within its dead-band, the current operational status remains.

However, it is noted that the change between Status 4 and Status 5 cannot be instantly implemented since an immediate shutdown of the operations of either HX1 or HX2 would increase the risk of operating instabilities in the EDAC system, even lead to a sudden compressor shutdown. Therefore, a transitional control program for switching between Status 4 and 5 is implemented, so that when switching between Status 4 and 5, the matching EEV for an operating HX will be gradually opened and the other EEV slowly closed, thus supporting a stable transition between the two statuses.

Furthermore, when the EDAC system is operated at Status 3, both indoor air temperature and RH can be directly controlled, with the help of VCD1, EEV1 and EEV2. According to the experimental results shown in Chapter 5, when the EDAC system is operated at Status 3, the output TCC of the EDAC system is increased monotonously in response to the decrease of VCD1 opening but would experience a unique variation trend of increasing, peaking and decreasing with the variation of EEV1 and EEV2 openings, while the E SHR is monotonic to the change of EEV1 and EEV2 openings. Therefore, if a PI-based controller is used, VCD1 acts in response to the indoor temperature while EEV1 to the indoor RH and EEV2 to the degree of refrigerant superheat of the EDAC system. Furthermore, in order to eliminate the input

disturbances thus avoiding frequent changes of the openings of VCD1 and EEV1, which is not beneficial to the stable operation of the EDAC system, a cascade control logic for Status 3 has been specially proposed. As shown in Fig. 7.2, there are two control loops for both temperature and humidity control: an inner PI loop with fast response to eliminate input disturbances and an outer PI loop to regulate output for the EDAC system.

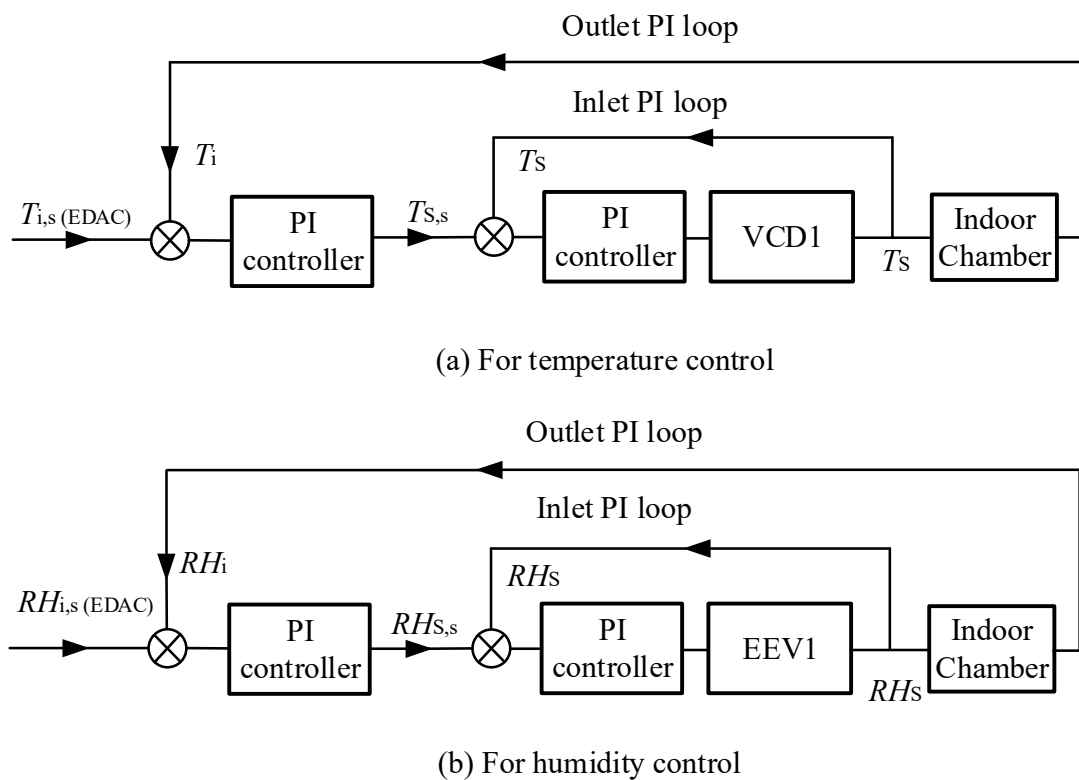


Fig. 7.2 Cascade PI controllers at Status 3

Although there are totally five statuses, except at Status 3, the EDAC system is the same as or similar to a conventional DX A/C system at the other four statuses. Furthermore, the PI control adopted at Status 3 has been commonly used. Therefore, the control principle for the EDAC system is simple and reliable, involving no complex calculation algorithms such as artificial neural network (ANN) [Li et al., 2012, 2013] and fuzzy logic [Li et al., 2015a; Yan et al., 2018], etc. The development cost of the EDAC system including the proposed control strategy is hence low.

7.3 Experimental conditions

In order to verify if the EDAC system was operational in different seasons to adequately deal with indoor sensible and latent loads, and to evaluate the operating performances of the developed control strategy, two Sets of experiments were carried out using the prototype experimental EDAC system described in Chapter 4, with Set A for the ADO mode and Set B the EDAC mode, as shown in Table 7.2. Furthermore, to carry out experimental work under all possible indoor sensible / latent loads was neither practical nor necessary, therefore, representative discrete values of indoor sensible / latent loads as shown in Table 7.2 were selected to represent the typical space cooling load characteristics in different seasons. For example, indoor sensible and latent load combination of 0 / 1000 W represented the cold and humid climate, 2000 / 900 W hot and dry climate, and 3100 / 1550 W hot and humid climate. Furthermore, air temperature and RH in the simulated outdoor space were respectively maintained at 25 °C, 80% RH in Set A experiments, and 33 °C, 68% RH in Set B experiments, respectively, in accordance with outdoor air conditions in different seasons, using the existing separate A/C system and the LGU placed there.

Table 7.2 Experimental conditions and cases

Set A Outdoor air temperature and RH: 25 °C, 80% RH (ADO mode)		
No	Fixed settings	Changed settings
A1 [#]	$T_{i,s(ADO)} / RH_{i,s(ADO)}$	Sensible / Latent load (W)
	26 °C / 50%	0 / 900 200 / 900 300 / 1100
A2 [*]	Sensible / Latent load (W)	$T_{i,s(ADO)} / RH_{i,s(ADO)}$
	0 / 1000	26 °C / 50% 25 °C / 50%
Set B Outdoor air temperature and RH: 33 °C, 68% RH (EDAC mode)		
No	Fixed settings	Changed settings
	$T_{i,s(EDAC)} / RH_{i,s(EDAC)}$	Sensible / Latent load (W)
B1 [#]	26 °C / 50%	2000 / 900 2100 / 1100
B2 [#]	26 °C / 50%	3100 / 1550 3200 / 1750
	Sensible / Latent load (W)	$T_{i,s(EDAC)} / RH_{i,s(EDAC)}$
B3 [*]	2000 / 1000	26 °C / 50% 25 °C / 50%
B4 [*]	3100 / 1650	26 °C / 50% 25 °C / 50%
B5 [*]	3100 / 1650	26 °C / 50% 26 °C / 40%

[#] disturbance rejection test ^{*} command following test

As shown in Table 7.2, there were two different types of tests in both test Sets, i.e., disturbance rejection test and command following test. In the disturbance rejection test, there were three tests (A1, B1 and B2), where indoor air temperature and RH settings remained unchanged at 26 °C and 50% RH, but the space cooling load in the indoor space was altered at a time. In the command following test (A2, B3, B4 and B5), while space sensible and latent cooling loads in the indoor room remained

unchanged during the tests, indoor air temperature set-points were changed from 26 °C to 25 °C at a time. Furthermore, given that the EDAC system was able to directly control indoor air RH when it was operated at Status 3, in Test B5, indoor air RH setting would also be changed from 50% to 40% to evaluate the performance with respect to indoor humidity control.

For each of the tests listed in Table 7.2, the test duration was 12000 s. Before changes were introduced, the experimental EDAC system was operated at a steady condition and all experimental conditions and control settings before the changes as shown in Table 7.2 maintained. The changes as specified in Table 7.2 were then introduced and each test went on for a further period till a further change was introduced or to the end of the test.

During experiments, the high speeds of the compressor, supply fan and condenser fan were set at 80%, 90% and 100% of their maximum speeds, or 4800 rpm, 1400 rpm and 2800 rpm, respectively, and their low speeds 40%, 45% and 50% of their maximum speeds, or 2400 rpm, 700 rpm and 1400 rpm, respectively. On the other hand, in order to prevent frequent change between each status, a dead-band of 0.5 °C for indoor air temperature and 5% for indoor air RH were respectively introduced. Furthermore, in order to simplify the experimental procedure, no fresh air was introduced as indoor thermal loads were fully represented by LGUs.

7.4 Experimental results and discussions

Using the experimental EDAC system and following the experimental conditions and cases presented in Section 7.3, extensive experiments have been conducted and experimental data collected. In this Section, the measured operating performances of

the experimental EDAC system at the ADO mode and the EDAC mode, expressed in terms of the variations of indoor air temperature and RH, are firstly presented in Sections 7.4.1 and 7.4.2, respectively. Secondly, the improved humidity control and energy saving potential when using the EDAC system at both modes are discussed based on the experimental results.

7.4.1 The measured operating performances of the EDAC system under the year-round control strategy at the ADO mode (Set A)

Figs. 7.3 and 7.4 show the experimental results of indoor air temperature and RH in Test A1 and A2 of Set A, respectively. In Set A, indoor space sensible load was low but latent load was high, thus the EDAC system was operated at ADO mode. As seen from Figs. 7.3 and 7.4, at ADO mode, the operational status of the EDAC system would be switched between Status 1 and Status 2. Indoor air temperature was raised at Status 1 and lowered at Status 2, while indoor RH level exhibited the same variation pattern but with a small variation range. This suggested that the EDAC system could output a larger reheat capacity but a slightly smaller dehumidification capacity during Status 1 than those during Status 2.

As seen from Fig. 7.3 for the results of Test A1, before the first change at 4000 s, indoor air temperature was oscillated around its set point but within its dead-band. After the indoor sensible load was increased at 4000 s, the EDAC system and the control strategy responded, so that the variation of indoor air temperature was within the expected control range. However, the operation duration of Status 2 was prolonged and that of Status 1 shortened, as a result of increased sensible load, leading to a slightly lower indoor air RH level. On the other hand, since the compressor speed and

supply fan speed were fixed, a longer On-period of condenser fan would result in a higher power input to the EDAC system from 0.83 kWh to 0.97 kWh. When indoor latent load was increased at 8200 s, the operation duration of Status 2 was further prolonged and that of Status 1 further shortened as a result of increased sensible load. However, indoor averaged air RH was increased from 47.8% to 50.9% due to the increased latent load and the power input into the EDAC system was increased from 0.97 kWh to 1.1 kWh due to a longer On-period of condenser fan.

Furthermore, as seen in Fig. 7.4 for the results of Test A2, as indoor air temperature setting was reduced by 1 °C at 6000 s, the operation duration of Status 2 was increased while that of Status 1 decreased as a result of reduced reheating demand by HX2. As seen, the EDAC system and the control strategy could appropriately respond, so that the new indoor air temperature setting of 25 °C was maintained. However, as the dehumidification ability of HX1 did not change much, a lower indoor air temperature would lead to a higher indoor air RH level. Therefore, the averaged indoor air RH was slightly increased from 49.8% to 51.4%. Correspondingly, the power input to the EDAC system was also increased due to a longer On-period of the condenser fan

From the results shown in Figs. 7.3 and 7.4 for both the disturbance reject test and command following test it is seen, while indoor air temperature could be controlled within the control range, indoor air RH could only be indirectly controlled and was mainly influenced by indoor thermal loads and indoor air temperature settings. The nature of directly controlling indoor air temperature and indirectly controlling RH when the EDAC system was operated at ADO mode as a dehumidifier, the robustness of the control strategy and the variations in the power input to the EDAC system are demonstrated in both figures.

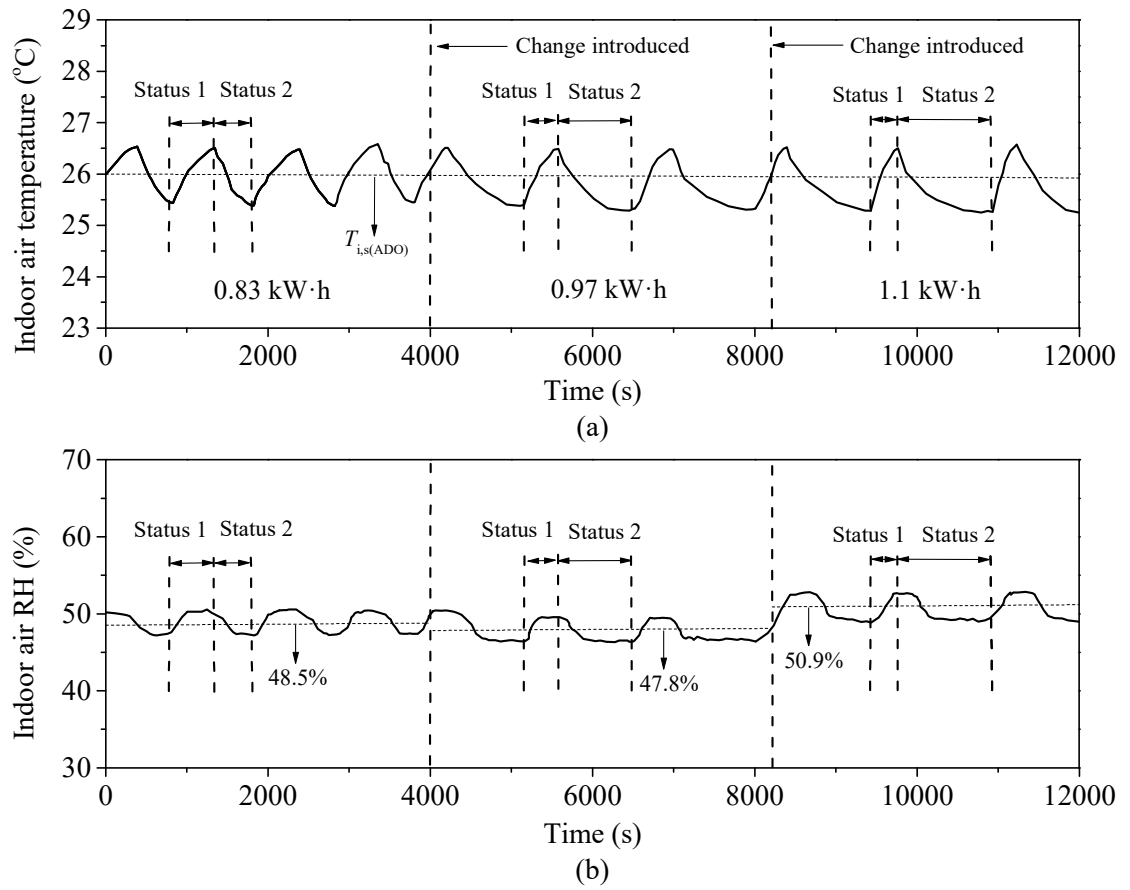


Fig. 7.3 Measured variations in indoor air temperature and RH in Test A1

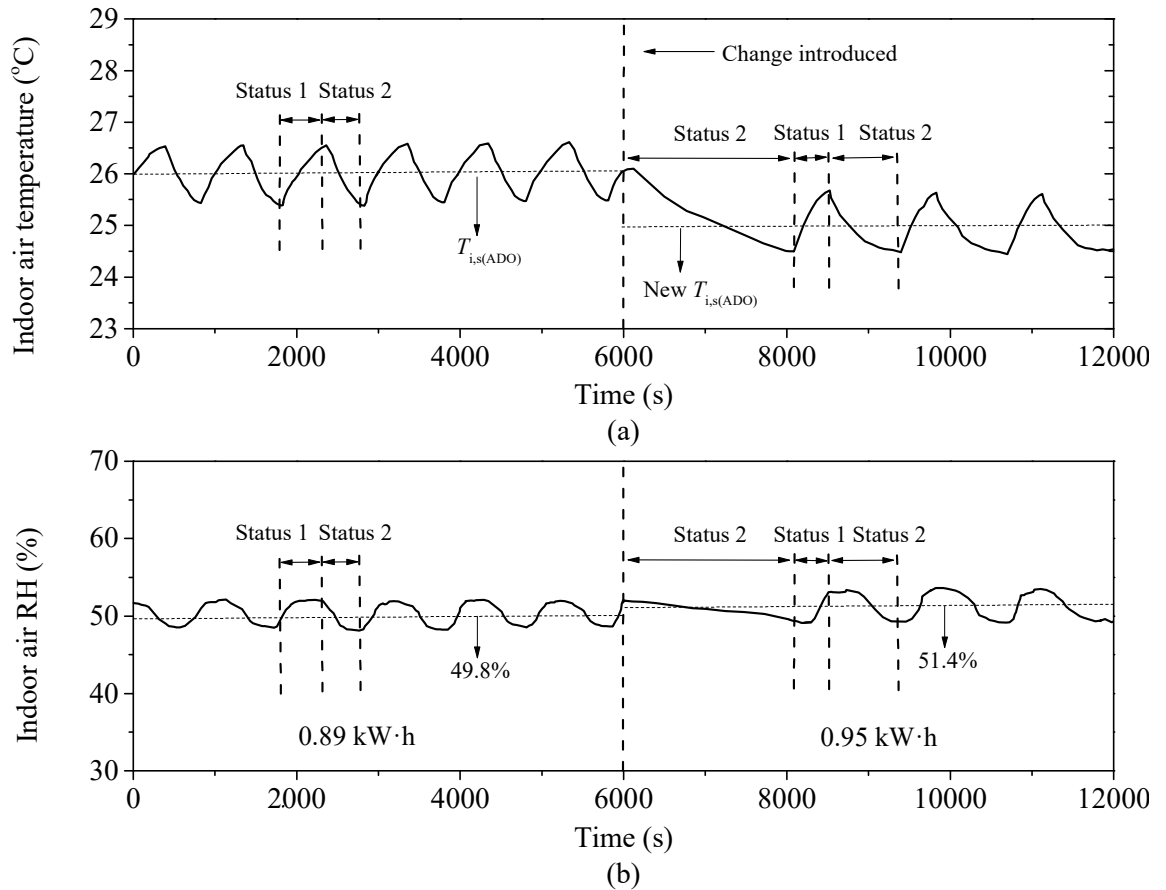


Fig. 7.4 Measured variations in indoor air temperature and RH in Test A2

7.4.2 The measured operating performances of the EDAC system under the year-round control strategy at the EDAC mode (Set B)

Fig. 7.5 to Fig. 7.9 show the experimental results of Tests B1 to B5 in Set B, respectively, when the EDAC system was operated at EDAC mode. As seen from the figures, when the sensible space load was high but latent load was low, the EDAC system was operated at either Statuses 4 or 5 (Test B1 and Test B3). The EDAC system was operated at Status 3 when both sensible and latent loads were high (Tests B2, B4 and B5). These were consistent with original intention when developing the control strategy. On the other hand, the measured variations in indoor air temperature and RH were different in these tests, with details as follows:

Test B1 and B3

Fig. 7.5 and Fig. 7.6 show the experimental results of Test B1 and B3, respectively. As seen from Figs. 7.5 and 7.6, the EDAC system could operate stably and significant temperature and RH fluctuations during switching between Statuses 4 and 5 were avoided using the transitional control program mentioned in Section 2.2. For the two tests, generally, indoor RH level was low but temperature was high at Status 5 but the other way around at Status 4, suggesting that a larger dehumidification ability and smaller sensible cooling capacity was provided by the EDAC system at Status 5 than at Status 4.

As seen from Fig. 7.5 for Test B1 results, indoor air temperature was stable, oscillating around the set point within the dead-band before both the sensible and latent loads were increased at 5300 s. After the changes, the operation duration at Status 4 was prolonged and that at Status 5 shortened for the EDAC system, resulting in an increased indoor RH level from 51.1% to 54.7%. However, the variation of indoor air temperature was still maintained within the control range. Therefore, the EDAC system and the control strategy could appropriately respond to the changes in this disturbance rejection test to maintain indoor air temperature at its control range, but with a slight increase in indoor RH, since latent load was increased. On the other hand, since the compressor and supply fan speeds at Status 4 were higher than those at Status 5, the power input to the EDAC system was therefore increased from 1.23 kWh to 1.42 kWh due to a longer operation duration at Status 4.

Furthermore, as seen from Fig. 7.6 for the results of Test B3, as indoor air temperature setting was reduced by 1 °C at 5200 s, the operation duration of Status 4 was increased while that of Status 5 reduced as a result of increased cooling demand by the EDAC

system. As seen, the EDAC system and the control strategy responded accordingly, so that indoor air temperature was maintained at its new setting of 25 °C. Since the dehumidification ability of the EDAC system at Status 5 was larger than that at Status 4, and indoor air temperature setting was reduced, a higher indoor air RH level from 48.3% to 52% would be resulted in. This demonstrated that in the command following test, the EDAC system and the control strategy could appropriately respond to the change in indoor air temperature setting, directly controlling indoor air temperature to its new setting, but passively controlling indoor air RH. For the power input to the EDAC system, it was increased from 1.33 kWh to 1.54 kWh due to a longer operation duration at Status 4.

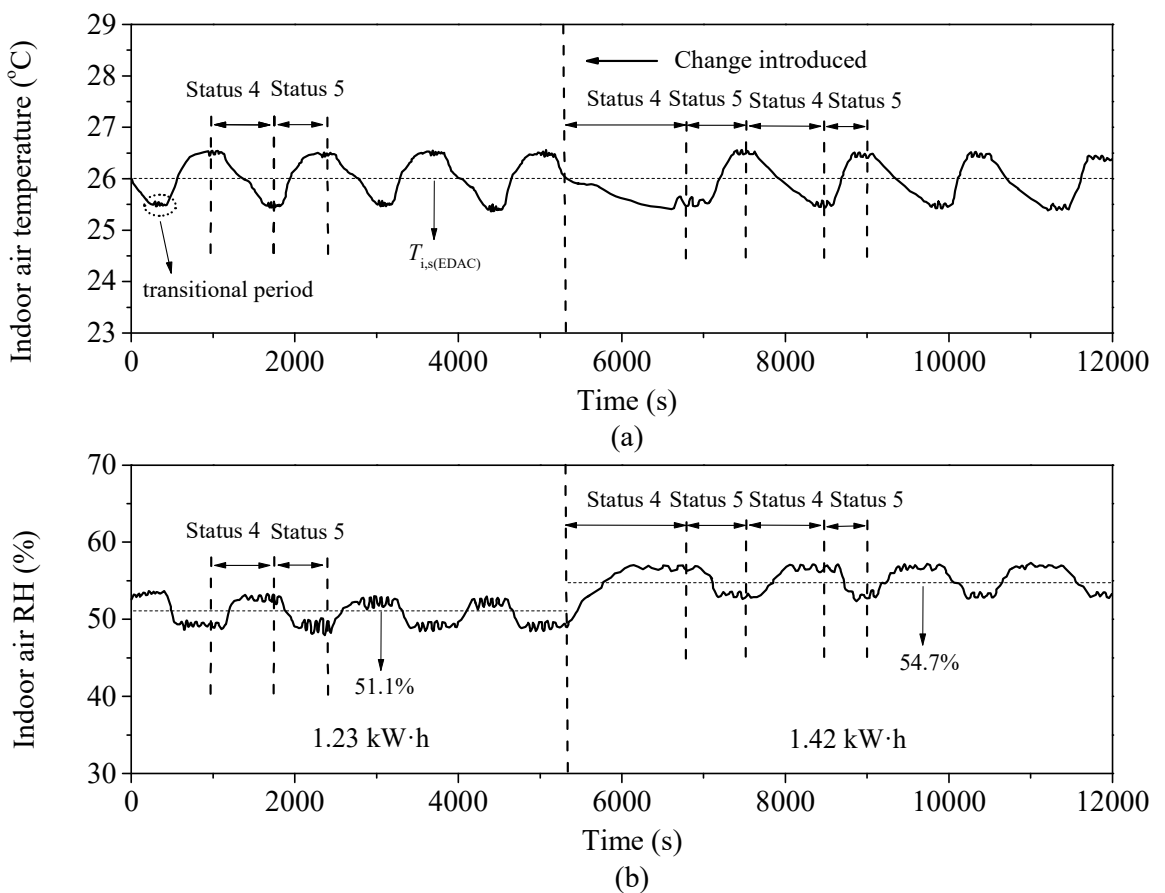


Fig. 7.5 Measured variations in indoor air temperature and RH in Test B1

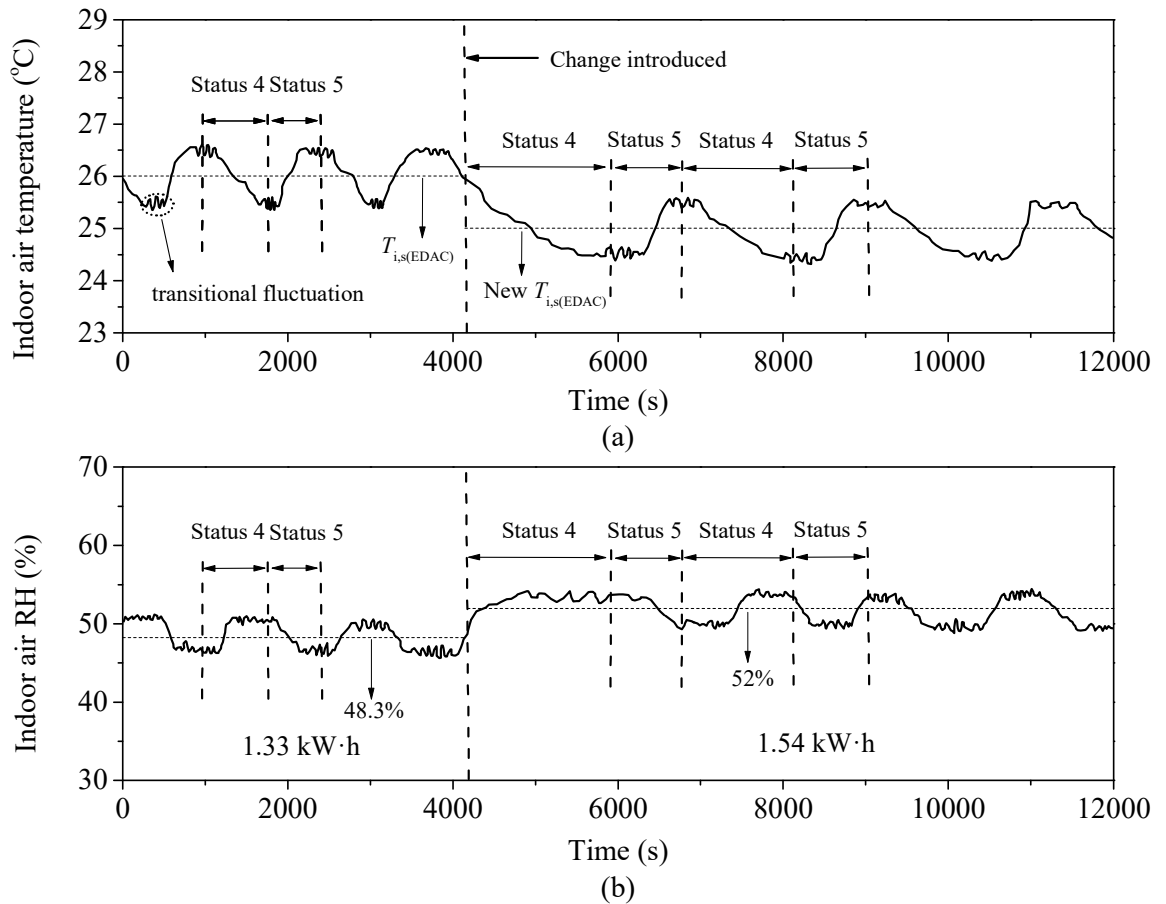


Fig. 7.6 Measured variations in indoor air temperature and RH in Test B3

Test B2, B4 and B5

Figs. 7.7 to 7.9 show the experimental results of Test B2, B4 and B5 respectively. As seen from the figures, unlike the EDAC system operated at other statuses when indoor air temperature can be directly controlled but indoor air RH indirectly controlled, at Status 3, both indoor air temperature and RH could be simultaneously controlled to their respective set points.

As seen from Fig. 7.7 for the measured results of Test B2, before sensible and latent loads were increased at 3600 s, both indoor air temperature and RH were controlled at around their respective settings but with small variations when using the developed Cascade PI controllers at Status 3. After the changes, the EDAC system and the control

strategy responded to output variable cooling and dehumidification capacities to match the new sensible and latent loads. Consequently, indoor air temperature and RH would fluctuate for a while during transition before returning to their respective settings.

As seen from Fig. 7.8 for the results of Test B4. After indoor air temperature setting was reduced by 1 °C at 3600 s, the cooling demand of indoor space was increased. However, the experimental EDAC system and the control strategy appropriately responded, so that indoor air temperature and RH could be controlled to, and maintained at its new setting. On the other hand, as seen from Fig. 7.9 for the test results of Test B5, as indoor air RH setting was decreased from 50% to 40%, suggesting increased dehumidification requirement in the indoor space, the EDAC system and the control strategy responded, so that both indoor air temperature and RH could also be controlled to their respective settings. Furthermore, the variation patterns of indoor air temperature and RH would be disturbed significantly when indoor air RH setting was altered as seen in Fig. 7.9. However, as seen in Fig. 7.8, the variation patterns were not remarkably affected when changing indoor air temperature setting.

Therefore, from the results shown in Figs. 7.7 to 7.9 for both the disturbance reject test and command following test, it can be seen that when the experimental EDAC system was operated at Status 3, it could not only provide variable cooling capacity to deal with variable sensible load as at the other statuses but also output variable dehumidification ability to handle variable latent load, thus maintaining both indoor air temperature and RH at their respective settings. Under the conditions of changing indoor space sensible and latent loads or altering indoor settings, the EDAC system and control strategy could suitably respond to the changes to simultaneously control

both indoor air temperature and RH. For the power input to the EDAC system, although the speeds for compressor, supply fan and condenser fan were fixed, it could be affected by the varying space loads and indoor settings.

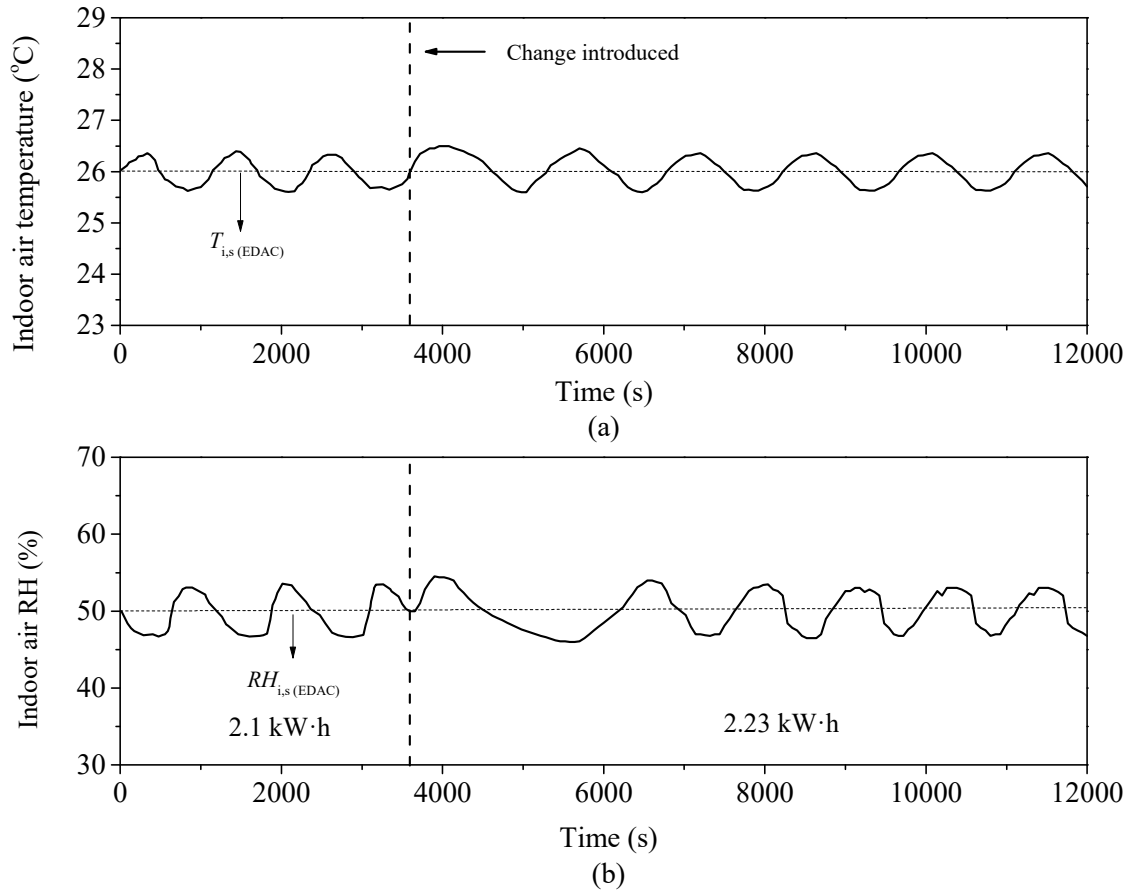


Fig. 7.7 Measured variations in indoor air temperature and RH in Test B2

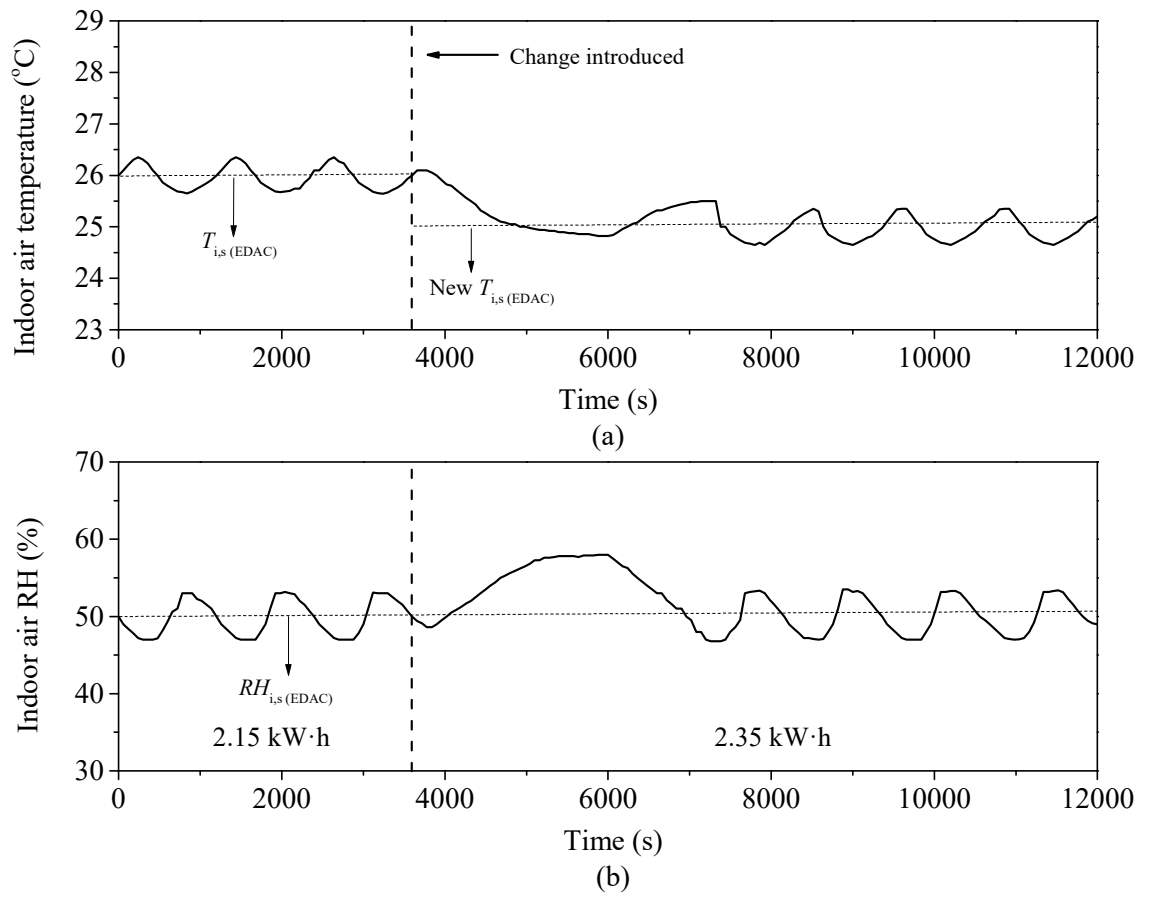


Fig. 7.8 Measured variations in indoor air temperature and RH in Test B4

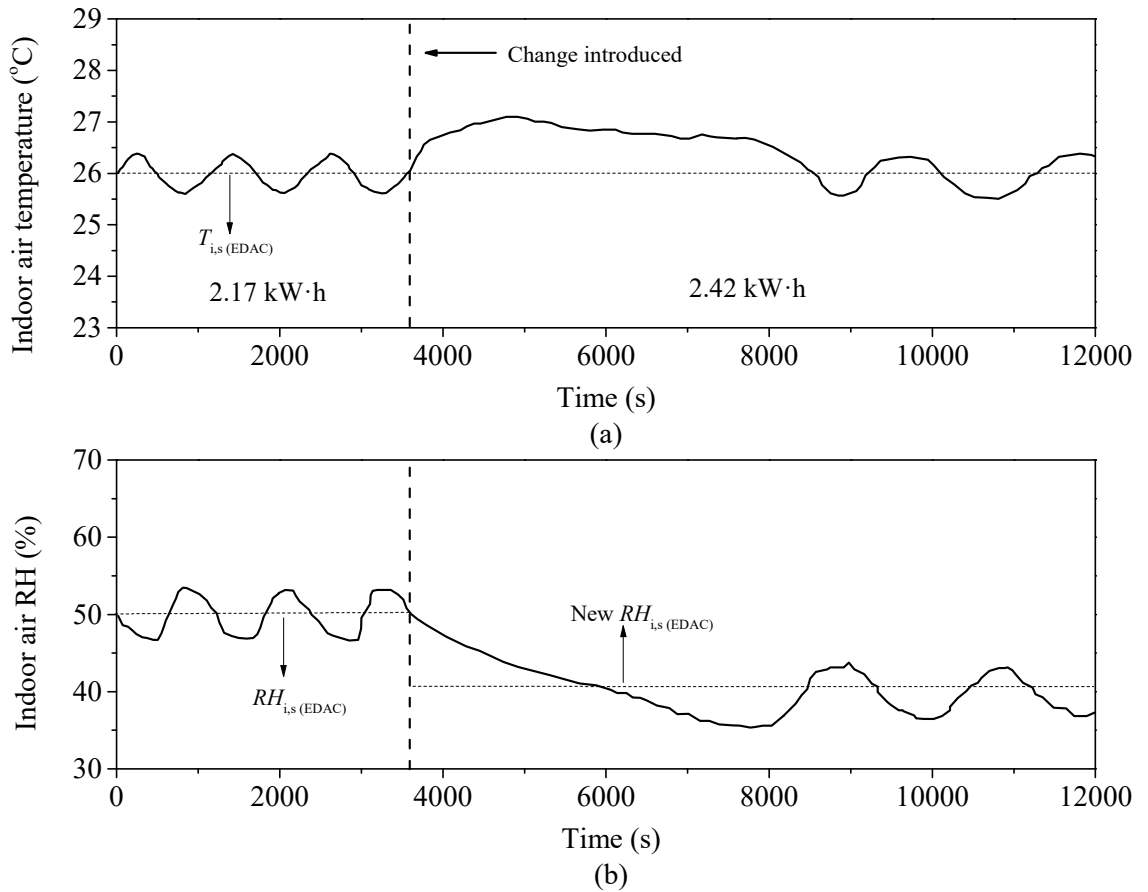


Fig. 7.9 Measured variations in indoor air temperature and RH in Test B5

7.4.3 Discussions

From the experimental results presented in Sections 7.4.1 and 7.4.2, it can be seen that unlike a conventional On-Off controlled single evaporator DX A/C system, the EDAC system could be operated at different statuses to match different space load characteristics in different seasons with the help of the developed year-round control strategy.

It was understandable that on the days when less or no additional cooling was required, a conventional On-Off controlled single evaporator DX A/C system cannot provide dehumidification unless space overcooling was allowed. However, as seen from Section 7.4.1, the EDAC system could be operated at ADO mode to provide

dehumidification while suitably controlling indoor air temperature. Furthermore, as seen from Section 7.4.2, at the EDAC mode, irrespective HX1 and / or HX2 of the EDAC system were independently or jointly operated, as long as indoor air RH setting was not met, even when indoor air temperature was already controlled to its setting, the compressor in the EDAC system would not be stopped, thereby avoiding the deterioration of dehumidification which usually took place during compressor's Off-time in an On-Off controlled single evaporator DX A/C system [Han et al., 2013; Xu et al., 2008]. In addition, the EDAC system would spend a large portion of its operating hours at Status 3, since space sensible and latent loads were often high in hot and humid climates at EDAC mode. This suggested that the EDAC system could simultaneously control indoor air temperature and RH over a relative long period, providing adequate humidity control. Therefore, improved year-round indoor humidity level could be achieved using the EDAC system.

Apart from the improved humidity control offered using the EDAC system as demonstrated above, the use of the EDAC system also lead to a higher operational energy efficiency than the use of a conventional On-Off controlled DX A/C system. The improvement in energy efficiency actually resulted from the following aspects:

- 1) When the EDAC system acted as a dehumidifier, the utilization of condensing heat can lead to a higher overall system efficiency
- 2) Since HX1 was only used when necessary at a high latent load condition, the EDAC system can be operated with a higher evaporating temperature and thus a higher efficiency when HX1 was not put into use.

- 3) With an improved indoor humidity control, indoor air dry-bulb temperature setting can be raised so that the resultant space sensible cooling load due to the temperature difference between indoor air and outdoor air was reduced.

7.5 Conclusions

A year-round control strategy was developed for the EDAC system for improved indoor humidity control and implemented in the experimental EDAC system as described in Chapter 4. Extensive experimental work has been carried out to examine both the operation of the proposed EDAC system and the controllability of the control strategy. Two sets of experiments with a total of seven tests were carried out when the EDAC system was operated at either ADO mode or EDAC mode. The experimental results suggested that the EDAC system was operational at both modes and the control strategy ensured the EDAC system to appropriately respond to the changes in both indoor thermal loads and setting during both disturbance rejection and command following tests. There were five indoor air statuses, and while indoor air temperature can be directly controlled at all statuses, indoor air RH can also be directly controlled at Status 3, and indirectly controlled due to better dehumidification at all the other statuses, as a result of changes in both indoor air temperature setting and actual latent loads.

The experimental results demonstrated that the proposed EDAC system was suitable for the use in different seasons, providing year-round improved indoor humidity control in hot and humid climates, at a higher energy efficiency.

Chapter 8

Conclusion and future work

8.1 Conclusions

A research project on firstly proposing a DX based standalone enhanced dehumidification air conditioning (EDAC) system, without employing any supplementary measures to provide variable dehumidification ability and establishing a prototype experimental EDAC system, secondly investigating the operational characteristics of the EDAC system at EDAC mode, thirdly developing and validating a steady-state physical-based mathematical model for the EDAC system also at EDAC mode and finally developing a year-round control strategy for the EDAC system for improved indoor humidity control, has been successfully carried out and is reported in this Thesis. The conclusions of the Thesis are:

- 1) An experimental study on the operational characteristics of the experimental EDAC system at the EDAC mode has been carried out and the study results are reported in Chapter 5. The results demonstrated that the EDAC system was able to provide variable dehumidification ability at a fixed inlet air state when the refrigerant and air mass flow rates to both evaporators in the experimental EDAC system was varied. The experimental results also demonstrated that inlet air temperature and relative humidity would significantly influence the operational characteristics of the EDAC system;
- 2) The development and experimental validation of a steady-state physical-based mathematical model for the experimental EDAC system is presented in Chapter 6. The model was experimentally validated, with an acceptable predicting accuracy.

Using the validated model, a follow-up modeling study confirmed that the EDAC system was able to provide variable dehumidification ability as compared to a conventional On-Off controlled single evaporator DX A/C system and a VS DX A/C system, and also suggested that using a lower ratio of surface area for the two evaporators in an EDAC system at the EDAC mode could enlarge the variation ranges in both TCC and E SHR, but at different magnitudes;

- 3) The development of a year-round control strategy of the EDAC system at both the ADO and EDAC mode for improved humidity control was developed and is presented in Chapter 7. Using the developed control strategy, the EDAC system was operational at the two operational modes to provide variable dehumidification ability and could appropriately respond to the changes in both indoor thermal loads and settings. Both indoor air temperature and RH can be directly controlled at Status 3 when both outdoor air temperature and RH were higher.

The main outcome of the proposed project is the development of a novel standalone DX based enhanced dehumidification air conditioning (EDAC) system, including the detailed experimental evaluations on its operational characteristics at different seasonal cooling loads and an experimentally validated steady-state mathematical model for the EDAC system, both at EDAC mode, and the year-round control strategy to operate the EDAC system at both ADO and EDAC modes, for improved year-round control over indoor air humidity.

The successful carrying out of the research project helped achieve better thermal comfort for occupants, improved IAQ and reduced energy use, using the EDAC systems that are less complicated and costly as compared to other technologies, so as

to save the capital and operational costs, and installation space of DX based air conditioning in buildings. The long-term significance of the research project is its contribution to sustainability through reducing energy use for air conditioning in buildings while improving the thermal comfort of building occupants, and to the advancement of DX A/C technology. While the project outcomes are expected to be applicable to all hot and humid climates, they will be particularly useful to Hong Kong where DX A/C systems are widely used and dehumidification using DX A/C systems has always been a grand challenge.

8.2 Proposed further work

Following the successful completion of the research project reported in this Thesis, a number of future possible studies are proposed as follows:

- 1) The experimental study reported in Chapter 5 illustrated the influences of the refrigerant and air mass flow rates passing through HX1 and HX2 and inlet air conditions on the operational characteristics of the EDAC system. However, other operating parameters, such as the compressor and supply fan speed could also affect the operational characteristics of an EDAC system. Therefore, it is suggested that the influences of the other operating parameters in an EDAC system on its operational characteristics should be further studied;
- 2) The predicting accuracy of the developed EDAC mathematical model may be further improved using the method mentioned in Section 6.4.3, i.e., developing a hybrid EDAC model which combines a distributed sub-model for its evaporators and empirical modules for all the other system components;

- 3) The developed steady-state EDAC model was experimentally validated with an acceptable predicting accuracy, as reported in Chapter 6. Nonetheless, a dynamic model for an EDAC system to simulate the transient system responses should be further developed, as a dynamic model is more useful in developing control strategies and diagnosing / detecting faults for EDAC systems;
- 4) The experimental study reported in Chapter 7 on the development of the year-round control strategy was carried out under finite combinations of indoor sensible / latent loads and indoor T/ RH settings, which may be insufficient in reflecting the operating performances of the experimental EDAC system over its entire operating range. More experimental cases should be carried out in the future
- 5) In order to further improve the efficiency and enlarge the variation range of TCC and E SHR for an EDAC system, the following two adjustments for the EDAC system could be considered in the future:
 - i) A solenoid valve SV2, with a variable opening area could be used.
 - ii) An ejector to reduce the irreversible pressure loss in the refrigerant mixing process at the compressor inlet could be used.

Appendix

Photos of the experimental EDAC system

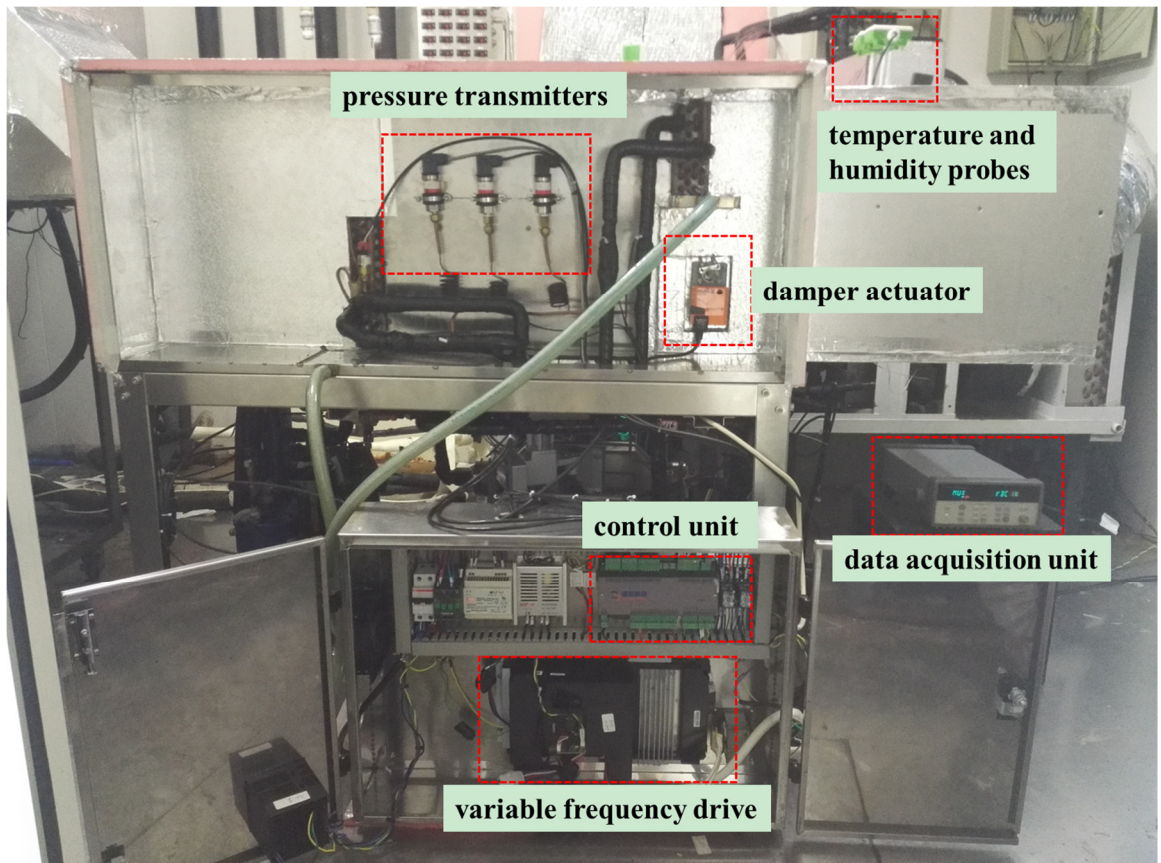


Photo 1 Overview of the experimental EDAC system (1)



Photo 2 Overview of the experimental EDAC system (2)

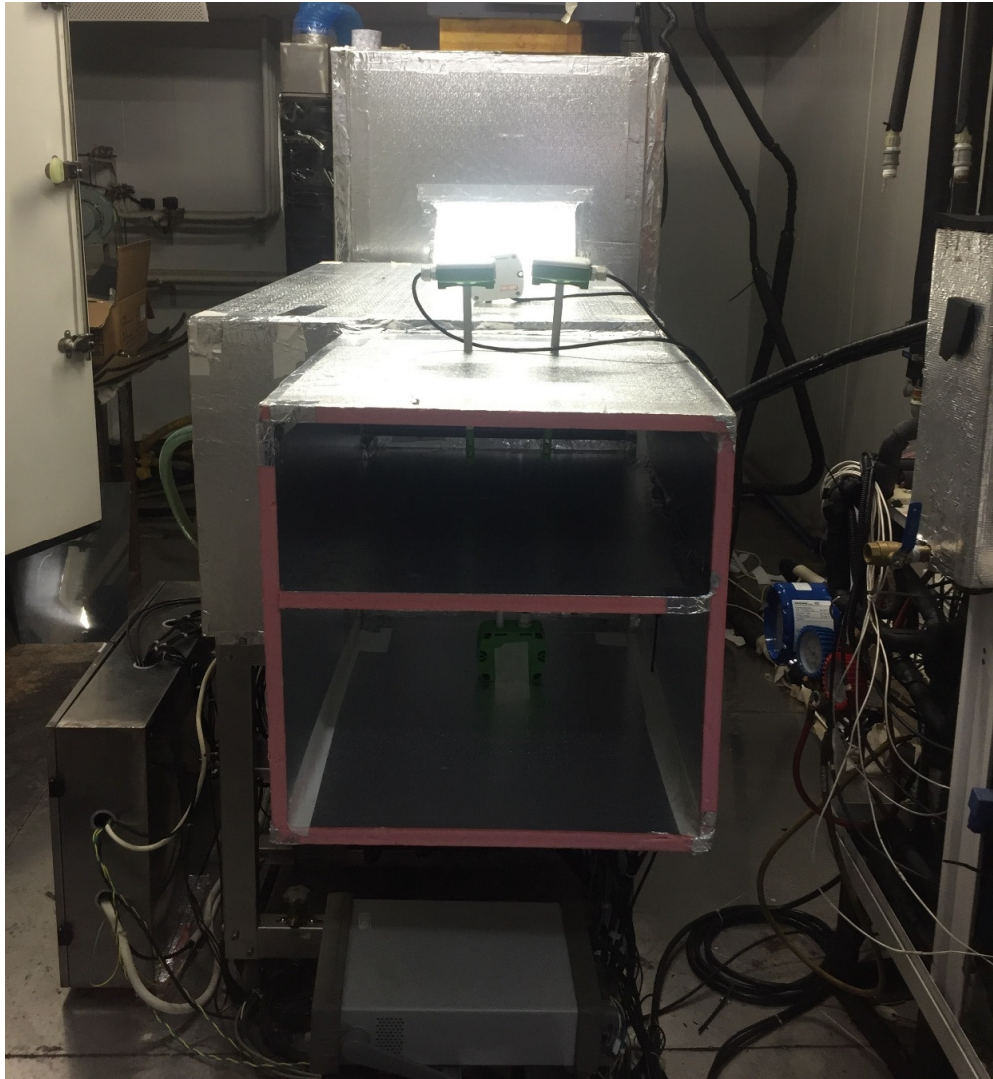


Photo 3 Overview of the air duct of the experimental EDAC system (1)

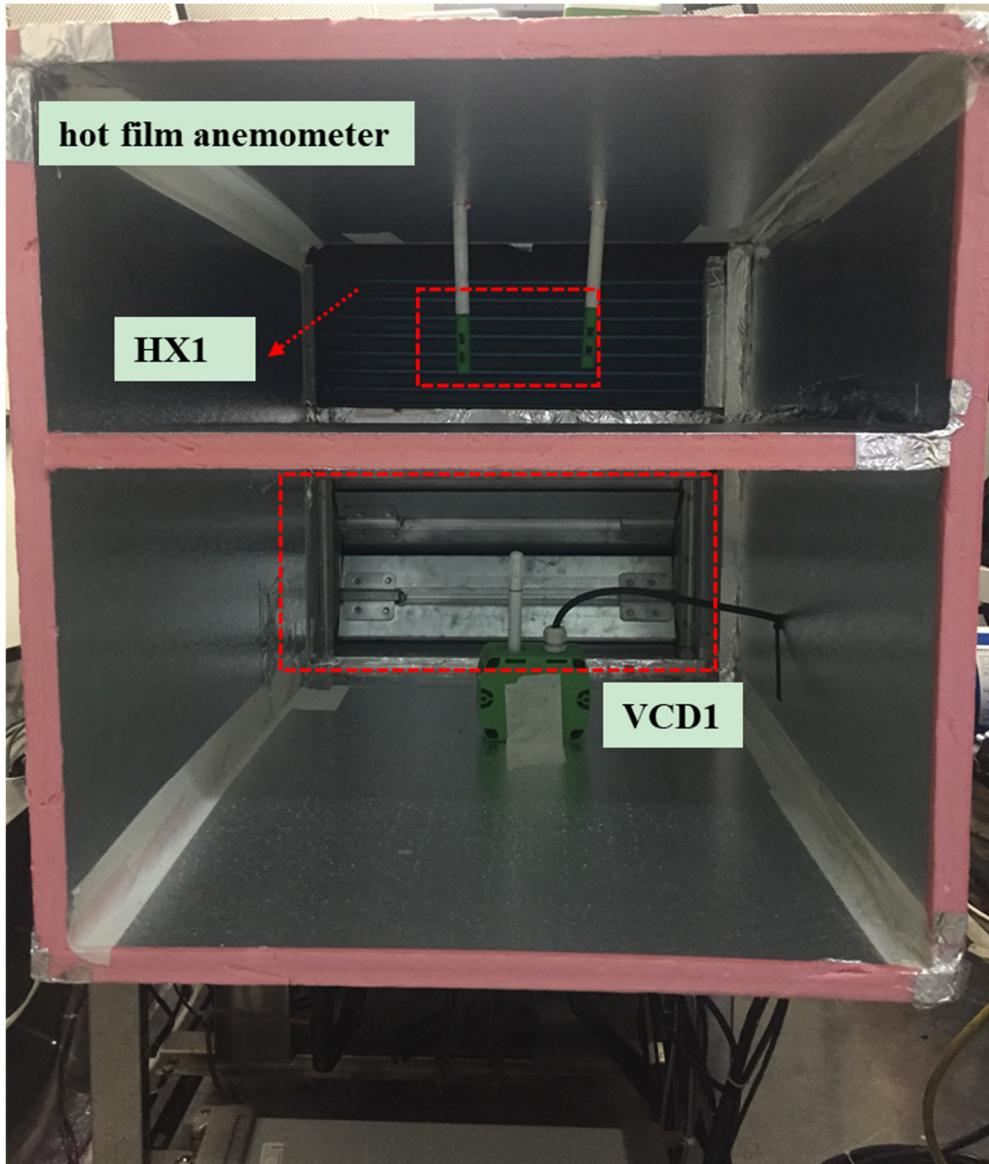


Photo 4 Overview of the air duct of the experimental EDAC system (2)

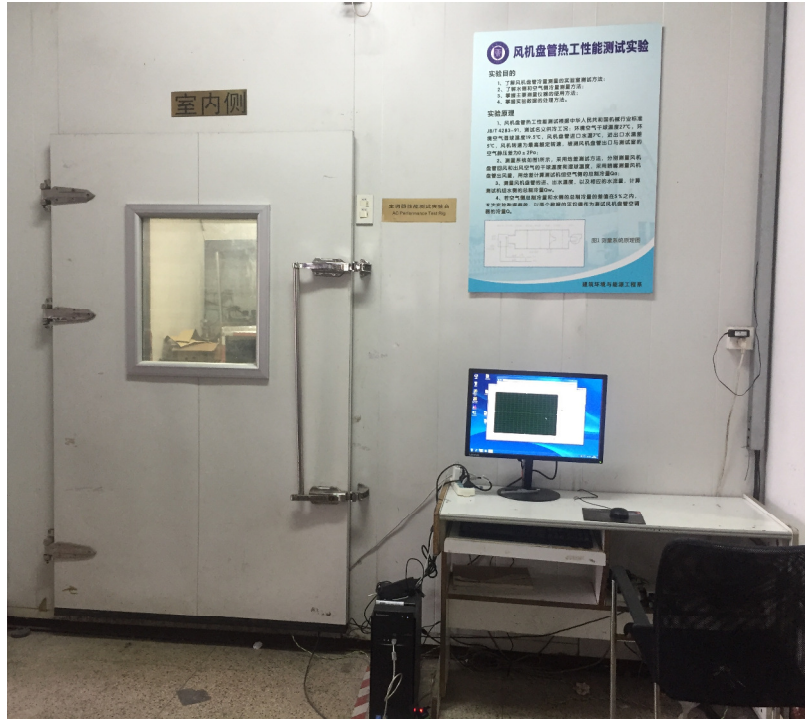


Photo 5 Indoor Chamber of the Laboratory



Photo 6 Outdoor Chamber of the Laboratory



Photo 7 Refrigerant mass flow meters



Photo 8 Load generation unit



Photo 9 Air sampling device

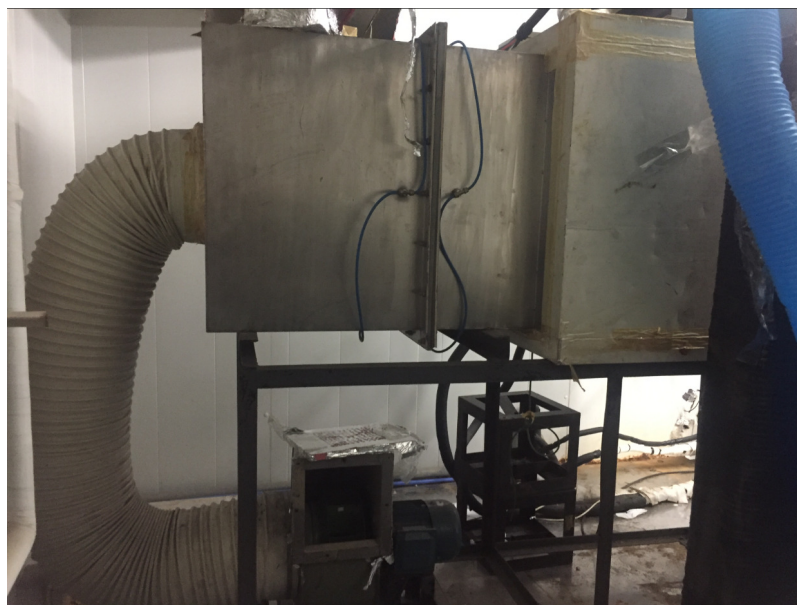


Photo 10 airflow rate measuring apparatus

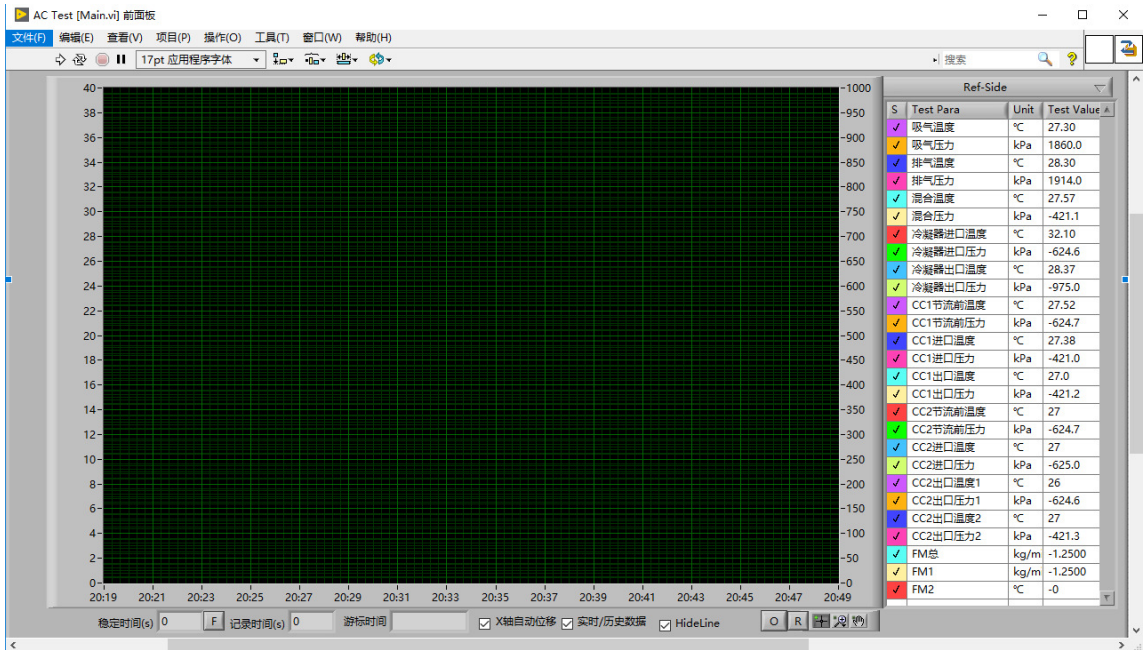


Photo 11 Logging supervisory program

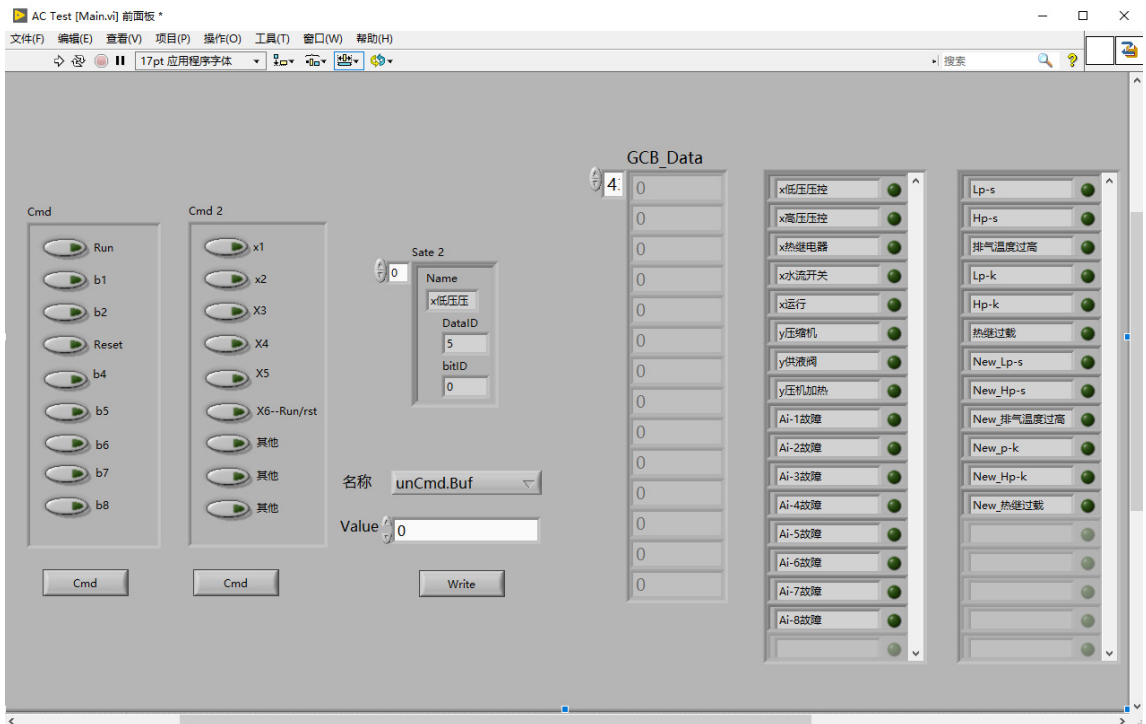


Photo 12 Control supervisory program

References

1. Alpuche et al. 2005
Alpuche M.G., Heard C., Best R. and Rojas J.
Exergy analysis of air cooling systems in buildings in hot humid climates. *Applied Thermal Engineering*, 25 (2005): 507-517.
2. Alsenz 2002.
Alsenz R.H.
Refrigeration sub-cooler and air conditioning dehumidifier. Google Patents.
3. Amrane et al. 2003
Amrane K., Hourahan G.C. and Potts G.
Latent performance of unitary equipment. *ASHRAE journal*, 45 (2003): 28.
4. Andrade and Bullard 2002
Andrade M.A. and Bullard C.W.
Modulating blower and compressor capacities for efficient comfort control/Discussion. *ASHRAE Transactions*, 108 (2002): 631.
5. Arens and Baughman 1996
Arens E.A. and Baughman A.
Indoor humidity and human health: part II--buildings and their systems. (1996).
6. ASHRAE 1986
ASHRAE Standard 41.1.
Standard Method for Temperature Measurement. American Society of Heating, Refrigerating and Air-Conditioning Engineers, Atlanta, GA, USA, (1986).
7. ASHRAE 1987
ASHRAE Standard 41.2.

- Standard methods for laboratory airflow measurement. American Society of Heating Refrigeration and Air Conditioning Engineers, Atlanta, GA, USA, (1987).
8. ASHRAE 2002.
ASHRAE Standard.
Ventilation for acceptable indoor air quality. American Society of Heating, Refrigerating and Air Conditioning Engineers, Atlanta, GA, USA, (2002).
 9. ASHRAE 2008
ASHRAE Standard. Chapter 37: Compressors. In:
ASHRAE Handbook: HVAC Systems and Equipment. American Society of Heating Refrigerating and Air Conditioning Engineers, Atlanta, GA, USA, (2008): 1-10.
 10. ASHRAE 2009
ASHRAE Handbook: Fundamentals.
American Society of Heating Refrigerating and Air Conditioning Engineers, Atlanta, GA, USA, (2009).
 11. Aynur et al. 2008a
Aynur T.N., Hwang Y. and Radermacher R.
Experimental evaluation of the ventilation effect on the performance of a VRV system in cooling mode—Part I: Experimental evaluation. HVAC&R Research, 14 (2008a): 615-630.
 12. Aynur et al. 2008b
Aynur T.N., Hwang Y. and Radermacher R.
Field performance measurements of a heat pump desiccant unit in dehumidification mode. Energy and Buildings, 40 (2008b): 2141-2147.
 13. Aynur et al. 2008c
Aynur T.N., Hwang Y. and Radermacher R.
A heat pump desiccant unit for dehumidification and humidification. (2008c).

14. Aynur et al. 2008d
Aynur T.N., Hwang Y. and Radermacher R.
Simulation evaluation of the ventilation effect on the performance of a VRV system in cooling mode—Part II, simulation evaluation. HVAC&R Research, 14 (2008d): 783-795.
15. Aynur et al. 2010a
Aynur T.N., Hwang Y. and Radermacher R.
Field performance measurements of a heat pump desiccant unit in heating and humidification mode. Energy and Buildings, 42 (2010a): 678-683.
16. Aynur et al. 2010b
Aynur T.N., Hwang Y. and Radermacher R.
Integration of variable refrigerant flow and heat pump desiccant systems for the cooling season. Applied Thermal Engineering, 30 (2010b): 917-927.
17. Aynur et al. 2010c
Aynur T.N., Hwang Y. and Radermacher R.
Integration of variable refrigerant flow and heat pump desiccant systems for the heating season. Energy and Buildings, 42 (2010c): 468-476.
18. Berglund 1998
Berglund L.G.
Comfort and humidity. ASHRAE journal, 40 (1998): 35.
19. Cao et al. 2017
Cao X., Zhang C.L. and Zhang Z.Y.
Stepped pressure cycle—A new approach to Lorenz cycle. International Journal of Refrigeration, 74 (2017): 283-294.
20. Chen 2005
Chen W.
Modeling and control of a direct expansion (DX) variable-air-volume (VAV) air conditioning (A/C) system. The Hong Kong Polytechnic University.

21. Chen and Deng 2006
Chen W. and Deng S.
Development of a dynamic model for a DX VAV air conditioning system. *Energy Conversion and Management*, 47 (2006): 2900-2924.
22. Chen et al. 2005
Chen W., Zhou X. and Deng S.
Development of control method and dynamic model for multi-evaporator air conditioners (MEAC). *Energy conversion and management*, 46 (2005): 451-465.
23. Cheung and Braun 2014
Cheung H. and Braun J.E.
Component-based, gray-box modeling of ductless multi-split heat pump systems. *International Journal of Refrigeration*, 38 (2014): 30-45.
24. Chi and Didion 1982
Chi J. and Didion D.
A simulation model of the transient performance of a heat pump. *International Journal of Refrigeration*, 5 (1982): 176-184.
25. Choi and Kim 2003
Choi J. and Kim Y.
Capacity modulation of an inverter-driven multi-air conditioner using electronic expansion valves. *Energy*, 28 (2003): 141-155.
26. Corberán and Melon 1998
Corberán J. and Melon M.G.
Modeling of plate finned tube evaporators and condensers working with R134a. *International journal of refrigeration*, 21 (1998): 273-284.
27. Dai et al. 2001
Dai Y., Wang R., Zhang H. and Yu J.

Use of liquid desiccant cooling to improve the performance of vapor compression air conditioning. *Applied Thermal Engineering*, 21 (2001): 1185-1202.

28. Damasceno et al. 1990
Damasceno G., Goldschmidt V. and Rooke S.
Comparison of three steady-state heat pump computer models. *ASHRAE Transactions (American Society of Heating, Refrigerating and Air-Conditioning Engineers);(United States)*, 96 (1990).
29. Davanagere et al. 1999
Davanagere B., Sherif S. and Goswami D.
A feasibility study of a solar desiccant air-conditioning system—Part II: Transient simulation and economics. *International Journal of Energy Research*, 23 (1999): 103-116.
30. Deng S. 2000
Deng S.
A dynamic mathematical model of a direct expansion (DX) water-cooled air-conditioning plant. *Building and Environment*, 35 (2000): 603-613.
31. Diaz et al. 1999
Diaz G., Sen M., Yang K. and McClain R.L.
Simulation of heat exchanger performance by artificial neural networks. *Hvac&R Research*, 5 (1999): 195-208.
32. Ding 2007
Ding G.l.
Recent developments in simulation techniques for vapour-compression refrigeration systems. *International Journal of Refrigeration*, 30 (2007): 1119-1133.
33. Domanski 1991
Domanski P.A.
Simulation of an evaporator with nonuniform one-dimensional air distribution.

34. Eicker et al. 2010
Eicker U., Schneider D., Schumacher J., Ge T. and Dai Y.
Operational experiences with solar air collector driven desiccant cooling systems. *Applied Energy*, 87 (2010): 3735-3747.
35. Elliott and Rasmussen 2008
Elliott M.S. and Rasmussen B.P.
Model-based predictive control of a multi-evaporator vapor compression cooling cycle, American Control Conference, 2008. IEEE, 1463-1468.
36. Elliott and Rasmussen 2013
Elliott M.S. and Rasmussen B.P.
Decentralized model predictive control of a multi-evaporator air conditioning system. *Control Engineering Practice*, 21 (2013): 1665-1677.
37. Fan et al. 2014
Fan H., Shao S. and Tian C.
Performance investigation on a multi-unit heat pump for simultaneous temperature and humidity control. *Applied Energy*, 113 (2014): 883-890.
38. Fanger 1970
Fanger P.O.
Thermal comfort. Analysis and applications in environmental engineering. *Thermal comfort. Analysis and applications in environmental engineering.*, (1970).
39. Fong et al. 2011
Fong K., Lee C.K., Chow T.T. and Fong A.
Investigation on solar hybrid desiccant cooling system for commercial premises with high latent cooling load in subtropical Hong Kong. *Applied Thermal Engineering*, 31 (2011): 3393-3401.
40. Fye et al. 2012
Fye C.K., Raghavan V.R. and Meng C.W.

Study on a two-evaporator system for humidity control, AIP Conference Proceedings. AIP, pp. 361-369.

41. Ge F., Guo X., Hu Z. and Chu Y. 2011
Ge F., Guo X., Hu Z. and Chu Y.
Energy savings potential of a desiccant assisted hybrid air source heat pump system for residential building in hot summer and cold winter zone in China. *Energy and Buildings*, 43 (2011): 3521-3527.
42. Ge et al. 2012
Ge T., Dai Y., Li Y. and Wang R.
Simulation investigation on solar powered desiccant coated heat exchanger cooling system. *Applied energy*, 93 (2012): 532-540.
43. Ge et al. 2010
Ge T., Dai Y., Wang R. and Peng Z.
Experimental comparison and analysis on silica gel and polymer coated fin-tube heat exchangers. *Energy*, 35 (2010): 2893-2900.
44. Gray and Webb 1986
Gray D. and Webb R.
Heat transfer and friction correlations for plate finned-tube heat exchangers having plain fins, *Proceedings of the 8th International Heat Transfer Conference*, 2745-2750.
45. Han and Zhang 2011
Han X. and Zhang X.
Experimental study on a residential temperature–humidity separate control air-conditioner. *Energy and buildings*, 43 (2011): 3584-3591.
46. Han et al. 2013
Han X., Zhang X., Wang L. and Niu R.
A novel system of the isothermal dehumidification in a room air-conditioner. *Energy and Buildings*, 57 (2013): 14-19.
47. Harriman 2002

- Harriman III L.G.
Dehumidification equipment advances. ASHRAE journal, 44 (2002): 22.
48. Holman and Gajda 2001
Holman J.P. and Gajda W.J.
Experimental methods for engineers. McGraw-Hill New York.
49. Hourahan 2004
Hourahan G.C.
How to properly size unitary equipment. ASHRAE Journal, 46 (2004): 15.
50. Huh and Brandemuehl 2008
Huh J.-H. and Brandemuehl M.J.
Optimization of air-conditioning system operating strategies for hot and humid climates. Energy and Buildings, 40 (2008): 1202-1213.
51. Hwang 2004
Hwang Y.
Potential energy benefits of integrated refrigeration system with microturbine and absorption chiller. International Journal of Refrigeration, 27 (2004): 816-829.
52. Jakob et al. 1987
Jakob F., Fischer R. and FLANIGAN L.
Experimental validation of the duct submodel for the SP43 simulation model. ASHRAE transactions, 93 (1987): 1499-1514.
53. Jia et al. 1995
Jia X., Tso C., Chia P. and Jolly P.
A distributed model for prediction of the transient response of an evaporator. International Journal of Refrigeration, 18 (1995): 336-342.
54. Jiang et al. 2006
Jiang W., Khan J. and Dougal R.A.

- Dynamic centrifugal compressor model for system simulation. *Journal of power sources*, 158 (2006): 1333-1343.
55. Jiang et al. 2013
Jiang Y., Ge T. and Wang R.
Performance simulation of a joint solid desiccant heat pump and variable refrigerant flow air conditioning system in EnergyPlus. *Energy and Buildings*, 65 (2013): 220-230.
56. Jiang et al. 2014a
Jiang Y., Ge T., Wang R. and Huang Y.
Experimental investigation on a novel temperature and humidity independent control air conditioning system—Part I: Cooling condition. *Applied Thermal Engineering*, 73 (2014a): 784-793.
57. Jiang et al. 2014b
Jiang Y., Ge T., Wang R. and Huang Y.
Experimental investigation on a novel temperature and humidity independent control air conditioning system—Part II: Heating condition. *Applied Thermal Engineering*, 73 (2014b): 775-783.
58. Keniar et al. 2015
Keniar K., Ghali K. and Ghaddar N.
Study of solar regenerated membrane desiccant system to control humidity and decrease energy consumption in office spaces. *Applied Energy*, 138 (2015): 121-132.
59. Kishi et al. 2009
Kishi R., Saijo Y., Kanazawa A., Tanaka M., Yoshimura T., Chikara H., Takigawa T., Morimoto K., Nakayama K. and Shibata E.
Regional differences in residential environments and the association of dwellings and residential factors with the sick house syndrome: a nationwide cross-sectional questionnaire study in Japan. *Indoor Air*, 19 (2009): 243-254.
60. Kittler 1996
Kittler R.

Mechanical dehumidification control strategies and psychrometrics. American Society of Heating, Refrigerating and Air-Conditioning Engineers, Inc., Atlanta, GA (United States).

61. Klein and Alvarado 2002
Klein S. and Alvarado F.
EES-Engineering Equation Solver. F-Chart Software.
62. Knight et al. 2008
Knight J.T., Bellah S.W. and Pickle S.B.
System and method for using hot gas reheat for humidity control. Google Patents.
63. Komor 1997
Komor P.
Space cooling demands from office plug loads. ASHRAE journal, 39 (1997): 41.
64. Krakow et al. 1995
Krakow K.I., Lin S. and Zeng Z.S.
Temperature and humidity control during cooling and dehumidifying by compressor and evaporator fan speed variation. American Society of Heating, Refrigerating and Air-Conditioning Engineers, Inc., Atlanta, GA (United States).
65. Kurtz 2003
Kurtz B.
Being size wise. ASHRAE journal, 45 (2003): 17.
66. Lam 1993
Lam J.
A survey of electricity consumption and user behaviour in some government staff quarters: Survey covering fire services' quarters in Hong Kong found

variable use of electricity consumption. *Building Research and Information*, 21 (1993): 109-116.

67. Lebrun 1995
Lebrun J.
Bringing simulation to application. Final proposal for IEA Annex, 30 (1995).
68. Lee et al. 2012
Lee W., Chen H., Leung Y. and Zhang Y.
Decoupling dehumidification and cooling for energy saving and desirable space air conditions in hot and humid Hong Kong. *Energy conversion and management*, 53 (2012): 230-239.
69. Legg 1986
Legg R.
Characteristics of single and multi-blade dampers for ducted air systems. *Building Services Engineering Research and Technology*, 7 (1986): 129-145.
70. Lemmon et al. 2013
Lemmon E., Huber M. and McLinden M.
NIST Standard Reference Database 23: Reference Fluid Thermodynamic and Transport Properties-REFPROP, Version 9.1, National Institute of Standards and Technology, Standard Reference Data Program, Gaithersburg, (2013).
71. Li et al. 2012
Li N., Xia L., Deng S., Xu X. and Chan M-Y.
Dynamic modeling and control of a direct expansion air conditioning system using artificial neural network. *Applied energy*, 91 (2012): 290-300.
72. Li et al. 2013
Li N., Xia L., Deng S., Xu X. and Chan M.-Y.
On-line adaptive control of a direct expansion air conditioning system using artificial neural network. *Applied thermal engineering*, 53 (2013): 96-107.
73. Li 2013a

- Li W.
Simplified modeling analysis of mass flow characteristics in electronic expansion valve. *Applied Thermal Engineering*, 53 (2013a): 8-12.
74. Li 2013b
Li W.
Simplified steady-state modeling for variable speed compressor. *Applied thermal engineering*, 50 (2013b): 318-326.
75. Li et al. 2018
Li Z., Chen J., Wang F., Cui L. and Qu M.
A simulation study for evaluating the performances of different types of household radiant air conditioning systems. *Applied Thermal Engineering*, 131 (2018): 553-564.
76. Li et al. 2006
Li Z., Chen W., Deng S. and Lin Z.
The characteristics of space cooling load and indoor humidity control for residences in the subtropics. *Building and environment*, 41 (2006): 1137-1147.
77. Li and Deng 2007a
Li Z. and Deng S.
A DDC-based capacity controller of a direct expansion (DX) air conditioning (A/C) unit for simultaneous indoor air temperature and humidity control–Part I: Control algorithms and preliminary controllability tests. *International journal of refrigeration*, 30 (2007a): 113-123.
78. Li and Deng 2007b
Li Z. and Deng S.
An experimental study on the inherent operational characteristics of a direct expansion (DX) air conditioning (A/C) unit. *Building and Environment*, 42 (2007b): 1-10.
79. Li et al. 2014
Li Z., Xu X., Deng S. and Pan D.

Further study on the inherent operating characteristics of a variable speed direct expansion air conditioning system. *Applied thermal engineering*, 66 (2014): 206-215.

80. Li et al. 2015a
Li Z., Xu X., Deng S. and Pan D.
A novel neural network aided fuzzy logic controller for a variable speed (VS) direct expansion (DX) air conditioning (A/C) system. *Applied Thermal Engineering*, 78 (2015a): 9-23.
81. Li et al. 2015b
Li Z., Xu X., Deng S. and Pan D.
A novel proportional-derivative (PD) law based fuzzy logic principles assisted controller for simultaneously controlling indoor temperature and humidity using a direct expansion (DX) air conditioning (A/C) system. *international journal of refrigeration*, 57 (2015b): 239-256.
82. Lin and Deng 2004
Lin Z. and Deng S.
A study on the characteristics of nighttime bedroom cooling load in tropics and subtropics. *Building and Environment*, 39 (2004): 1101-1114.
83. Lin and Deng 2006
Lin Z. and Deng S.
Sizing room air conditioners used in sleeping environments in the subtropics. *Energy conversion and management*, 47 (2006): 1851-1856.
84. Ling et al. 2010
Ling J., Hwang Y. and Radermacher R.
Theoretical study on separate sensible and latent cooling air-conditioning system. *international journal of refrigeration*, 33 (2010): 510-520.
85. Ling et al. 2011
Ling J., Kuwabara O., Hwang Y. and Radermacher R.

Experimental evaluation and performance enhancement prediction of desiccant assisted separate sensible and latent cooling air-conditioning system. international journal of refrigeration, 34 (2011): 946-957.

86. Ling et al. 2013

Ling J., Kuwabara O., Hwang Y. and Radermacher R.
Enhancement options for separate sensible and latent cooling air-conditioning systems. International Journal of Refrigeration, 36 (2013): 45-57.

87. Liu et al. 2004

Liu J., Wei W., Ding G., Zhang C., Fukaya M., Wang K. and Inagaki T.
A general steady state mathematical model for fin-and-tube heat exchanger based on graph theory. International Journal of Refrigeration, 27 (2004): 965-973.

88. Lstiburek 2002

Lstiburek J.
Residential ventilation and latent loads. ASHRAE journal, 44 (2002): 18.

89. Lu et al. 2009

Lu H., Chen H., Xie J., Tao H. and Hu Y.
Refrigerant flow distributary disequilibrium caused by configuration of two phase fluid pipe network. Energy Conversion and Management, 50 (2009): 730-738.

90. MacArthur and Grald 1987

MacArthur J. and Grald E.
Prediction of cyclic heat pump performance with a fully distributed model and a comparison with experimental data. ASHRAE Trans, 93 (1987).

91. Masy 2006

Masy G.

Dynamic simulation on simplified building models and interaction with heating systems, 7th International Conference on System Simulation in Buildings, Liège, Belgium.

92. McGahey 1998
McGahey K.
New commercial applications for desiccant-based cooling. ASHRAE journal, 40 (1998): 41.
93. Mei and Levermore 2002
Mei L. and Levermore G.
Simulation and validation of a VAV system with an ANN fan model and a non-linear VAV box model. Building and Environment, 37 (2002): 277-284.
94. Muñoz et al. 2017
Muñoz F., Sanchez E.N., Xia Y. and Deng S.
Real-time neural inverse optimal control for indoor air temperature and humidity in a direct expansion (DX) air conditioning (A/C) system. International Journal of Refrigeration, 79 (2017): 196-206.
95. Murphy 2002
Murphy J.
Dehumidification performance of HVAC systems. ASHRAE journal, 44 (2002): 23.
96. Niu et al. 2002
Niu J., Zhang L. and Zuo H.
Energy savings potential of chilled-ceiling combined with desiccant cooling in hot and humid climates. Energy and Buildings, 34 (2002): 487-495.
97. Osanyintola and Simonson 2006
Osanyintola O.F. and Simonson C.J.
Moisture buffering capacity of hygroscopic building materials: Experimental facilities and energy impact. Energy and Buildings, 38 (2006): 1270-1282.

98. Paasi et al. 2001
Paasi J., Nurmi S., Vuorinen R., Strengell S. and Maijala P.
Performance of ESD protective materials at low relative humidity. *Journal of Electrostatics*, 51 (2001): 429-434.
99. Pacheco-Vega et al. 2001
Pacheco-Vega A., Sen M., Yang K. and McClain R.L.
Neural network analysis of fin-tube refrigerating heat exchanger with limited experimental data. *International Journal of Heat and Mass Transfer*, 44 (2001): 763-770.
100. Pan et al. 2012
Pan Y., Xu X., Xia L. and Deng S.
A modeling study on the effects of refrigerant pipeline length on the operational performance of a dual-evaporator air conditioning system. *Applied thermal engineering*, 39 (2012): 15-25.
101. Park et al. 2007
Park C., Cho H., Lee Y. and Kim Y.
Mass flow characteristics and empirical modeling of R22 and R410A flowing through electronic expansion valves. *International Journal of Refrigeration*, 30 (2007): 1401-1407.
102. Qi 2009
Qi Q.
Multivariable control of air temperature and humidity in a space served by a direct expansion (DX) air conditioning (A/C) system. The Hong Kong Polytechnic University.
103. Qi and Deng 2009
Qi Q. and Deng S.
Multivariable control of indoor air temperature and humidity in a direct expansion (DX) air conditioning (A/C) system. *Building and Environment*, 44 (2009): 1659-1667.

104. Rasmussen and Alleyne 2004
Rasmussen B.P. and Alleyne A.G.
Control-oriented modeling of transcritical vapor compression systems. *Journal of dynamic systems, measurement, and control*, 126 (2004): 54-64.
105. Reinikainen and Jaakkola 2003
Reinikainen L. and Jaakkola J.
Significance of humidity and temperature on skin and upper airway symptoms. *Indoor air*, 13 (2003): 344-352.
106. Seo et al. 2014
Seo J.-M., Song D. and Lee K.H.
Possibility of coupling outdoor air cooling and radiant floor cooling under hot and humid climate conditions. *Energy and Buildings*, 81 (2014): 219-226.
107. Shah et al. 2004
Shah R., Alleyne A.G. and Bullard C.W.
Dynamic Modeling and Control of Multi-Evaporator Air-Conditioning Systems. *ASHRAE transactions*, 110 (2004).
108. Shirey 1993.
Shirey D.
Demonstration of efficient humidity control techniques at an art museum, the 1993 Winter Meeting of ASHRAE Transactions. Part 1, Chicago, IL, USA, 01/23-27/93, pp. 694-703.
109. Shirey III and Henderson Jr 2004
Shirey III D.B. and Henderson Jr H.I.
Dehumidification at Part Load. *ASHRAE Journal*, 46 (2004): 42.
110. Shirey III et al. 2006.
Shirey III D.B., Henderson Jr H.I. and Raustad R.A.
Understanding the Dehumidification Performance of Air-Conditioning Equipment at Part-Load Conditions. University of Central Florida.
111. Singh et al. 2006

Singh J., Singh N. and Sharma J.
Fuzzy modeling and control of HVAC systems—A review. (2006).

112. Song et al. 2008
Song D., Kim T., Song S., Hwang S. and Leigh S.-B.
Performance evaluation of a radiant floor cooling system integrated with dehumidified ventilation. *Applied Thermal Engineering*, 28 (2008): 1299-1311.
113. Subramanyam et al. 2004
Subramanyam N., Maiya M. and Murthy S.S.
Application of desiccant wheel to control humidity in air-conditioning systems. *Applied thermal engineering*, 24 (2004): 2777-2788.
114. Sunwoo et al. 2006
Sunwoo Y., Chou C., Takeshita J., Murakami M. and Tochihara Y.
Physiological and subjective responses to low relative humidity in young and elderly men. *Journal of physiological anthropology*, 25 (2006): 229-238.
115. Toftum and Fanger 1999
Toftum J. and Fanger P.O.
Air humidity requirements for human comfort. *ASHRAE transactions*, 105 (1999): 641.
116. Toftum et al. 1998a
Toftum J., Jørgensen A.S. and Fanger P.O.
Upper limits for indoor air humidity to avoid uncomfortably humid skin. *Energy and Buildings*, 28 (1998a): 1-13.
117. Toftum et al. 1998b
Toftum J., Jørgensen A.S. and Fanger P.O.
Upper limits of air humidity for preventing warm respiratory discomfort. *Energy and Buildings*, 28 (1998b): 15-23.
118. Trent 2003

- Trent R.W.
Advanced, energy efficient air conditioning, dehumidification and reheat method and apparatus. Google Patents.
119. Tu et al. 2017
Tu Y., Wang R., Ge T. and Zheng X.
Comfortable, high-efficiency heat pump with desiccant-coated, water-sorbing heat exchangers. *Scientific reports*, 7 (2017): 40437.
120. Tuo et al. 2012
Tuo H., Bielskus A. and Hrnjak P.
Experimentally validated model of refrigerant distribution in a parallel microchannel evaporator. *SAE International Journal of Materials and Manufacturing*, 5 (2012): 365-374.
121. Turaga et al. 1988
Turaga M., Lin S. and Fazio P.
Correlations for heat transfer and pressure drop factors for direct expansion air cooling and dehumidifying coils. *ASHRAE transactions*, 94 (1988): 616-630.
122. Vargas and Parise 1995
Vargas J. and Parise J.
Simulation in transient regime of a heat pump with closed-loop and on-off control. *International Journal of Refrigeration*, 18 (1995): 235-243.
123. Villarino et al. 2017
Villarino J.I., Villarino A. and Fernández F.Á.
Experimental and modeling analysis of an office building HVAC system based in a ground-coupled heat pump and radiant floor. *Applied energy*, 190 (2017): 1020-1028.
124. Wang et al. 1999
Wang C.C., Lee C.J., Chang C.T. and Lin S.P.

- Heat transfer and friction correlation for compact louvered fin-and-tube heat exchangers. *International journal of heat and mass transfer*, 42 (1999): 1945-1956.
125. Wang et al. 2000
Wang C.C., Lin Y.T. and Lee C.J.
Heat and momentum transfer for compact louvered fin-and-tube heat exchangers in wet conditions. *International journal of heat and mass transfer*, 43 (2000): 3443-3452.
126. Wang and Toubert 1991
Wang H. and Toubert S.
Distributed and non-steady-state modeling of an air cooler. *International Journal of Refrigeration*, 14 (1991): 98-111.
127. Wang et al. 2013
Wang N., Zhang J. and Xia X.
Desiccant wheel thermal performance modeling for indoor humidity optimal control. *Applied energy*, 112 (2013): 999-1005.
128. Webb 1990
Webb R.
Air-side heat transfer correlations for flat and wavy plate fin-and-tube geometries. *ASHRAE transactions*, 96 (1990): 445-449.
129. Westphalen 2004
Westphalen D.
New approach to energy savings for rooftop AC. *ASHRAE journal*, 46 (2004): 38.
130. Whitman et al. 2012.
Whitman B., Johnson B., Tomczyk J. and Silberstein E.
Refrigeration and air conditioning technology. Cengage Learning.
131. Winkler et al. 2008

Winkler J., Aute V. and Radermacher R.

Comprehensive investigation of numerical methods in simulating a steady-state vapor compression system. *International Journal of Refrigeration*, 31 (2008): 930-942.

132. Xia et al. 2010

Xia L., Chan M.Y, Deng S. and Xu X.

Analytical solutions for evaluating the thermal performances of wet air cooling coils under both unit and non-unit Lewis Factors. *Energy Conversion and Management*, 51 (2010): 2079-2086.

133. Xia et al. 2017

Xia Y., Deng S.and Chan M.Y.

Inherent operational characteristics and operational stability of a variable speed direct expansion air conditioning system. *Applied Thermal Engineering*, 113 (2017): 268-277.

134. Xia et al. 2018

Xia Y., Yan H., Deng S. and Chan M.Y.

A new capacity controller for a direct expansion air conditioning system for operational safety and efficiency. *Building Services Engineering Research and Technology*, 39 (2018): 21-37.

135. Xu and Deng 2012

Xu X. and Deng S.

A novel rule set establishment method for a pid-type fuzzy logic controller in HVAC systems, 2nd Asian-US-European Thermophysics Conference in Hong Kong Thermal Science for Sustainable World, Hong Kong.

136. Xu et al. 2008

Xu X., Deng S. and Chan M.Y.

A new control algorithm for direct expansion air conditioning systems for improved indoor humidity control and energy efficiency. *Energy conversion and management*, 49 (2008): 578-586.

137. Xu et al. 2014
Xu X., Deng S., Han X. and Zhang X.
A control-oriented semi-physical model for a direct expansion air conditioning system. *Building Services Engineering Research and Technology*, 35 (2014): 585-599.
138. Xu et al. 2010
Xu X., Xia L., Chan M. and Deng S.
Inherent correlation between the total output cooling capacity and equipment sensible heat ratio of a direct expansion air conditioning system under variable-speed operation (XXG SMD SHR DX AC unit). *Applied thermal engineering*, 30 (2010): 1601-1607.
139. Xu et al. 2017
Xu X., Zhong Z., Deng S. and Zhang X.
A review on temperature and humidity control methods focusing on air-conditioning equipment and control algorithms applied in small-to-medium-sized buildings. *Energy and Buildings*, (2017).
140. Xu et al. 1996
Xu Z., Gotham D., Collins M., Coney J., Sheppard C. and Merdjani S.
A numerical and experimental study of turbulent flow through the evaporator coil in an air-conditioning unit. *International journal of refrigeration*, 19 (1996): 369-381.
141. Yan et al. 2016
Yan H., Deng S. and Chan M.
Developing and validating a dynamic mathematical model of a three-evaporator air conditioning (TEAC) system. *Applied Thermal Engineering*, 100 (2016): 880-892.
142. Yan et al. 2018
Yan H., Xia Y., Xu X. and Deng S.

Inherent operational characteristics aided fuzzy logic controller for a variable speed direct expansion air conditioning system for simultaneous indoor air temperature and humidity control. *Energy and Buildings*, 158 (2018): 558-568.

143. Zhang and Yoshino 2010
Zhang H. and Yoshino H.
Analysis of indoor humidity environment in Chinese residential buildings. *Building and Environment*, 45 (2010): 2132-2140.
144. Zhang and Zhang 2006
Zhang W.J. and Zhang C.L.
A generalized moving-boundary model for transient simulation of dry-expansion evaporators under larger disturbances. *International Journal of Refrigeration*, 29 (2006): 1119-1127.
145. Zhao et al. 2011
Zhao K., Liu X.H., Zhang T. and Jiang Y.
Performance of temperature and humidity independent control air-conditioning system in an office building. *Energy and Buildings*, 43 (2011): 1895-1903.
146. Zhou et al. 2002
Zhou X.X., Wu Y.Q. and Shao Y.
Modeling and research on the characteristics of double-evaporator air conditioner with inverter. *Journal of Shanghai Jiaotong University*, 36 (2002): 1675-1679. (In chinses)